Network Models of Epidemic Spread: Applications and Analysis

By

CARL THOMAS CORCORAN
DISSERTATION

Submitted in partial satisfaction of the requirements for the degree of

DOCTOR OF PHILOSOPHY

in

Applied Mathematics

in the

OFFICE OF GRADUATE STUDIES

of the

UNIVERSITY OF CALIFORNIA

DAVIS

Approved:

Alan Hastings, Chair

Timothy Lewis

Thilo Gross

Committee in Charge

2021

To my mother, Cheryl Corcoran, my greatest advocate.

Contents

Abstract v

Acknowledgments vii

Chapter 1. Introduction 1

1.1. Compartment Models 2

1.2. Networks 5

1.3. Pairwise Models 9

1.4. Description of Chapters 12

Chapter 2. A Low-Dimensional Network Model for an SIS Epidemic: Analysis of the Super Compact Pairwise Model 14

2.1. Introduction 14

2.2. Model 17

2.3. Epidemic Threshold 20

2.4. The Endemic Equilibrium 22

2.5. Discussion 32

Appendix 33

Chapter 3. Adaptive Network Modeling of Social Distancing Interventions 43

3.1. Introduction 43

3.2. Model 46

3.3. Analysis of Interventions 54

3.4. Discussion 68

Appendix 70

Chapter 4. A Simple Dynamic Process on Bipartite Networks 77

4.1. Introduction 77
4.2. Model Construction 79
4.3. Analysis of the SIS with BRLAD model 89
4.4. Seasonal Forcing in Activation/Deletion and Transmission 92
4.5. Discussion 97

Bibliography 100

Network Models of Epidemic Spread: Applications and Analysis

Abstract

Over the past century, mathematical epidemiology has grown to be one of the triumphs of applied mathematics and mathematical biology. It has drawn influence and insight from a variety of related fields, including mathematics, physics, chemistry, biology, ecology, and social science, among others. With tools ranging from simple ordinary differential equation models to highly complex stochastic simulations, mathematical models of epidemic spread have had significant theoretical and practical impacts. In the past two decades, the development of network science as a discipline has lead to a new modeling paradigm in mathematical epidemiology. Networks can capture aspects of social structure that are critical to disease spread, allowing for models that balance parsimony and complexity.

In this dissertation, I consider questions of model construction, analysis, and application that are united under the framework of modeling epidemics on networks. In Chapter 2, we consider an existing low-dimensional model of an SIS disease on a network. We perform a bifurcation analysis of the model to determine the epidemic threshold and derive asymptotic approximations of the endemic equilibrium under two parameter regimes. As well, we perform sensitivity analysis on the results for the endemic equilibrium with respect to network parameters, and find implications for public health interventions that are in line with previous studies.

Chapters 3 and 4 both model processes of social dynamics using adaptive networks, or networks whose edges change dynamically over time. In Chapter 3, we introduce an SEIR model on a heterogeneous, clustered network with random link activation/deletion dynamics. With this framework, we develop realistic mechanisms for social distancing policies using piecewise constant activation/deletion rates for edges in the network. These mechanisms are able to produce rich qualitative behavior and provide insight into what makes for an effective social distancing intervention. Chapter 4 extends this examination of changing social behavior. I introduce a novel dynamical process where random link activation/deletion occurs on a bipartite network where individuals connect to mixing locations and consider its implications for the corresponding unipartite contact network. This new process is analyzed in conjunction with an SIS-type disease spreading on the

contact network. Furthermore, I consider the implication for seasonal social dynamics, including how separate sources of seasonality (transmission and social behavior) impact how disease dynamics unfold.

Acknowledgments

To my advisor, Alan Hastings, I will be forever in your debt for your mentorship as a scientist and mathematician. Graduate school has been a transformational experience beyond my expectations, and it is in large part due to you. You have righted my ship in times of self-doubt, and given me opportunities I felt were beyond my reach. It is a privilege to have had the independence to pursue research that motivated me, and you have been more encouraging than I ever could have hoped for with an advisor.

To my dissertation committee members, Tim Lewis and Thilo Gross, you have shaped my graduate school experience in different but essential ways, for which I will always be grateful. Tim, from my first campus visit to serving on my dissertation committee, you have been an irreplaceable teacher, friend, and mentor. Thilo, you have always been extremely gracious and accommodating in helping with this dissertation, and without your early work on adaptive networks, I would not have been able to write Chapters 3 and 4.

To the past and current Math Department staff here at UC Davis, especially Tina Denena, Sarah Driver, Victoria Whistler, and Vanessa Bravo, thank you for helping me navigate some of the trickiest parts of graduate school with patience and positivity. To my professors in the UC Davis Math Department, especially the mathematical biology faculty, thank you for giving me the skills to succeed as a mathematician and scientist, and always being open and available to me.

To the faculty of the ‘Dynamics and data in the COVID-19 pandemic” at the American Institute of Mathematics, thank you for the opportunity to pursue cutting-edge projects on a highly-relevant topic. To my Chapter 3 collaborator John Michael Clark, thank you for agreeing to take on a challenging project in such a short amount of time.

To the faculty of Macalester College Mathematics Department, thank you for bringing me wholly into the world of mathematics and setting me on my path ahead. And to Karen Saxe, my undergraduate advisor, thank you for introducing me to mathematical research with such patience and enthusiasm.

To my former colleagues in the Saint Paul Academy Mathematics Department, thank you for shaping the way I think about mathematics and its teaching. With your guidance, I learned that the communication of mathematics is as essential as its practice.

To my friends from Minnesota to California (and now throughout the country), thank you for keeping me grounded and reminding me to enjoy a life outside of graduate school. All the trivia nights, wine tasting, barbecues, camping trips, and getaways to the Bay Area are memories I will treasure for the rest of my life.

To my family—my mother Cheryl and my brothers William, Mitchell, and Joseph, and to my father Grant and Madhavi Deshpande and the rest of my family too numerous to list—thank you for providing a loving and loyal upbringing. It has been constant comfort knowing that you all were in my corner. To Rachel Ferreira, thank you for picking me up off the floor when the tasks of graduate school seemed insurmountable, and for putting up with all my late nights spent writing this dissertation. And finally, thank you to Dwight D. Eisenmeower, my cat, with whom I have weathered many storms. Even in the loneliest moments of graduate school, you were always by my side.

CHAPTER 1

Introduction

Mathematical epidemiology has been an extremely active and impactful branch of mathematical biology in the past century. Rather than modeling biological systems for their own sake, epidemiological models are invaluable for public health practitioners and have saved an untold number of lives. Models have been applied to numerous infectious diseases: some examples include malaria (Ross, 1915), measles (London and Yorke, 1973), influenza (Ferguson et al., 2006), and recently COVID-19 (Ferguson et al., 2020). Mathematical models of epidemic spread have always sought to balance realism with complexity and tractability. Early modeling approaches included simple compartment models (e.g. Kermack and McKendrick (1927)) which continue to find use today, while increasingly abundant computing power has led to complex agent-based simulation models (e.g. Eubank et al. (2004)) in recent decades.

The trade-off between realism and complexity is underscored by the features that make each modeling approach successful. Compartment models elucidate the fundamental mechanisms of disease spread, and their analysis has spawned many essential epidemiological indicators (see Section 1.1). However, these models often require strong simplifying assumptions that limit their effectiveness in the face of real-world epidemics: one particularly notable assumption that a population is well mixed. Conversely, agent-based simulations can describe individual behavior in great detail, which leads to more accurate, data-driven predictive models which have become indispensable to public health scientists and policymakers. However, the level of detail can obfuscate some of the underlying mechanisms of a particular epidemic's spread, and the computational requirements can make exploring the parameter space of a given model prohibitively expensive.

With the development of network science in recent decades, a new and influential modeling paradigm has emerged. Network-based models of epidemic spread offer something of a compromise between compartment models and agent-based simulations (see Kiss et al. (2017) or Pastor-Satorras et al. (2015) for an overview of network models of epidemics). Many network models can capture

the complexity of social structure addressed explicitly by agent-based simulations in the framework of dynamical systems (similar to compartment models). Studies on mixing patterns (Read et al., 2008) and social networks (Christakis and Fowler, 2010; Salathe et al., 2010) reinforce that a central aspect of social structure is heterogeneity in the number of contacts an individual has, and that other network characteristics play a role as well. As such, the construction of a network under consideration plays an integral role in how an epidemic unfolds. Gaining a deeper understanding of the effects of this structure is the theme of this dissertation.

Chapters 2 through 4 of this dissertation cover three modeling projects that explore how heterogeneity in network structure and the dynamics of social behavior influence the trajectory of an epidemic. Each chapter is intended to be published as a standalone academic paper. Chapter 2 was published in the *Bulletin of Mathematical Biology* (Corcoran and Hastings, 2021) with Alan Hastings. Chapter 3 began as a project with John Michael Clark at the American Institute of Mathematics summer school 'Dynamics and data in the COVID-19 pandemic," and has been submitted for review. Chapter 4 is currently in preparation for submission. As the topics of each chapter share related foundations, in the remaining sections of this chapter I provide the necessary background for the rest of this dissertation. In Section 1.1, I cover the basics of compartment models; in Section 1.2, I present some essential features of networks that play a role in epidemic spread; in Section 1.3, I introduce the pairwise model, which is the foundational network model on which all three chapters rely.

1.1. Compartment Models

For much of the twentieth century, compartment models (introduced by Kermack and McKendrick (1927), see Diekmann and Heesterbeek (2000) for an overview of modern approaches) have been the foundation of mathematical epidemiology. Compartment models track how an infectious disease progresses through a population by categorizing individuals in terms of their condition relative to the disease natural history. Compartment models exhibit some flexibility as a framework—models can be stochastic or deterministic, and take place in discrete or continuous time. In the remainder of this section, deterministic, continuous-time models are considered. Two of the most common compartment models are the SIR (susceptible-infectious-recovered) and SIS

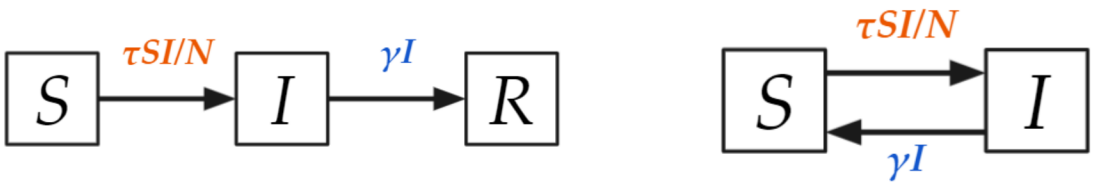

(a) (b)

FIGURE 1.1. Compartment diagrams for an (a) SIR and (b) SIS disease. Compartments are labeled for susceptible (S), infectious (I), and recovered (R) subpopulations, and arrows indicate the direction and rate of transfer between compartments.

(susceptible-infectious-susceptible) models. In both models, susceptible individuals may have a disease transmitted to them, become infectious, and eventually recover. With the SIR model, individuals gain long-term immunity upon recovery and move to the recovered compartment. With the SIS model, no long-term immunity is gained by recovery, and individuals become susceptible to contracting the disease again. Compartment diagrams for the two models are shown in Figure 1.1, along with rates of transfer between compartments. The corresponding system of differential equations for the SIS model (Fig. 1.1b) are

$$\dot{S} = -\tau SI/N + \gamma I, \tag{1.1}$$

$$\dot{I} = \tau SI/N - \gamma I, \tag{1.2}$$

where τ is the transmission rate and γ is the recovery rate. Without vital dynamics (i.e. the total population N is fixed), the system satisfies the conservation equation $S + I = N$, which allows the SIS model to be written with a single equation. The system may have two steady states: the disease-free equilibrium $I = 0$ and the endemic equilibrium $I = N(1 - \gamma/\tau)$. The endemic equilibrium exists and is stable when the basic reproductive number $R_0 = \tau/\gamma > 1$. If $R_0 < 1$, the disease-free equilibrium is stable. Examples of solution trajectories of the SIS model can be found in Figure 1.2b.

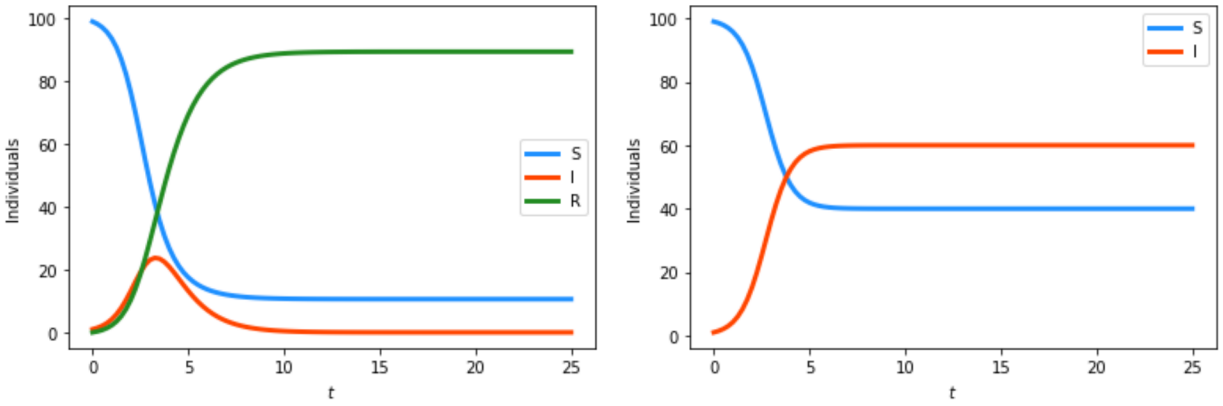

(a) (b)

FIGURE 1.2. Solution trajectories for the (a) SIR and (b) SIS models. Both populations have $N = 100$ individuals, and are initialized with $I(0) = 1$ infectious individuals. For both models, $\tau = 2.5$ and $\gamma = 1$.

For the SIR model (Fig. 1.1a), the corresponding system of differential equations is

$$\dot{S} = -\tau SI/N, \tag{1.3}$$

$$\dot{I} = \tau SI/N - \gamma I, \tag{1.4}$$

$$\dot{R} = \gamma I. \tag{1.5}$$

An epidemic occurs if $R_0 = \tau/\gamma > 1$, however as all infectious individuals eventually move to the recovered compartment, as $t \to \infty$, we have $I \to 0$. Examples of solution trajectories of the SIR model can be found in Figure 1.2a. A critical epidemiological quantity with the SIR model is the final size of the epidemic R_∞. Writing (1.3) as $\dot{S} + \tau SI/N = 0$ and multiplying by $\exp\left(\frac{\tau R}{N\gamma}\right)$, it follows that $S \exp\left(\frac{\tau R}{N\gamma}\right)$ is constant with respect to time, with the constant being determined by the initial number of susceptibles $S(0)$. Assuming that there are no recovered individuals at the beginning of the epidemic ($R(0) = 0$) and that there are no infections at the end of the epidemic ($S_\infty + R_\infty = N$), the final size R_∞ can be determined from the implicit equation

$$N - R_\infty = S(0) \exp\left(-\frac{\tau R_\infty}{N\gamma}\right). \tag{1.6}$$

A critical assumption made by the simple SIR and SIS models is known as the homogeneous mixing assumption: any individual can come into contact with another. This is reflected in the

transmission term $\tau SI/N$ in both models, where τI is the total rate at which infectious contacts are formed and S/N is the proportion of those contacts which are made with a susceptible individual. While the homogeneous mixing assumption can be useful for certain populations, it is clear that in many cases social contacts are complex, varied, and structured. In rolling back this assumption to improve epidemiological models, new mathematical tools have to be introduced.

1.2. Networks

With the removal of the homogeneous mixing assumption, network topology is required to define the structure of individual contacts. Characterization of this structure reflects the distinct lineages of network science: some concepts and metrics are derived from traditional graph theory in mathematics, while others are born from modern applications in physics, computer science, ecology, and social science (see Newman (2010) for an overview). Construction of the networks themselves is a separate challenge, and many random graph creation algorithms have been proposed that satisfy certain network properties. For network models of epidemics, both graph metrics and network generation are crucial pieces of the field.

Graphs are the mathematical objects that underpin contemporary network science. A graph is a collection of N nodes (or vertices) connected by E edges (or links). The exact connectivity structure of a graph can be detailed by its adjacency matrix A: an $N \times N$ matrix with entries $a_{ij} = 1$ if nodes i and j are connected by an edge and $a_{ij} = 0$ otherwise. Though this exact characterization appears in some network models of epidemics (Van Mieghem (2011), for example), for large networks it can be unavailable or of a prohibitive size for computational purposes. With many network models, the vital quantification of structure is the degree distribution. The degree of a node is the number of neighbors (or equivalently edges) to which it is connected, and the degree distribution of a network details the proportion of nodes of a given degree: $p_k = N_k/N$ where N_k is the number of nodes of degree k. In the context of epidemics on networks, many important properties can be derived from the degree distribution. Perhaps the most critical is the average degree of the network, defined as

$$\langle k \rangle = \sum_{k=0}^{N} k p_k. \tag{1.7}$$

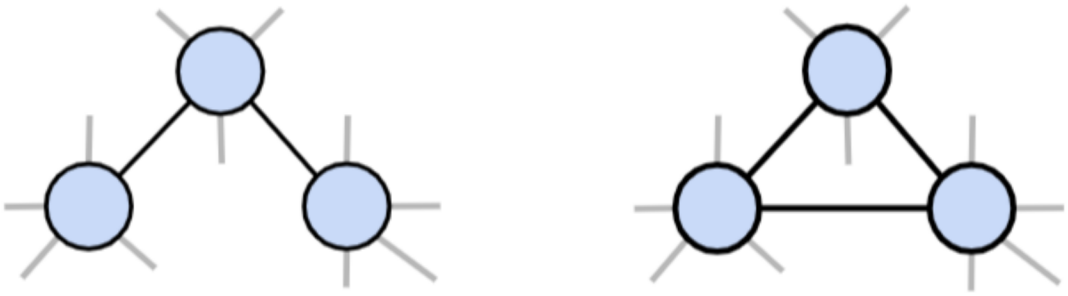

(a) (b)

FIGURE 1.3. Simple diagrams of (a) a connected triple and (b) a triangle that occur in networks.

Higher moments of the degree distribution can be calculated similarly, as $\langle k^n \rangle = \sum_{k=0}^{N} k^n p_k$. These higher moments are particularly relevant in Chapter 2, where network motifs are approximated in terms of these moments. Perhaps the most concrete use of these moments is the average number of connected triples (Fig. 1.3a) per node (counted twice), which is given by

$$\langle k^2 - k \rangle = \sum_{k=0}^{N} k(k-1)p_k. \tag{1.8}$$

This formula can be made sense of from a combinatorial perspective by recognizing that each degree i node is the center of $2\binom{i}{2} = i(i-1)$ triples (when counted twice). As Section 1.3 will show, connected triples play an important role in disease transmission on networks.

From a computational perspective, a useful and elegant characterization of the degree distribution can be made using probability generating functions (see Wilf (2006) for a comprehensive treatment). The probability generating function (or PGF) is a power series whose coefficients correspond to the proportion of nodes in a network with a given degree[1]:

$$G(x) = \sum_{k=0}^{\infty} p_k x^k. \tag{1.9}$$

The machinery of generating functions are used in Chapter 3 and extensively in Chapter 4, in particular the property that differentiating with respect to x and evaluating at $x = 1$ can retrieve the moments of the degree distribution. In those chapters, networks that change dynamically

[1]Characterizing the PGF as an infinite series is standard notation; we consider $p_i = 0$ when i is greater than the maximum degree of the network.

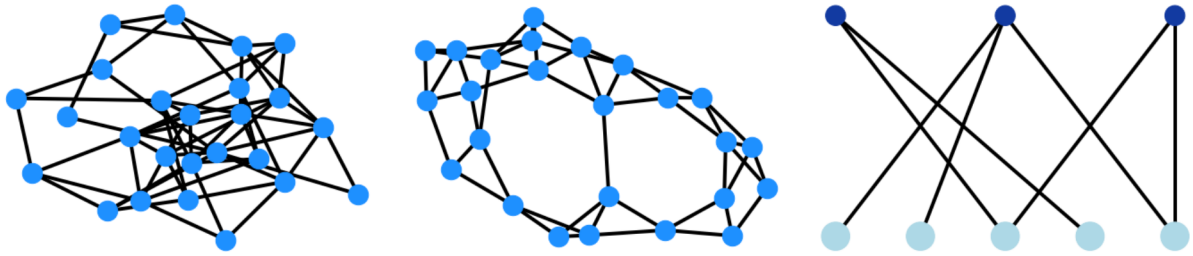

(a) (b) (c)

FIGURE 1.4. Examples of (a) Erdős-Renyi, (b) Watts-Strogatz, and (c) bipartite networks. Examples of both the Erdős-Renyi and Watts-Strogatz networks have $N = 25$ nodes. For the Erdős-Renyi network, $p = 0.2$ and for the Watts-Strogatz network, $c = 4$ and $p = 0.2$.

through time are considered: thus p_k is time-dependent, and the generating function takes a two variable form

$$G(x,t) = \sum_{k=0}^{\infty} p_k(t) x^k. \tag{1.10}$$

An advantage of this formulation is that the time evolution of the degree distribution can be described with partial differential equations for the PGF.

The final network metric that warrants introduction is the clustering coefficient, which is defined as three times the ratio of triangles (Fig. 1.3b) to connected triples:

$$\phi = \frac{3 \cdot \text{Number of Triangles}}{\text{Number of Connected Triples}}. \tag{1.11}$$

The clustering coefficient reflects the density of connections in a network, and clustering can have a significant effect on epidemic spread. Moreover, the propensity for social contacts to form triangles (i.e. high clustering coefficient) has been an observed phenomenon in real-world networks (Read et al., 2008).

A challenge with network models of real-world systems is the difficulty of determining the exact structure of real-world contact networks. Nonetheless, a number of algorithms for generating graphs with given statistical properties are well-known. Two common random graphs that are used in this dissertation are Erdős-Renyi random graphs (Erdös and Renyi, 1959; Gilbert, 1959) and Watts-Strogatz ('small-world") networks (Watts and Strogatz, 1998). Erdős-Renyi random graphs are

formed by taking N nodes and considering all possible pairs and connecting them independently with probability p (Fig. 1.4a). The degree distribution for Erdős-Renyi random graphs tends to the Poisson distribution for large N. Watts-Strogatz networks are formed by placing N nodes in a ring and connecting each node to its c nearest neighbors (with c being even), and then independently rewiring each edge with probability p (Fig. 1.4b). If an edge is rewired, the 'first" node of the pair is randomly connected to another node in the network. Notable features of Watts-Strogatz networks are short average path lengths and relatively high clustering for suitable values of p. Another common method for generating networks is the configuration model (Molloy and Reed, 1995). With configuration model networks, the degree distribution and number of nodes is specified in advance. Nodes are randomly assigned a degree from the distribution and given the corresponding number of half-edges. Half-edges are then connected at random (forming the edges of the network) until no half edges remain. While configuration models offer great flexibility in the ability to fit an observed degree distribution, they lack some features of empirical social networks, as the clustering coefficient vanishes in the large N limit (Newman, 2010). Nonetheless, they are some of the most widely-used random graphs, and play an important role in constructing networks in Chapters 2 through 4.

Finally, two other network concepts play an important role in this dissertation. First, bipartite networks are used in Chapters 3 and 4 to generate contact networks on which the epidemic spreads. Bipartite networks (Fig. 1.4c) consist of two disjoint sets of nodes $\mathcal{A}$ and $\mathcal{B}$, and every edge connects a node in $\mathcal{A}$ to a node in $\mathcal{B}$. Bipartite networks find a natural application in representing a social mixing network. One set of nodes represents individuals, and the other set of nodes represents mixing locations or social groups. A contact network where the epidemic unfolds can be formed by connecting two individuals if they both have an edge to the same mixing location—the resulting contact network between individuals is the unipartite projection of the bipartite network onto the set of individuals. The unipartite contact networks formed this way can exhibit significant heterogeneity and clustering (see Newman et al. (2001) for properties that can be derived with probability generating functions). Second, adaptive networks are the central focus of Chapters 3 and 4. Up until this point, only networks whose edges do not change over time (static networks) have been addressed. Adaptive networks (see Gross and Blasius (2008) for an overview) allow

for the edge structure of the network to evolve through time. In particular, the dynamics of the network structure and the disease transmission dynamics unfold on comparable timescales, and can lead to rich qualitative dynamics. Adaptive network models allow us to study phenomena not captured by static networks, and as such network dynamic processes are applied in Chapters 3 and 4 to model changing social dynamics resulting from public health interventions.

1.3. Pairwise Models

With the concepts of networks established, combining network topology and disease dynamics is the final step in constructing models for epidemics on networks. Chapters 2 through 4 all rely on pairwise models, which are mean-field models for a stochastic transmission (and recovery) process unfolding on a network. As one might expect, individuals are represented by nodes and potential disease-transmitting contacts are represented by edges. At any point in time, each individual has a status determined by the disease natural history. For example, with an SIR model, each individual can be in one of the three states, while with an SIS model, each individual can be in one of two states. In a network with N nodes, this means that there are a total of 3^N possible states for the entire network with an SIR disease, and there are 2^N possible states for an SIS disease. If transmission and recovery are modeled as Poisson processes, the disease dynamics form a continuous-time Markov chain with m^N- dimensional state space where m is the number of possible states for each individual node.

By solving the Kolmogorov equations of the system, the probabilities of the network being in each state at a given time can be found. Through a process known as 'lumping" (Simon et al., 2011; Taylor et al., 2012), these equations can be arranged and combined to yield differential equations for the expected number of nodes in each state. Bracket notation is used to denote the expected number of nodes in each state, i.e. $[S]$ for the expected number of susceptible nodes, $[I]$ for the expected number of infectious nodes, and $[R]$ for the expected number of recovered nodes. The transmission process depends on the expected number of susceptible-infectious pairs $[SI]$, which necessitates equations for the expected number of pairs in each possible state. These equations depend on the expected number of triples in each state, the equations for which depend on higher-order motifs. For an SIS disease on a static network, the system is as follows (Eames and Keeling,

2002):

$$[\dot{S}] = -\beta[SI] + \gamma[I], \tag{1.12}$$

$$[\dot{I}] = \beta[SI] - \gamma[I], \tag{1.13}$$

$$[\dot{SS}] = -2\beta[SSI] + 2\gamma[SI], \tag{1.14}$$

$$[\dot{SI}] = \beta([SSI] - [ISI] - [SI]) + \gamma([II] - [SI]), \tag{1.15}$$

$$[\dot{II}] = 2\beta([ISI] + [SI]) - 2\gamma[II], \tag{1.16}$$

where β is the rate at which SI pairs transmit the infection[2] and γ is the recovery rate. The full system requires evolution equations for the expected number of triples $[SSI]$ and $[ISI]$, and higher-order motifs, though the equations are rarely written. The number of nodes N being fixed leads to the conservation equation $[S] + [I] = N$. Furthermore, for a static network the pairs obey the conservation equation $[SS] + 2[SI] + [II] = N\langle k\rangle$, where $\langle k\rangle$ is the average degree, and $N\langle k\rangle$ is twice the number of edges in the network. The equations for SIR dynamics on a network are similar:

$$[\dot{S}] = -\beta[SI], \tag{1.17}$$

$$[\dot{I}] = \beta[SI] - \gamma[I], \tag{1.18}$$

$$[\dot{SS}] = -2\beta[SSI], \tag{1.19}$$

$$[\dot{SI}] = \beta([SSI] - [ISI] - [SI]) - \gamma[SI], \tag{1.20}$$

$$[\dot{II}] = 2\beta([ISI] + [SI]) - 2\gamma[II]. \tag{1.21}$$

Equations for the expected number of recovered nodes $[R]$ and pairs involving them $[SR]$, $[IR]$, $[RR]$ are not necessary, as $[R]$ can be determined from the conservation equation $[S] + [I] + [R] = N$.

Useful heuristics for understanding the derivation of the SIS model (1.12)-(1.16) and the SIR model (1.17)-(1.21) are compartment diagrams for the expected number of nodes and pairs in each state (Fig. 1.5). Like the diagrams for simple compartment models in Figure 1.1, the transfer

[2]The transmission rate τ in the simple compartment models and the transmission rate β in the pairwise models are slightly different characterizations, but are related by $\tau = \beta N$.

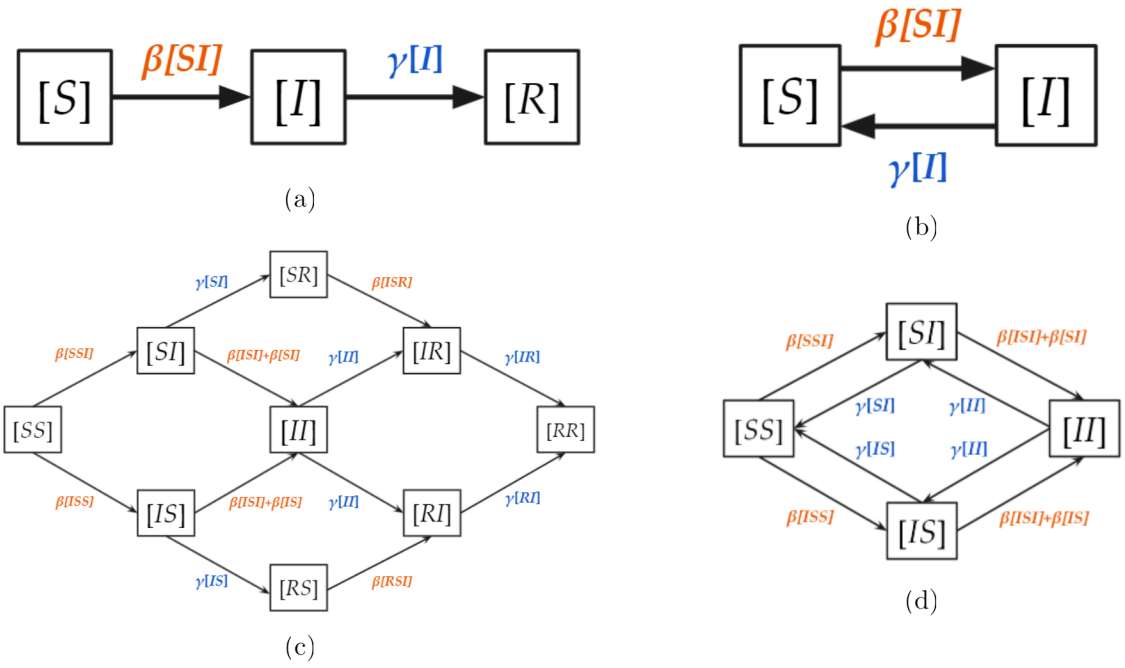

FIGURE 1.5. Compartment diagrams for the pairwise models of (a),(c) SIR and (b),(d) SIS diseases. Diagrams for the expected number of nodes in each state are shown in (a) and (b). Diagrams for the expected number of pairs of nodes in each state are shown in (c) and (d). Note that when connecting the pairwise models to these diagrams, the order of the pairs does not matter (e.g. the $[SI]$ and $[IS]$ compartments are modeled by the $[SI]$ equation).

from the $[S]$ to $[I]$ compartments depends on the (expected) number of susceptible-infectious pairs. In simple compartment models, this is the product SI, while in the pairwise models, it defined explicitly in network terms as $[SI]$ (Figs. 1.5), which requires tracking the expected number of pairs and necessitates compartments for the pairs of all states. The rates of transfer between pair compartments can be determined from the transmission and recovery processes, yielding the diagrams in Figures 1.5c and 1.5d. Again, transmission between pairs depends on triples, which necessitates further compartment diagrams to arrive at the full pairwise SIR and SIS models.

At this point, the dependence of the pairwise models on triples and higher-order motifs warrants comment. Though further equations are omitted in (1.12)-(1.16) and (1.17)-(1.21), for the exact dynamics (in terms of expectation) they are required. This makes the full pairwise models prohibitively large for any sort of analysis. The most common approach to overcome this limitation is to approximate the expected number of triples in terms of lower-order state variables and

network metrics. Known as triple approximations (Keeling, 1999), these assumptions close the full pairwise models forming dynamical systems of manageable size. Chapter 2 analyzes a system that is closed by a triple approximation developed in House and Keeling (2011) and Simon and Kiss (2016), while Chapters 3 and 4 use a novel closure based on one introduced in Keeling (1999).

1.4. Description of Chapters

The remaining three chapters of this dissertation are united by their consideration of pairwise models of epidemics on networks. A low-dimensional model of an SIS disease on a network was introduced by Simon and Kiss (2016), termed the 'super compact pairwise model." In their article, Simon and Kiss derived a well-performing triple closure but did not analyze the epidemic threshold or the endemic equilibrium of the model (though they noted that both presented fruitful future directions). In Chapter 2, bifurcation analysis is done to find the epidemic threshold, and asymptotic techniques are employed to find accurate approximations of the endemic equilibrium in two regimes of transmission and recovery rates. Moreover, a sensitivity analysis of the approximations of the endemic equilibrium suggests public health conclusions related to screening versus contact tracing in line with existing work, though from a network structure perspective.

Chapters 3 and 4 both concern adaptive network models and are strongly influenced by the COVID-19 pandemic. Chapter 3 uses a simple process of network dynamics known as random link activation/deletion (Kiss et al., 2012) to model the effects of social distancing and lockdown policies in conjunction with an SEIR (susceptible-exposed-infectious-recovered) disease on a network. Two mechanisms for social distancing are introduced using piecewise constant activation and deletion rates, and effects on the overall outcome of the epidemic are measured. Significantly, the severity of an intervention and the threshold prevalence to trigger it are found to have a greater impact on the outcome than the length of time over which the intervention occurs. Chapter 4 develops a novel process for network dynamics which occur on a bipartite mixing network, while disease dynamics occur on the corresponding unipartite contact network. Leveraging probability generating functions to determine the effects of the process on the contact network, this chapter introduces a realistic adaptive network process inspired by now-ubiquitous mobile phone mobility data. This process is

also used to analyze seasonality in disease patterns, separating periodicity in transmission dynamics from social contact dynamics.

CHAPTER 2

A Low-Dimensional Network Model for an SIS Epidemic: Analysis of the Super Compact Pairwise Model

2.1. Introduction

In the past few decades, network-based models of epidemic spread have become a central topic (Kiss et al., 2017; Pastor-Satorras et al., 2015) in epidemiology. Their ability to capture mathematically the complex structure of transmission interactions makes them an invaluable theoretical paradigm. Mathematically, a network is modeled as a graph consisting of a set of nodes that are connected by a set of links (called edges). In the context of epidemiology, typically nodes represent individuals, and edges represent interactions that can transmit the infection. Used in conjunction with compartment models, the disease natural history determines the number of possible states an individual node might be in at any point in time. When disease spread is modeled as a continuous time Markov chain, the network size and disease natural history can lead to high dimensional state spaces. For example, in a network with N nodes where individual nodes can be in m possible states, the size of the state space for the network is m^N. Efforts to describe this process with a system of ordinary differential equations are similarly hampered by size—the Kolmogorov equations governing this system are exact, but prohibitively large. Thus, an important goal in network-based modeling has been to find a (relatively) low-dimensional system that accurately approximates the underlying high-dimensional system.

Many approaches (Barnard et al., 2019; Karrer and Newman, 2010; Miller et al., 2012; Pastor-Satorras and Vespignani, 2001; Pastor-Satorras et al., 2015) in recent years have sought to introduce models with systems of a manageable size. Pairwise models (Eames and Keeling, 2002; House and Keeling, 2011; Keeling, 1999) have been a popular and fruitful approach to this question. Derived from the Kolmogorov equations and exact in their unclosed form (Taylor et al., 2012), pairwise

models consider the evolution of not just the expected number of nodes in a given state, but also pairs and triples of nodes. The dynamical variables are of the form $[A]$ (the expected number of nodes in state A), $[AB]$ (the expected number of pairs in state $A-B$), and $[ABC]$ (the expected number of triples in state $A-B-C$). Higher-order groupings of nodes are also considered but rarely written, as dimension-reduction efforts often focus on approximating the expected number of triples in terms of pairs and individual nodes. Pairwise models have been successful with a variety of different network types, with models developed for networks with heterogeneous degree (Eames and Keeling, 2002), weighted networks (Rattana et al., 2013), directed networks (Sharkey et al., 2006), and networks with motifs (House et al., 2009; Keeling et al., 2016) to name a few. Moreover, pairwise models have been developed for a variety of disease natural histories, with particular focus on SIR (susceptible-infectious-recovered) and SIS (susceptible-infectious-susceptible) models.

In this chapter, we consider an SIS pairwise model for networks with heterogeneous degree. SIS dynamics are used to model diseases where no long term immunity is conferred upon recovery, leading to their frequent application to sexually transmitted infections such as chlamydia or gonorrhea (Eames and Keeling, 2002). Contact networks for diseases of this type frequently involve heterogeneity in the number of contacts for individuals, and thus node degree becomes an essential concept. The degree of a node in a network is the number of edges to which the node is connected, and thus the number of potential infectious contacts. In this way, heterogeneous networks can capture complex disease dynamics. An essential tool when working with such networks is the degree distribution, defined by p_k which is the probability a randomly selected node has degree k. The degree distribution has played an important role in dimension reduction approximations for pairwise models.

For the SIR-type diseases, accurate low-dimensional models have been derived from the pairwise family using probability generating functions (Miller et al., 2012), complete with conditions for finding the final size of the epidemic. Despite the successes of the SIR case, the dimension reduction techniques in Miller et al. (2012) do not apply to the SIS case. Instead, the development of low-dimensional models of SIS-type disease spread on networks have relied on moment closure approximations. Under the assumption of a heterogeneous network with no clustering, House and Keeling (2011) introduced an approximation reducing the system size from $\mathcal{O}(N^2)$ to $\mathcal{O}(N)$, where

N is the number of nodes in the network. Termed the compact pairwise model (CPW), it has shown good agreement with stochastic simulations despite its considerably smaller size. However, the number of model equations still grows as the maximum degree of the network, making its application challenging for large networks with significant degree heterogeneity. Perhaps the most successful model in reducing the number of equations of the CPW for SIS-type diseases is the super compact pairwise model (SCPW) (Simon and Kiss, 2016). The system consists of only four equations, with network structure being encoded to the model through the first three moments of the degree distribution. While Simon and Kiss demonstrated excellent agreement between the CPW and the SCPW, bifurcation analysis of the model and an explicit formula for the endemic steady state remain to be done.

This chapter sets out on that analysis of the SCPW model. A common point of investigation among models of SIS-type diseases is the disease-free equilibrium (DFE) that loses stability as a relevant parameter passes a critical value known as the epidemic threshold (Boguña and Pastor-Satorras, 2002; Pastor-Satorras and Vespignani, 2001, 2002). The epidemic threshold serves as a dividing point between two qualitatively different types of outbreaks. Below the epidemic threshold, any outbreak will die out; above the epidemic threshold, the system converges asymptotically to a stable equilibrium where the disease remains endemic in the population. Many studies follow the 'next generation matrix" approach for the basic reproduction number R_0 (van den Driessche and Watmough, 2002) to characterize the epidemic threshold. We follow a more conventional bifurcation analysis to derive the epidemic threshold and offer a proof that the system undergoes a transcritical bifurcation, as one might expect. Perhaps more importantly, the SCPW's small fixed number of equations presents an excellent opportunity to investigate the endemic equilibrium for SIS models on heterogeneous networks, which has been heretofore inhibited by large system size. We present a novel asymptotic approach to approximating the endemic equilibrium, leveraging the low-dimensionality of the model. Furthermore, the approximations allow us to perform a sensitivity analysis, investigating how the endemic equilibrium responds to changes in network parameters. The results presented further our understanding of the SCPW model specifically, and suggest potential new avenues in the challenging problem of analytically determining the nontrivial steady state of pairwise models of SIS-type diseases.

The chapter is structured as follows: in Section 2.2, we nondimensionalize the model and reduce the number of equations to 3 to facilitate computations. In Section 2.3, we derive the epidemic threshold and show that the system undergoes a forward transcritical bifurcation. In Section 2.4, we tackle the endemic steady state that emerges through the bifurcation. We use asymptotic methods to approximate the size of the endemic steady state under two regimes—the system near the epidemic threshold and the system far away from the epidemic threshold—and give examples of the efficacy of these approximations on prototypical networks. Finally, we examine the implications of these two approximations. In line with existing studies (Eames and Keeling, 2002), we find that control measures for reducing the prevalence at the endemic equilibrium may require different tactics depending on the regime.

2.2. Model

Pairwise models of SIS-type diseases provide a network-based analog of the classical SIS model (Diekmann and Heesterbeek, 2000).The essential characteristics of pairwise models of SIS epidemics are dynamical equations for not just the expected number of nodes in each state, but also pairs and triples of nodes. At the node level, $[S]$ and $[I]$ are the expected number of susceptible and infectious nodes respectively. At the pair level, $[SI]$ is the expected number of connected pairs of susceptible and infectious nodes, while $[SS]$ and $[II]$ are the expected numbers of connected susceptible-susceptible and infectious-infectious pairs respectively. The full pairwise model (Eames and Keeling, 2002) further requires equations for the expected number of triples ($[SSI]$ and $[ISI]$) and higher motifs as well:

$$
\begin{aligned}
\dot{[S]} &= \gamma[I] - \beta[SI], \\
\dot{[I]} &= \beta[SI] - \gamma[I], \\
\dot{[SI]} &= \gamma([II] - [SI]) + \beta([SSI] - [ISI] - [SI]), \\
\dot{[SS]} &= 2\gamma[SI] - 2\beta[SSI], \\
\dot{[II]} &= -2\gamma[II] + 2\beta([ISI] + [SI]).
\end{aligned}
$$

The CPW closes the system by approximating the expected number of triples as

$$[ASI] \approx [AS][SI]\frac{S_2 - S_1}{S_1^2},$$

where $A \in \{S, I\}$ and S_1 and S_2 are the first and second moments of the distribution of susceptible nodes; that is

$$S_1 = \sum_k k[S_k] = [SS] + [SI], \quad S_2 = \sum_k k^2[S_k],$$

where $[S_k]$ is the expected number of susceptible nodes with degree k. Unfortunately S_2 cannot be expressed exactly in terms of $[S], [I], [SI], [SS]$, and $[II]$ only, so the SCPW model offers an approximation that depends on these variables and moments of the degree distribution.

The SCPW model derived in Simon and Kiss (2016) is given as

$$[\dot{S}] = \gamma[I] - \beta[SI], \tag{2.1}$$

$$[\dot{I}] = \beta[SI] - \gamma[I] \tag{2.2}$$

$$[\dot{SI}] = \gamma([II] - [SI]) - \beta[SI] + \beta[SI]([SS] - [SI])Q, \tag{2.3}$$

$$[\dot{SS}] = 2\gamma[SI] - 2\beta[SI][SS]Q, \tag{2.4}$$

$$[\dot{II}] = -2\gamma[II] + 2\beta[SI] + 2\beta[SI]^2Q, \tag{2.5}$$

where

$$Q = \frac{1}{n_S[S]}\left(\frac{\langle k^2\rangle(\langle k^2\rangle - \langle k\rangle n_S) + \langle k^3\rangle(n_S - \langle k\rangle)}{n_S(\langle k^2\rangle - \langle k\rangle^2)} - 1\right), \; n_S = \frac{[SI] + [SS]}{[S]},$$

$\langle k^n\rangle$ is the nth moment of the degree distribution, β is the transmission rate, and γ is the recovery rate. Here, the quantity Q serves as an approximation of $(S_2 - S_1)/S_1^2$. As well, the quantities $[S], [I], [SI], [SS], [II]$ satisfy conservation equations

$$[S] + [I] = N, \tag{2.6}$$

$$2[SI] + [SS] + [II] = \langle k\rangle N. \tag{2.7}$$

We note that $\langle k\rangle N$ is twice the number of edges, and in (2.7) the term $2[SI]$ accounts for both $S - I$ and $I - S$ pairs. With the goal of performing bifurcation and asymptotic analyses in mind, nondimensionalizing the SCPW model is a natural first step. To do so, we will rearrange

the equations (2.3)-(2.5) so that the network parameters $\langle k\rangle, \langle k^2\rangle, \langle k^3\rangle$ are consolidated into more workable constants. First, we rewrite Q as

$$Q = \frac{\alpha[S]}{([SI]+[SS])^2} + \frac{\tilde{\beta}}{[SI]+[SS]}, \tag{2.8}$$

where

$$\alpha = \frac{\langle k^2\rangle^2 - \langle k\rangle\langle k^3\rangle}{\langle k^2\rangle - \langle k\rangle^2}, \quad \tilde{\beta} = \frac{\langle k^3\rangle - \langle k^2\rangle\langle k\rangle}{\langle k^2\rangle - \langle k\rangle^2} - 1. \tag{2.9}$$

A natural nondimensionalization of this system is to scale the number of nodes and links in each state to the proportion of nodes and pairs in each state: $v = [S]/N, w = [I]/N, x = [SI]/(\langle k\rangle N), y = [SS]/(\langle k\rangle N), z = [II]/(\langle k\rangle N)$. As well, a natural rescaling of time is $T = t/\gamma$, which prompts the defining of the transmission-recovery rate ratio $\delta = \beta/\gamma$. The introduction of δ consolidates the two epidemiological parameters β and γ into a single nondimensional parameter, so any changes to epidemiology of the disease will be captured in δ alone. With these substitutions, the system (2.1)-(2.5) becomes

$$\dot{v} = w - \langle k\rangle\delta x, \tag{2.10}$$

$$\dot{w} = \langle k\rangle\delta x - w, \tag{2.11}$$

$$\dot{x} = z - (\delta+1)\,x + \frac{\alpha\delta}{\langle k\rangle}\cdot\frac{vx(y-x)}{(x+y)^2} + \tilde{\beta}\delta\cdot\frac{x(y-x)}{x+y}, \tag{2.12}$$

$$\dot{y} = 2x - \frac{2\alpha\delta}{\langle k\rangle}\cdot\frac{vxy}{(x+y)^2} - 2\tilde{\beta}\delta\cdot\frac{xy}{x+y}, \tag{2.13}$$

$$\dot{z} = -2z + 2\delta x + \frac{2\alpha\delta}{\langle k\rangle}\cdot\frac{vx^2}{(x+y)^2} + 2\tilde{\beta}\delta\cdot\frac{x^2}{x+y}, \tag{2.14}$$

where the dot notation is defined to represent the derivative with respect to the nondimensional time variable $\frac{d}{dT}$. The conservation equations (2.6) and (2.7) become

$$v + w = 1, \tag{2.15}$$

$$2x + y + z = 1, \tag{2.16}$$

respectively.

At this point, the conservation equations can be used to reduce the system to 3 equations. However, the elimination of different equations for different analyses will be convenient. For characterizing the bifurcation undergone by the disease-free equilibrium (DFE), it is convenient to work with variables that are 0 at the DFE. For approximating the endemic steady state using asymptotic methods, the most parsimonious equations will make the algebraic manipulation required easier. Thus, we will work with slightly different (but equivalent) characterizations of (2.10)-(2.14) in the sections that follow.

2.3. Epidemic Threshold

To derive the epidemic threshold, we consider the stability of the DFE in terms of the epidemiological parameter δ. We will show that as δ increases through a critical value δ_c, the DFE loses stability. Typically as the DFE loses stability, an asymptotically stable endemic equilibrium emerges. The SCPW is no exception, and here we derive the epidemic threshold, with a proof that the system undergoes a transcritical bifurcation (and thus an endemic equilibrium emerges) when $\delta = \delta_c$ included in Appendix Section 2.5.1.

First, we use the conservation equations (2.15) and (2.16) to eliminate equations (2.10) and (2.13). The resulting system is

$$\dot{w} = \langle k \rangle \delta x - w, \tag{2.17}$$

$$\dot{x} = z - (\delta + 1)\, x + \frac{\alpha\delta}{\langle k \rangle} \cdot \frac{(1-w)x(1-3x-z)}{(1-x-z)^2} + \tilde{\beta}\delta \cdot \frac{x(1-3x-z)}{1-x-z}, \tag{2.18}$$

$$\dot{z} = -2z + 2\delta x + \frac{2\alpha\delta}{\langle k \rangle} \cdot \frac{(1-w)x^2}{(1-x-z)^2} + 2\tilde{\beta}\delta \cdot \frac{x^2}{1-x-z}. \tag{2.19}$$

Though ostensibly a messier choice of equation reduction, we note that at the DFE, $[I] = [SI] = [II] = 0$, so $w = x = z = 0$. The notation

$$\dot{\mathbf{x}} = \begin{bmatrix} \dot{w} \\ \dot{x} \\ \dot{z} \end{bmatrix} = \begin{bmatrix} F_1(w,x,z) \\ F_2(w,x,z) \\ F_3(w,x,z) \end{bmatrix} = \mathbf{F}(\mathbf{x}) \tag{2.20}$$

will be convenient moving forward. To determine the stability of the DFE, we compute the Jacobian at $\mathbf{x} = \bar{0}$:

$$D\mathbf{F} = \begin{bmatrix} -1 & \langle k \rangle \delta & 0 \\ 0 & \left(\frac{\alpha}{\langle k \rangle} + \tilde{\beta} \right) \delta - (\delta + 1) & 1 \\ 0 & 2\delta & -2 \end{bmatrix}. \tag{2.21}$$

A straightforward computation shows that

$$\frac{\alpha}{\langle k \rangle} + \tilde{\beta} = \frac{\langle k^2 \rangle - \langle k \rangle}{\langle k \rangle} = \bar{k}. \tag{2.22}$$

We can write $D\mathbf{F}$ as a block triangular matrix as

$$D\mathbf{F} = \begin{bmatrix} -1 & A \\ 0 & B \end{bmatrix},$$

where the dimensions A and B respectively are 1×2 and 2×2. The properties of determinants of block matrices tell us that the eigenvalues of $D\mathbf{F}$ are -1 and the eigenvalues of B, which will determine the stability of the DFE.

We appeal here to the trace-determinant theorem, which tells us the eigenvalues ξ of the 2×2 matrix B are given by

$$\xi = \frac{\mathrm{Tr}(B)}{2} \pm \frac{\sqrt{(\mathrm{Tr}(B))^2 - 4\,\mathrm{Det}(B)}}{2}.$$

First, we observe that these eigenvalues are real, as

$$\mathrm{Tr}(B)^2 - 4\,\mathrm{Det}(B) = (\delta(\bar{k} - 1) + 1)^2 + 8\delta, \tag{2.23}$$

which is clearly positive. As a consequence, for the DFE to be stable we must have $\mathrm{Tr}(B) < 0$ and $\mathrm{Det}(B) > 0$. The determinant can be written

$$\mathrm{Det}(B) = 2(1 - \delta\bar{k}), \tag{2.24}$$

and is thus positive if and only if $\delta < 1/\bar{k}$. Moreover, if $\delta < 1/\bar{k}$, then

$$\mathrm{Tr}(B) < (\bar{k} - 1)/\bar{k} - 3 = -2 - 1/\bar{k} < 0.$$

Therefore, we conclude that the DFE is stable for $\delta < 1/\bar{k}$ and unstable for $\delta > 1/\bar{k}$. Thus, the epidemic threshold is the critical value of the bifurcation parameter δ :

$$\delta_c = \frac{1}{\bar{k}} = \frac{\langle k \rangle}{\langle k^2 \rangle - \langle k \rangle}. \tag{2.25}$$

Notably, this threshold value is identical to that of the CPW as shown in Kiss et al. (2017). However the type of bifurcation that occurs here remains to be shown, and also that an asymptotically stable endemic steady state emerges. To prove this, we apply a theorem of Castillo-Chavez et al. (2004) in Appendix Section 2.5.1. We note that both the CPW and SCPW models are approximations to the true SIS dynamics on a network, so while (2.25) is a good approximation of the true epidemic threshold, it may not be appropriate in some cases. For instance, (2.25) is greater than zero for networks with a power law degree distribution ($p_k \sim k^{-d}$) with $d > 3$ in the large network limit ($N \to \infty$). However, exact results show that the true epidemic threshold is zero in the large network limit (Chatterjee and Durrett, 2009).

2.4. The Endemic Equilibrium

With the existence of an endemic steady state established, we turn to the question of finding an approximate analytic expression. In general, this is a difficult proposition with epidemic models on networks owing to the frequently high-dimensional nature of the dynamical systems. An exact closed-form expression for the endemic equilibrium of the SCPW model requires solving a system of polynomial equations in multiple variables, which we do not attempt here. However, with asymptotic techniques, a workable approximation can be derived for two cases of δ: near the epidemic threshold ($\delta \approx \delta_c$), and far away from it ($\delta >> \delta_c$). We do not have a good approximation in the intermediate case. Two challenges are apparent. First, how to eliminate equations to facilitate asymptotic expansions of the equilibrium and second, the choice of small nondimensional parameter in each case.

Unlike in Section 2.3, the most parsimonious characterization of (2.10)-(2.14) is desirable. So we eliminate (2.11) and (2.14) with the conservation equations. To promote the finding of a small nondimensional parameter, we rewrite the resulting system using $\delta = \delta_c \cdot \frac{\delta}{\delta_c}$ and incorporate the

constants $\sigma = \langle k \rangle \delta_c$, $\lambda = \alpha \delta_c / \langle k \rangle$, $\mu = \tilde{\beta} \delta_c$. With these substitutions, the system becomes

$$\dot{v} = 1 - v - \sigma \frac{\delta}{\delta_c} x, \tag{2.26}$$

$$\dot{x} = 1 - y - \left(3 + \delta_c \frac{\delta}{\delta_c} \right) x + \lambda \frac{\delta}{\delta_c} \frac{vx(y-x)}{(x+y)^2} + \mu \frac{\delta}{\delta_c} \frac{x(y-x)}{x+y}, \tag{2.27}$$

$$\dot{y} = 2x - 2\lambda \frac{\delta}{\delta_c} \frac{vxy}{(x+y)^2} - 2\mu \frac{\delta}{\delta_c} \frac{xy}{x+y}. \tag{2.28}$$

At the endemic equilibrium, $\dot{v} = \dot{x} = \dot{y} = 0$. We can solve (2.26) for v and substitute into (2.27) and (2.28). With some rearrangement of terms and a little algebra (and adding (2.28) to (2.27)) we arrive at the system of polynomial equations that determines the endemic steady state:

$$\begin{aligned} 0 = &\left(\frac{\delta_c}{\delta} \right)^2 (1 - y - 2x)(x+y)^2 - \frac{\delta_c}{\delta} \left(\delta_c x (x+y)^2 + \lambda x^2 + \mu x (x+y) \right) \\ &+ \lambda \sigma x^3 = P(x, y), \end{aligned} \tag{2.29}$$

$$0 = \left(\frac{\delta_c}{\delta} \right)^2 (x+y)^2 - \frac{\delta_c}{\delta} \left(\lambda y + \mu y (x+y) \right) + \lambda \sigma x y = Q(x, y). \tag{2.30}$$

Note that in (2.30), we have dropped a factor of x that corresponds to the DFE. For the endemic steady state, we are interested in knowing the prevalence when the system is at equilibrium: w^*. We use the following procedure to approximate the solution:

(1) Express δ_c / δ in terms of a small parameter.

(2) Use the Implicit Function Theorem to linearize $P(x, y) = 0$ as

$$y \approx \tilde{y} - \frac{P_x(\tilde{x}, \tilde{y})}{P_y(\tilde{x}, \tilde{y})} (x - \tilde{x})$$

around a point $(\tilde{x}, \tilde{y})$ that is mathematically and/or biologically justified for the given regime.

(3) Expand x, y, and other relevant quantities in terms of the small parameter.

(4) Substitute the expansions into $Q(x, y) = 0$ and obtain a regular perturbation problem and find an asymptotic solution for the equilibrium value x, which approximates x^*.

(5) Apply the relation $w^* = (\delta_c / \delta)^{-1} \sigma x^*$ to obtain an asymptotic series for the prevalence at the endemic equilibrium.

We describe the results of this procedure for each case in the remainder of this section—the details of the computations are included in Appendix Section 2.5.2.

2.4.1. Case 1: Near the epidemic threshold ($\delta \approx \delta_c$). When $\delta \approx \delta_c$, an endemic steady state has just emerged, so we can view this equilibrium as a small perturbation to the steady state $x = 0$, $y = 1$. Therefore we set $\eta = 1 - \delta_c/\delta$ as a small parameter. In terms of this small parameter, (2.29) and (2.30) become

$$\begin{aligned} 0 = {} & (1-\eta)^2(1-y-2x)(x+y)^2 \\ & - (1-\eta)\left(\delta_c x(x+y)^2 + \lambda x^2 + \mu x^2(x+y)\right) + \lambda\sigma x^3, \end{aligned} \tag{2.31}$$

$$0 = (1-\eta)^2(x+y)^2 - (1-\eta)\left(\lambda y + \mu y(x+y)\right) + \lambda\sigma xy. \tag{2.32}$$

Linearizing $P(x, y) = 0$ about this point gives

$$y \approx 1 - \left(2 + \frac{\delta_c}{1-\eta}\right) x. \tag{2.33}$$

Expanding

$$2 + \frac{\delta_c}{1-\eta} = 2 + \delta_c(1 + \eta + \eta^2 + \mathcal{O}(\eta^3)), \tag{2.34}$$

$$x^* = x_0 + x_1\eta + x_2\eta^2 + \mathcal{O}(\eta^3), \tag{2.35}$$

we have

$$\begin{aligned} y \approx {} & (1 - (2+\delta_c)x_0) - (\delta_c x_0 + (2+\delta_c)x_1)\eta \\ & - (\delta_c x_0 + (2+\delta_c)x_2 + \delta_c x_1)\eta^2 + \mathcal{O}(\eta^3). \end{aligned} \tag{2.36}$$

Substituting into (2.32) and equating coefficients to 0, we find an η-order expansion of the approximate equilibrium value x^* as

$$x^* \approx \frac{1}{\lambda\sigma + \mu\delta_c + \mu - \delta_c}\eta + \mathcal{O}(\eta^2). \tag{2.37}$$

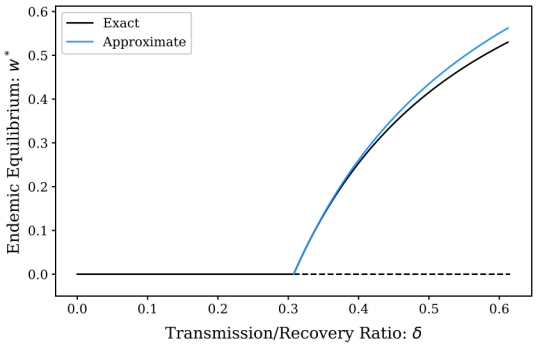

(a)

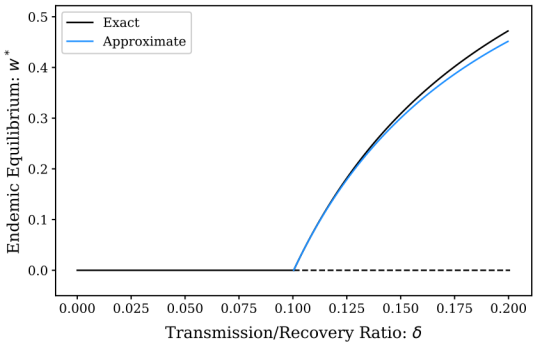

(b)

FIGURE 2.1. Exact (numerical) and approximate endemic equilibrium prevalence in the $\delta \approx \delta_c$ regime for (a) a bimodal (two degree) network with 5000 degree 3 nodes and 5000 degree 5 nodes and (b) a configuration-model network with a Poisson degree distribution with $10,000$ nodes and $\langle k \rangle = 10$. Moments of the degree distribution for the bimodal network (a) are $\langle k \rangle = 4, \langle k^2 \rangle = 17, \langle k^3 \rangle = 76$, with $\delta_c = 0.31$, and higher moments of the degree distribution for the Poisson network (b) are $\langle k^2 \rangle \approx 110, \langle k^3 \rangle \approx 1309$, with $\delta_c = 0.1$. Solid lines denote stable equilibria, while dashed lines denote unstable. The equilibrium with $w^* = 0$ is the DFE.

Using the relation $w^* = \frac{\sigma}{1-\eta} x^* = \sigma x^* + \mathcal{O}(\eta)$, we have

$$w^* \approx \frac{\sigma}{\lambda\sigma + \mu\delta_c + \mu - \delta_c}\eta + \mathcal{O}(\eta^2). \tag{2.38}$$

To demonstrate the efficacy of this approximation, we compare the approximation (2.38) to the actual endemic equilibrium using bifurcation diagrams (Fig. 2.1). We consider two example configuration model random networks (Molloy and Reed, 1995) with $N = 10,000$. In Figure 2.1a,

a bimodal (two degree) network is considered with 5000 degree 3 nodes and 5000 degree 5 nodes. In Figure 2.1b, a network with a Poisson degree distribution (with average degree $\langle k \rangle = 10$) is considered. As is clear in both examples, the agreement between the actual and approximate endemic equilibrium is quite good near the epidemic threshold. Interestingly, the approximate value of w^* is greater than the exact value for the bimodal network and less than the exact value for the Poisson network. We suspect that this is due to network structure and higher order terms in the asymptotic expansion, which we have not computed. An analogous situation is found in the $\delta >> \delta_c$ case.

2.4.2. Case 2: Far away from the epidemic threshold ($\delta >> \delta_c$). For $\delta >> \delta_c$, when the system is far from the epidemic threshold, our small parameter of choice is $\varepsilon = \delta_c/\delta$. We can rewrite (2.29) and (2.30) in terms of this parameter:

$$\begin{aligned} 0 &= \varepsilon^2(1-y-2x)(x+y)^2 \\ &\quad - \varepsilon\left(\delta_c x(x+y)^2 + \lambda x^2 + \mu x^2(x+y)\right) + \lambda\sigma x^3, \end{aligned} \tag{2.39}$$

$$0 = \varepsilon^2(x+y)^2 - \varepsilon\left(\lambda y + \mu y(x+y)\right) + \lambda\sigma xy. \tag{2.40}$$

When $\delta >> \delta_c$, the transmission rate β is large relative to the recovery rate γ. Thus, we expect the disease to affect much of the population, and consequently there will be very few remaining $[SS]$ links, and therefore $y \approx 0$.

Solving $P(\phi, 0) = 0$ for ϕ yields

$$\phi(\varepsilon) = \frac{\varepsilon^2 - \lambda\varepsilon}{2\varepsilon^2 + (\delta_c + \mu)\varepsilon - \lambda\sigma}, \tag{2.41}$$

and slope of the linearization is then

$$\psi(\varepsilon) = -\frac{P_x(\phi, 0)}{P_y(\phi, 0)} = -\frac{(\varepsilon - \lambda)(2\varepsilon^2 + (\delta_c + \mu)\varepsilon - \lambda\sigma)}{\varepsilon(\varepsilon^2 - (\mu + 5\lambda)\varepsilon - \lambda(2\delta_c + \mu - 2\sigma))}, \tag{2.42}$$

so

$$y \approx \psi(x - \phi). \tag{2.43}$$

Next, we seek to expand y in terms of ε only. The relevant expansions for ϕ, ψ, and x are

$$\phi(\varepsilon) = \frac{1}{\sigma}\varepsilon + \frac{\delta_c + \mu - \sigma}{\lambda\sigma^2}\varepsilon^2 + \mathcal{O}(\varepsilon^3), \tag{2.44}$$

$$\psi(\varepsilon) = \frac{\lambda\sigma}{2\delta_c + \mu - 2\sigma}\varepsilon^{-1} - \frac{2\delta_c^2 + 3\delta_c\mu + \sigma(5\lambda + 2\sigma) + \mu^2}{(2\delta_c + \mu - 2\sigma)^2} + \mathcal{O}(\varepsilon), \tag{2.45}$$

$$x(\varepsilon) = x_0 + x_1\varepsilon + x_2\varepsilon^2 + \mathcal{O}(\varepsilon^2). \tag{2.46}$$

To ease the writing of coefficients, we let ϕ_α and ψ_α refer to the coefficients on ε^α for the respective series. From this, it follows that

$$\begin{aligned} y \approx\ & (\psi_{-1}x_0)\varepsilon^{-1} + (\psi_{-1}x_1 + \psi_0 x_0 - \psi_{-1}\phi_1) \\ & + (\psi_{-1}x_2 + \psi_1 x_0 + \psi_0 x_1 - \psi_{-1}\phi_2 - \psi_0\phi_1)\varepsilon + \mathcal{O}(\varepsilon^2). \end{aligned} \tag{2.47}$$

Substituting into (2.40), and equating the coefficients to 0, we find that we need the coefficients up to order ε^4 in order to find a ε^2 order expansion of the approximate equilibrium value of x^*. The result is

$$x^* \approx \frac{1}{\sigma}\varepsilon + \frac{\delta_c + \mu - \sigma}{\lambda\sigma^2}\varepsilon^2 + \mathcal{O}(\varepsilon^3). \tag{2.48}$$

Finally, as $w^* = \sigma\varepsilon^{-1}x^*$, we arrive at an $\varepsilon-$order approximation for size of the endemic steady state as

$$w^* \approx 1 + \frac{\delta_c + \mu - \sigma}{\lambda\sigma}\varepsilon + \mathcal{O}(\varepsilon^2). \tag{2.49}$$

As with the $\delta \approx \delta_c$ case, we compare the approximation (2.49) to the actual endemic equilibrium in Figure 2.2 for the same networks as previously described. Again, the agreement is quite good, even for relatively small values of δ. In this case, the approximation for the endemic equilibrium also provides an approximation to the epidemic threshold. Whether this approximation is an overestimate or underestimate of the exact threshold depends on network structure. If $\langle k^2\rangle \geq \langle k\rangle^2 + \langle k\rangle$, the approximation is an overestimate. On the other hand, if $\langle k^2\rangle < \langle k\rangle^2 + \langle k\rangle$, the approximation being an overestimate or underestimate depends on the relationship between $\langle k^3\rangle$ and the other two moments.

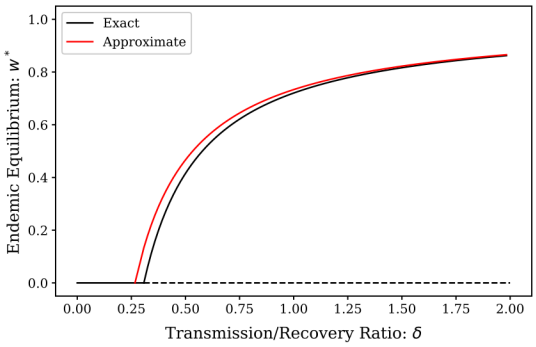

(a)

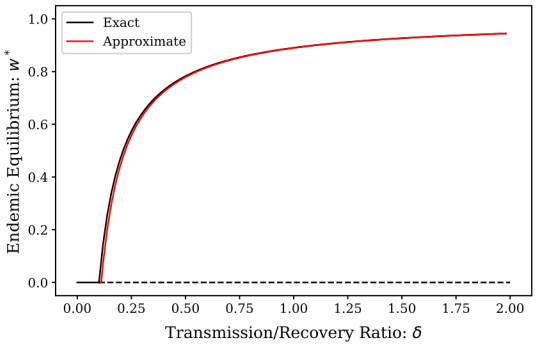

(b)

FIGURE 2.2. Exact (numerical) and approximate endemic equilibrium prevalence in the $\delta >> \delta_c$ regime for (a) a bimodal (two degree) network with 5000 degree 3 nodes and 5000 degree 5 nodes and (b) a configuration-model network with a Poisson degree distribution with $10,000$ nodes and $\langle k \rangle = 10$. Moments of the degree distribution for the bimodal network (a) are $\langle k \rangle = 4, \langle k^2 \rangle = 17, \langle k^3 \rangle = 76$, with $\delta_c = 0.31$, and higher moments of the degree distribution for the Poisson network (b) are $\langle k^2 \rangle \approx 110, \langle k^3 \rangle \approx 1309$, with $\delta_c = 0.1$. Solid lines denote stable equilibria, while dashed lines denote unstable. The equilibrium with $w^* = 0$ is the DFE.

2.4.3. Sensitivity Analysis. With any model of infectious disease, its implications in preventing or mitigating spread should be considered. For network models, some pharmaceutical and non-pharmaceutical interventions can alter the contact network structure in the effort to contain or mitigate outbreaks (Salathe and Jones, 2010). For an SIS-type disease, particularly when containment is impossible, one such goal may be to decrease the size of the endemic equilibrium. To that end, we examine the sensitivity of our approximations of w^* to network parameters in the

TABLE 2.1. Partial Derivatives for $\delta \approx \delta_c$

$\frac{\partial w^*}{\partial \langle k \rangle}_{\delta=\delta_c}$	$=$	$-\frac{\langle k^2 \rangle}{\langle k \rangle - 2\langle k^2 \rangle + \langle k^3 \rangle}$
$\frac{\partial w^*}{\partial \langle k^2 \rangle}_{\delta=\delta_c}$	$=$	$\frac{\langle k \rangle}{\langle k \rangle - 2\langle k^2 \rangle + \langle k^3 \rangle}$
$\frac{\partial w^*}{\partial \langle k^3 \rangle}_{\delta=\delta_c}$	$=$	0

SCPW model. One benefit of explicit asymptotic expressions for the endemic equilibrium is that sensitivity analyses are straightforward to implement.

For a fixed δ, we have a three-dimensional parameter space. To visualize these parameter combinations, we use two-dimensional heat maps taken at slices of the third network parameter. In this case, we have decided to look at several fixed values of $\langle k^3 \rangle$, and draw sensitivity heat maps in the variables $(\langle k \rangle, \langle k^2 \rangle)$. Further complicating matters is the fact that moments of a distribution are subject to many inequalities which restrict the domain of the sensitivity heat maps. Two natural restrictions to include are the results of Jensen's Inequality and the Cauchy-Schwarz Inequality respectively:

$$\langle k^2 \rangle \geq \langle k \rangle^2,$$

$$\langle k^2 \rangle^2 \leq \langle k^3 \rangle \langle k \rangle.$$

For a fixed value of $\langle k^3 \rangle$, these restrictions give a wedge-shaped feasible region of $(\langle k \rangle, \langle k^2 \rangle)$. We plot the sensitivities for $\langle k^3 \rangle = 20, 100,$ and 400 to display a range of possible parameter combinations.

In the $\delta \approx \delta_c$ case, calculating the partial derivatives is straightforward. To compute the sensitivities, we evaluate the partial derivatives at the epidemic threshold: $\delta = \delta_c$. Table 2.1 shows the expressions for these sensitivities, and Figure 2.3 shows corresponding plots. Clearly $\frac{\partial w^*}{\partial \langle k \rangle} \leq 0$ and $\frac{\partial w^*}{\partial \langle k^2 \rangle} \geq 0$, with more extreme values near the upper-right corner of the feasible region.

For the $\delta >> \delta_c$ case, the partial derivatives (Table 2.2) all depend on a factor of $1/\delta$, so the choice of δ for computing sensitivities does not affect the relative magnitudes of the partial

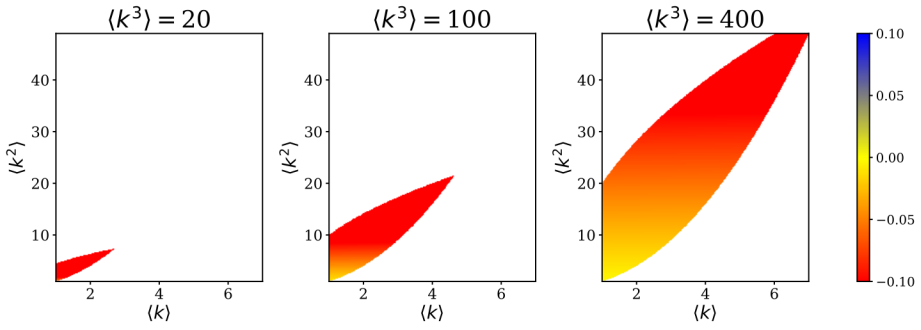

(a)

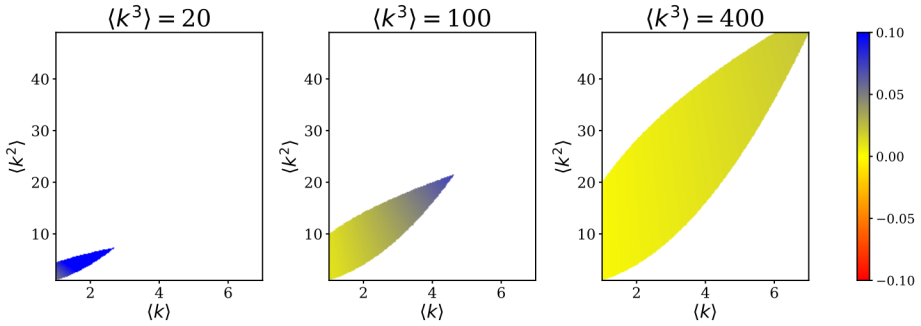

(b)

FIGURE 2.3. Sensitivities (a) $\frac{\partial w^*}{\partial \langle k \rangle}$ and (b) $\frac{\partial w^*}{\partial \langle k^2 \rangle}$ for the $\delta \approx \delta_c$ approximation. White denotes regions of the $(\langle k \rangle, \langle k^2 \rangle)$ plane outside of the feasible region. Sensitivities are evaluated at $\delta = \delta_c$.

TABLE 2.2. Partial Derivatives for $\delta >> \delta_c$

$$\frac{\partial w^*}{\partial \langle k \rangle} = \frac{\langle k^3 \rangle^2 + 3\langle k \rangle^2 \langle k^2 \rangle^2 - 2(\langle k \rangle^3 \langle k^3 \rangle + \langle k^2 \rangle^3)}{(\langle k^2 \rangle^2 - \langle k^3 \rangle \langle k \rangle)^2} \frac{1}{\delta}$$

$$\frac{\partial w^*}{\partial \langle k^2 \rangle} = -\frac{2(\langle k \rangle^2 - \langle k^2 \rangle)(\langle k \rangle \langle k^2 \rangle - \langle k^3 \rangle)}{(\langle k^2 \rangle^2 - \langle k^3 \rangle \langle k \rangle)^2} \frac{1}{\delta}$$

$$\frac{\partial w^*}{\partial \langle k^3 \rangle} = \frac{(\langle k \rangle^2 - \langle k^2 \rangle)^2}{(\langle k^2 \rangle^2 - \langle k^3 \rangle \langle k \rangle)^2} \frac{1}{\delta}$$

derivatives. For convenience, we select $\delta = 1.5$. The sensitivity plots in Figure 2.4 show that $\frac{\partial w^*}{\partial \langle k \rangle} \geq 0$, $\frac{\partial w^*}{\partial \langle k^2 \rangle} \leq 0$, and $\frac{\partial w^*}{\partial \langle k^3 \rangle} \geq 0$, with the greatest sensitivity near the curve $\langle k^2 \rangle^2 = \langle k^3 \rangle \langle k \rangle$, though the large magnitude appears to be due to the partial derivatives being undefined there.

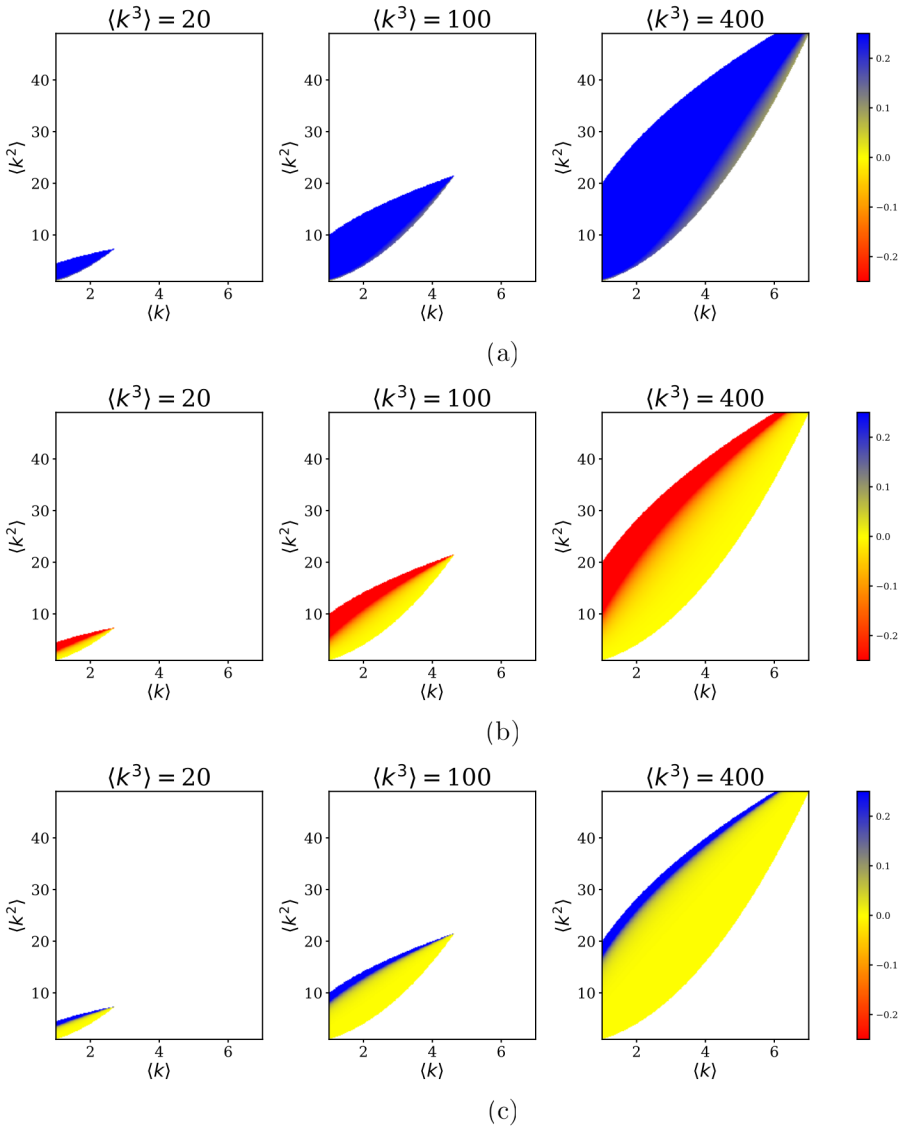

FIGURE 2.4. Sensitivities (a) $\frac{\partial w^*}{\partial \langle k\rangle}$, (b) $\frac{\partial w^*}{\partial \langle k^2\rangle}$, and (c) $\frac{\partial w^*}{\partial \langle k^3\rangle}$ for the $\delta >> \delta_c$ approximation. White denotes regions of the $(\langle k\rangle, \langle k^2\rangle)$ plane outside of the feasible region. Sensitivities are evaluated at $\delta = 5\delta_c$.

A significant observation from these sensitivities is that $\frac{\partial w^*}{\partial \langle k\rangle}$ and $\frac{\partial w^*}{\partial \langle k^2\rangle}$ change signs depending on the regime considered. If the goal of an intervention is to reduce the size of the endemic equilibrium, near the epidemic threshold, this can be accomplished in principle by increasing $\langle k\rangle$ or decreasing $\langle k^2\rangle$, which will in effect increase δ_c as well. This is intuitive, as an effort to push the system below the epidemic threshold would also decrease the endemic equilibrium for a fixed

δ. However, in the $\delta >> \delta_c$ regime, the system is far from the epidemic threshold, and reducing the size of the endemic equilibrium can be accomplished by decreasing $\langle k \rangle$ or increasing $\langle k^2 \rangle$. This suggests that containment and mitigation strategies that depend on altering the structure of the contact network may require different goals in terms of the moments of the degree distribution.

2.5. Discussion

In this chapter, we have analyzed the super compact pairwise model presented in Simon and Kiss (2016). A non-dimensional version of the model was considered, and a bifurcation analysis was performed demonstrating that the SCPW and CPW models share an epidemic threshold. Moreover, we derived approximate formulas for the endemic equilibrium in two regimes: when the transmission/recovery ratio is near the epidemic threshold, and far away from it. While the asymptotic techniques used here are ad hoc, similar techniques may prove fruitful in other low-dimensional models of infectious disease spread on networks. However, an exact expression for the endemic equilibrium remains elusive.

Before explaining the advantages of our approach, we acknowledge two limitations of our approximation. First, approximations of the endemic equilibrium for diseases between the two regimes is lacking. Second, while the examples of simulated networks show good agreement between the exact and approximate prevalence, we have not quantified the approximation error generally. As such, there may be types of networks for which our approximation of the endemic equilibrium is less accurate or inappropriate.

Our approximation of the endemic equilibrium is very useful in providing a more detailed look into the interactions of the moments of the degree distribution as they relate to the size of an outbreak. This has implications for disease control measures, particularly those that work by altering the contact network structure. Our results suggest that for SIS-type diseases, strategies to contain (near the epidemic threshold) or mitigate (far away from the epidemic threshold) an outbreak may require different goals. In the mitigation scenario where the prevalence is high, measures might be employed that decrease the first moment $\langle k \rangle$ of the degree distribution. In effect, this may mean initiatives aimed at reducing the number of contacts of individuals alone. On the other hand, in the containment scenario where the prevalence is low, decreasing the second moment

$\langle k^2 \rangle$ may be efficient. When couched in degree distribution terms this goal is hard to conceptualize, but using probability generating functions (Newman et al., 2001) one can show that $\langle k^2 \rangle$ is the average number of first and second neighbors of nodes in the network. Thus, measures that reduce both the contacts of individuals and their partners are effective in this scenario. This suggests the importance of contact tracing. We note that the sensitivities also suggest that increasing $\langle k^2 \rangle$ in the high prevalence case and increasing $\langle k \rangle$ in the low prevalence case may lead to a reduction of the size of the endemic equilibrium, though it is not clear why from a biological perspective.

Our results complement the findings of Eames and Keeling (2002), who observed that the effectiveness of two common control measures, screening and contact tracing, depend on the prevalence at the endemic equilibrium. Screening, which targets and treats individuals, is efficient when the prevalence is high. Contact tracing, which targets and treats individuals and their partners, if efficient when the prevalence is low. Unlike this chapter, Eames and Keeling implement these measures through epidemiological parameters (rather than through changing network structure). In this way, our results can be viewed as a network-structure analog for their conclusions and confirm that control measures appropriate in a network setting can be found. Further work in this area may include investigating this phenomenon with alternative models of SIS diseases on networks.

Appendix

2.5.1. Bifurcation Analysis. We begin with Theorem 4.1 from Castillo-Chavez et al. (2004), referring to the specific conditions that will be relevant for this analysis. Consider a system of ODEs with a parameter ϕ :

$$\frac{dx}{dt} = \mathbf{F}(x, \phi), \qquad \mathbf{F} : \mathbb{R}^n \times \mathbb{R} \to \mathbb{R}^n \text{ and } \mathbf{F} \in C^2(\mathbb{R}^n \times \mathbb{R}). \tag{2.50}$$

Assume that 0 is an equilibrium for all values of ϕ. Assume further that $D_x f(0, 0) = \left(\frac{\partial F_i}{\partial x_j}(0, 0) \right)$ is the linearization matrix of (2.50) around the equilibrium 0 and with $\phi = 0$, and zero is a simple eigenvalue of this matrix with all other eigenvalues having negative real parts. Assume as well that this matrix has a nonnegative right eigenvector $\mathbf{w}$ and left eigenvector $\mathbf{v}$ corresponding to the zero

eigenvalue. Let F_k be the kth component of f and

$$a = \sum_{k,i,j=1}^{n} v_k w_i w_j \frac{\partial^2 F_k}{\partial x_i \partial x_j}(0,0). \tag{2.51}$$

$$b = \sum_{k,i=1}^{n} v_k w_i \frac{\partial^2 F_k}{\partial x_i \partial \phi}(0,0). \tag{2.52}$$

If $a < 0$ and $b > 0$, then when ϕ changes from negative to positive, 0 changes its stability from stable to unstable. Correspondingly, a negative unstable equilibrium becomes positive and locally asymptotically stable.

We apply this theorem to (2.17) – (2.19), where the equilibrium occurs at $w = x = z = 0$. Moreover, we define a bifurcation parameter $\phi = \delta - \delta_c$, so $\phi = 0$ corresponds to $\delta = \delta_c$, and $\frac{\partial}{\partial \phi} = \frac{\partial}{\partial \delta}$. For consistency with previously established notation, we will treat δ as our parameter, with ϕ increasing through 0 as δ increases through δ_c. The Jacobian given in (2.21) when $w = 0, x = 0, z = 0$, and $\delta = \delta_c$ is

$$J = \begin{bmatrix} -1 & \langle k \rangle \delta_c & 0 \\ 0 & -\delta_c & 1 \\ 0 & 2\delta_c & -2 \end{bmatrix}. \tag{2.53}$$

and the characteristic polynomial is given by

$$0 = \xi(\xi + 1)(\xi - (-2 - \delta_c)). \tag{2.54}$$

The left and right eigenvectors ($\mathbf{v}$ and $\mathbf{w}$ respectively) corresponding to the eigenvalue $\xi = 0$ are

$$\mathbf{v} = \begin{bmatrix} 0 & 2 & 1 \end{bmatrix}, \mathbf{w} = \begin{bmatrix} \langle k \rangle & \delta_c^{-1} & 1 \end{bmatrix}^T. \tag{2.55}$$

To compute a and b, it is convenient to express (2.51) and (2.52) in matrix-vector form:

$$a = \mathbf{w}^T (2H_2 + H_3)\mathbf{w}, \tag{2.56}$$

$$b = \mathbf{v} \frac{\partial J}{\partial \delta}(0, \delta_c)\mathbf{w}, \tag{2.57}$$

where H_2 and H_3 are the Hessians of F_2 and F_3 respectively at $\bar{0}$. These Hessians are

$$H_2 = \begin{bmatrix} 0 & -\frac{\alpha\delta_c}{\langle k\rangle} & 0 \\ -\frac{\alpha\delta_c}{\langle k\rangle} & -2-2\tilde{\beta}\delta_c & \frac{\alpha\delta_c}{\langle k\rangle} \\ 0 & \frac{\alpha\delta_c}{\langle k\rangle} & 0 \end{bmatrix}, H_3 = \begin{bmatrix} 0 & 0 & 0 \\ 0 & 4 & 0 \\ 0 & 0 & 0 \end{bmatrix}. \tag{2.58}$$

Thus,

$$\begin{aligned} a &= \begin{bmatrix} \langle k\rangle & \delta_c^{-1} & 1 \end{bmatrix} \begin{bmatrix} 0 & -\frac{2\alpha\delta_c}{\langle k\rangle} & 0 \\ -\frac{2\alpha\delta_c}{\langle k\rangle} & -4\tilde{\beta}\delta_c & \frac{2\alpha\delta_c}{\langle k\rangle} \\ 0 & \frac{2\alpha\delta_c}{\langle k\rangle} & 0 \end{bmatrix} \begin{bmatrix} \langle k\rangle \\ \delta_c^{-1} \\ 1 \end{bmatrix} \\ &= \begin{bmatrix} \langle k\rangle & \delta_c^{-1} & 1 \end{bmatrix} \begin{bmatrix} -\frac{2\alpha}{\langle k\rangle} \\ -2\alpha\delta_c - 4\tilde{\beta} + \frac{2\alpha\delta_c}{\langle k\rangle} \\ \frac{2\alpha}{\langle k\rangle} \end{bmatrix} \\ &= -2\alpha - 2\alpha - 4\tilde{\beta}/\delta_c + 2\frac{\alpha}{\langle k\rangle} + 2\frac{\alpha}{\langle k\rangle} \\ &= -4\left(\alpha\left(\frac{1}{\langle k\rangle}+1\right) + \tilde{\beta}\left(\frac{\langle k^2\rangle}{\langle k\rangle}+1\right)\right) \\ &= -4\left(\frac{\langle k^3\rangle}{\langle k\rangle}-1\right). \end{aligned} \tag{2.59}$$

As $\langle k^3\rangle > \langle k\rangle$, it follows that $a < 0$.

The computation for b is simpler. We note that

$$\frac{\partial J}{\partial \delta}(0,\delta_c) = \begin{bmatrix} 0 & \langle k\rangle & 0 \\ 0 & \delta_c^{-1}-1 & 0 \\ 0 & 2 & 0 \end{bmatrix}. \tag{2.60}$$

Thus

$$b = \begin{bmatrix} 0 & 2 & 1 \end{bmatrix} \begin{bmatrix} 0 & \langle k \rangle & 0 \\ 0 & \delta_c^{-1} - 1 & 0 \\ 0 & 2 & 0 \end{bmatrix} \begin{bmatrix} \langle k \rangle \\ \delta_c^{-1} \\ 1 \end{bmatrix}$$

$$= \begin{bmatrix} 0 & 2 & 1 \end{bmatrix} \begin{bmatrix} 0 & \langle k \rangle \delta_c^{-1} & 0 \\ 0 & \delta_c^{-1}(\delta_c^{-1} - 1) & 0 \\ 0 & 2\delta_c^{-1} & 0 \end{bmatrix}$$

$$= 2\delta_c^{-1}(\delta_c^{-1} - 1) + 2\delta_c^{-1} = 2\delta_c^{-2} > 0. \tag{2.61}$$

Finally, as $a < 0$ and $b > 0$, we conclude that as δ increases through δ_c, a positive, asymptotically stable equilibrium emerges, which is the endemic equilibrium.

2.5.2. Asymptotic Approximations of the Endemic Equilibrium. The full derivations of the approximations (2.38) and (2.49) are presented in this appendix.

2.5.2.1. *Near the epidemic threshold ($\delta \approx \delta_c$).* We begin with (2.31) and (2.32) and seek the linear approximation of $P(x, y) = 0$ at $(0, 1)$. We compute

$$\frac{\partial P}{\partial x} = 2(1-\eta)^2 \left((1 - y - 2x)(x + y) - (x + y)^2\right)$$

$$- (1 - \eta) \left(\delta_c(x + y)(3x + y) + 2\lambda x + \mu x(3x + 2y)\right) + 3\lambda\sigma x^2, \tag{2.62}$$

$$\frac{\partial P}{\partial y} = (1 - \eta) \left(-2\delta_c x(x + y) - \mu x^2 + (1 - \eta)(x + y)(2 - 5x - 3y)\right). \tag{2.63}$$

The slope of the linear approximation is then

$$-\frac{\partial P/\partial x}{\partial P/\partial y}_{(0,1)} = -\frac{-2(1-\eta)^2 - \delta_c(1-\eta)}{-(1-\eta)^2} = -2 - \frac{\delta_c}{1-\eta}, \tag{2.64}$$

and thus we approximate

$$y \approx 1 + \left(-2 - \frac{\delta_c}{1-\eta}\right) x. \tag{2.65}$$

We now expand x as $x = x_0 + x_1\eta + \dots$ and $\frac{\delta_c}{1-\eta} = \delta_c(1 + \eta + \eta^2 + \dots)$ as a geometric series. Incorporating these with (2.65), we get the approximate expansion of y as

$$\begin{aligned} y &\approx 1 - \big(2 + \delta_c(1 + \eta + \eta^2 + \dots)\big)\,(x_0 + x_1\eta + x_2\eta^2 \dots) \\ &= 1 - (2 + \delta_c)x_0 - (\delta_c x_0 + (2 + \delta_c)x_1)\eta \\ &\qquad - (\delta_c x_0 + \delta_c x_1 + (2 + \delta_c)x_2)\eta^2 + \dots \end{aligned} \tag{2.66}$$

For easier bookkeeping, define y_α to be the coefficient of η^α in (2.66). As well, the following expansions will prove useful:

$$x^2 = x_0^2 + 2x_0x_1\eta + (x_1^2 + 2x_0x_2)\eta^2 + \dots, \tag{2.67}$$

$$y^2 = y_0^2 + 2y_0y_1\eta + (y_1^2 + 2y_0y_2)\eta^2 + \dots, \tag{2.68}$$

$$xy = x_0y_0 + (x_0y_1 + x_1y_0)\eta + (x_0y_2 + x_1y_1 + x_2y_0)\eta^2 + \dots \tag{2.69}$$

Now, we apply (2.66)-(2.69) to (2.32) yielding

$$\begin{aligned} 0 &= (1 - 2\eta + \eta^2)\,\big(x_0^2 + 2x_0y_0 + y_0^2 + 2(x_0x_1 + x_0y_1 + x_1y_0 + y_0y_1)\eta + \dots\big) \\ &\quad - (1 - \eta)\,(\lambda y_0 + \mu y_0(x_0 + y_0) + (\lambda y_1 + \mu(x_0y_1 + x_1y_0 + 2y_0y_1))\eta + \dots) \\ &\quad + \lambda\sigma\,(x_0y_0 + (x_0y_1 + x_1y_0)\eta + \dots)\,. \end{aligned} \tag{2.70}$$

Equating the $\mathcal{O}(1)$ terms to zero, we have

$$\begin{aligned}
0 &= x_0^2 + 2x_0y_0 + y_0^2 - \lambda y_0 - \mu y_0(x_0 + y_0) + \lambda\sigma x_0 y_0 \\
&= (1 - (1+\delta_c)x_0)^2 - \lambda(1 - (2+\delta_c)x_0) \\
&\quad - \mu(1 - (2+\delta_c)x_0)(1 - (1-\delta_c)x_0) \\
&\quad + \lambda\sigma x_0(1 - (2+\delta_c)x_0) \\
&= 1 - 2(1+\delta_c)x_0 + x_0^2 - \lambda + \lambda(2+\delta_c)x_0 - \mu(1 - (3+2\delta_c)x_0) \\
&\quad - \mu(1+\delta_c)(2+\delta_c)x_0^2 + \lambda\sigma x_0 - \lambda\sigma(2+\delta_c)x_0^2 \\
&= (1 - \lambda - \mu) + (\lambda\sigma + \lambda(2+\delta_c) + \mu(3+2\delta_c) - 2(1+\delta_c))\, x_0 \\
&\quad + (1 - \mu(1+\delta_c)(2+\delta_c) - \lambda\sigma(2+\delta_c))\, x_0^2 \\
&= x_0\,[\lambda\sigma + \lambda(2+\delta_c) + \mu(3+2\delta_c) - 2(1+\delta_c) \\
&\quad + (1 - \mu(1+\delta_c)(2+\delta_c) - \lambda\sigma(2+\delta_c))\, x_0]\,. \qquad (2.71)
\end{aligned}$$

where we avail ourselves of (2.22) for the last equality. For the solution were interested, we have $x_0 = 0$ and $y_0 = 1$.

We rewrite (2.70) as

$$\begin{aligned}
0 &= (1 - 2\eta + \eta^2)\,(1 + (x_1 + 2y_1)\eta + \dots) \\
&\quad - (1 - \eta)\,(\lambda + \mu + (\lambda y_1 + \mu(x_1 + 2y_1))\eta + \dots) \\
&\quad + \lambda\sigma\,(x_1\eta + \dots)\,. \qquad (2.72)
\end{aligned}$$

Equating the coefficients of the $\mathcal{O}(\eta)$ terms to zero gives

$$\begin{aligned} 0 &= -2 + 2x_1 + 2y_1 + (\lambda + \mu) - (\lambda y_1 + \mu(x_1 + 2y_1)) + \lambda\sigma x_1 \\ &= -2 + 2x_1 - 2(2 + \delta_c)x_1 + 1 + \lambda(2 + \delta_c)x_1 \\ &\quad - \mu(x_1 - 2(2 + \delta_c)x_1) + \lambda\sigma x_1 \\ &= -1 + x_1\left(2 - 2(2 + \delta_c) + \lambda(2 + \delta_c) - \mu(1 - 2(2 + \delta_c)) + \lambda\sigma\right) \\ &= -1 + x_1\left(\lambda\sigma + \mu\delta_c + \mu - \delta_c\right). \end{aligned} \tag{2.73}$$

Thus,

$$x_1 = \frac{1}{\lambda\sigma + \mu\delta_c + \mu - \delta_c}. \tag{2.74}$$

Now that we have a first order approximation of x, we obtain an first order approximation of the endemic equilibrium:

$$\begin{aligned} w^* &= \frac{\sigma}{1 - \eta}x^* \\ &= \sigma(1 + \eta + \eta^2 + \dots)(x_0 + x_1\eta + \dots) \\ &= \sigma x_1\eta + \mathcal{O}(\eta^2). \end{aligned} \tag{2.75}$$

and thus

$$w^* \approx \frac{\sigma}{\lambda\sigma + \mu\delta_c + \mu - \delta_c}\eta + \mathcal{O}(\eta^2). \tag{2.76}$$

2.5.2.2. *Far away from the epidemic threshold ($\delta >> \delta_c$).* We begin with (2.39) and (2.40) and seek the linear approximation of $P(x, y) = 0$ at $(\phi, 0)$ where ϕ is given by (2.41). We compute

$$\begin{aligned} \frac{\partial P}{\partial x} &= -2\varepsilon^2(x + y)(3x + 2y - 1) \\ &\quad - \varepsilon\left(\delta_c(3x^2 + 4xy + y^2) + 2\lambda x + \mu x(3x + 2y)\right) + 2\lambda\sigma x^2, \end{aligned} \tag{2.77}$$

$$\frac{\partial P}{\partial y} = \varepsilon\left(-2\delta_c x(x + y) - \mu x^2 - \varepsilon(x + y)(5x + 3y - 2)\right). \tag{2.78}$$

The slope of the linear approximation is then

$$
\begin{aligned}
-\frac{\partial P/\partial x}{\partial P/\partial y}_{(\phi,0)} &= \frac{-2\varepsilon^2\phi(3\phi-1)-3\varepsilon\delta_c\phi^2+3\lambda\phi+3\mu\phi^2+2\lambda\sigma\phi^2}{\varepsilon\left(-2\delta_c\phi^2-\mu\phi^2-\varepsilon\phi(5\phi-2)\right)} \\
&= \frac{-(\varepsilon^2-\varepsilon\lambda)\phi}{\phi(-\varepsilon\phi(2\delta_c+\mu)-\varepsilon^2(5\phi-2))} \\
&= \frac{-(\varepsilon-\lambda)(2\varepsilon^2+\varepsilon(\delta_c+\mu)-\lambda\sigma)}{\varepsilon\left(\varepsilon^2-\varepsilon(\mu+5\lambda)+2\lambda\sigma-\lambda(2\delta_c+\mu)\right)} = \psi(\varepsilon). \qquad (2.79)
\end{aligned}
$$

Thus, the linear approximation at $(\phi, 0)$ is

$$y \approx \psi(x-\phi). \qquad (2.80)$$

We now expand ψ and ϕ in powers of ε :

$$
\begin{aligned}
\psi(\varepsilon) &= \psi_{-1}\varepsilon^{-1}+\psi_0+\mathcal{O}(\varepsilon) \\
&= \frac{\lambda\sigma}{2\delta_c+\mu-2\sigma}\varepsilon^{-1}-\frac{2\delta_c^2+3\delta_c\mu+\sigma(5\lambda+2\sigma)+\mu^2}{(2\delta_c+\mu-2\sigma)^2}+\mathcal{O}(\varepsilon), \qquad (2.81)
\end{aligned}
$$

$$
\begin{aligned}
\phi(\varepsilon) &= \phi_1\varepsilon+\phi_2\varepsilon+\mathcal{O}(\varepsilon^3) \\
&= \frac{1}{\sigma}\varepsilon+\frac{\delta_c+\mu-\sigma}{\lambda\sigma^2}\varepsilon^2+\mathcal{O}(\varepsilon^3). \qquad (2.82)
\end{aligned}
$$

Now, we expand x as well and reorganize to express y as a power series in ε :

$$
\begin{aligned}
y &\approx \left(\psi_{-1}\varepsilon^{-1}+\psi_0+\dots\right)\left(\left(x_0+x_1\varepsilon_1+x_2\varepsilon^2+\dots\right)-\left(\phi_1\varepsilon+\phi_2\varepsilon^2+\dots\right)\right) \\
&= \psi_{-1}x_0\varepsilon^{-1}+(\psi_{-1}x_1+\psi_0x_0-\psi_{-1}\phi_1) \\
&\quad +(\psi_{-1}x_2+\psi_0x_1+\psi_1x_0-(\psi_{-1}\phi_2+\psi_0\phi_1))\,\varepsilon+\mathcal{O}(\varepsilon^2). \qquad (2.83)
\end{aligned}
$$

For easier bookkeeping, we define y_α to be the coefficient of ε^α in (2.83). Again, the following expansions will prove useful:

$$x^2 = x_0^2+2x_0x_1\varepsilon+(x_1^2+2x_0x_2)\varepsilon^2+\dots, \qquad (2.84)$$

$$y^2 = y_{-1}\varepsilon^{-2}+2y_{-1}y_0\varepsilon^{-1}+(y_0^2+2y_{-1}y_1)+\dots, \qquad (2.85)$$

$$xy = x_0y_{-1}\varepsilon^{-1}+(x_0y_0+x_1y_{-1})+(x_0y_1+x_1y_0+x_2y_{-1})\varepsilon+\dots. \qquad (2.86)$$

We now apply (2.83)-(2.86) to (2.40) and multiply by ε, yielding

$$
\begin{aligned}
0 = \varepsilon^3 \big(& y_{-1}^2 \varepsilon^{-2} + (2y_{-1}y_0 + 2x_0y_{-1})\varepsilon^{-1} \\
& + \left(x_0^2 + x_0y_0 + x_1y_{-1} + y_0^2 + 2y_{-1}y_1\right) \\
& + 2\left(x_0x_1 + x_0y_1 + x_1y_0 + x_2y_{-1} + y_{-1}y_2 + y_0y_1\right)\varepsilon + \dots \big) \\
- \varepsilon^2 \big(& \mu y_{-1}^2 \varepsilon^{-2} + (\lambda y_{-1} + \mu(x_0y_{-1} + 2y_{-1}y_0))\varepsilon^{-1} \\
& + \lambda y_0 + \mu(x_0y_0 + x_1y_{-1} + y_0^2 + 2y_{-1}y_1) \\
& + (\lambda y_1 + \mu\left(x_0y_1 + x_1y_0 + x_2y_{-1} + 2y_{-1}y_2 + 2y_0y_1\right))\varepsilon \\
& + (\lambda y_2 + \mu\left(x_0y_2 + x_1y_1 + x_2y_0 + x_3y_{-1} + y_1^2 + 2y_{-1}y_3 + 2y_0y_2\right))\varepsilon^2 \\
& + \dots \big) \\
+ \varepsilon\lambda\sigma \big(& x_0y_{-1}\varepsilon^{-1} + (x_0y_0 + x_1y_{-1}) + (x_0y_1 + x_1y_0 + x_2y_{-1})\varepsilon \\
& + (x_0y_2 + x_1y_1 + x_2y_0 + x_3y_{-1})\varepsilon^2 \\
& + (x_0y_3 + x_1y_2 + x_2y_1 + x_3y_0 + x_4y_{-1})\varepsilon^3 \dots \big) .
\end{aligned} \tag{2.87}
$$

Equating the $\mathcal{O}(1)$ terms to zero, we have

$$
0 = \lambda\sigma x_0y_{-1} - \mu y_{-1}^2 = x_0^2(\lambda\sigma\psi_{-1} - \mu\psi_{-1}^2), \tag{2.88}
$$

and thus $x_0 = y_{-1} = 0$. Equating the $\mathcal{O}(\varepsilon)$ terms to zero, we have

$$
0 = y_{-1}^2 + \lambda y_{-1} + \mu(x_0y_{-1} + 2y_{-1}y_0) + \lambda\sigma(x_0y_0 + x_1y_{-1}), \tag{2.89}
$$

which is seen to be trivially satisfied as a result of (2.88). Therefore, we look to the $\mathcal{O}(\varepsilon^2)$ terms to determine x_1. Equating those coefficients to zero leads to

$$
\begin{aligned}
0 &= 2y_{-1}y_0 + 2x_0y_{-1} - \lambda y_0 - \mu(x_0y_0 + x_1y_{-1} + y_0^2 + 2y_{-1}y_1) \\
&\quad + \lambda\sigma(x_0y_1 + x_1y_0 + x_2y_{-1}) \\
&= -\lambda y_0 - \mu y_0^2 + \lambda\sigma x_1y_0 \\
&= -\psi_{-1}(x_1 - \phi_1)(\lambda - \mu\psi_{-1}\phi_1 + (\mu\psi_{-1} - \lambda\sigma)x_1).
\end{aligned} \tag{2.90}
$$

Of the two solutions to this equation, we are interested in $x_1 = \phi_1 = 1/\sigma$, which in turn implies that $y_1 = 0$.

Looking now for x_2, we equate the $\mathcal{O}(\varepsilon^3)$ coefficients to zero:

$$\begin{aligned} 0 = {} & x_0^2 + x_0 y_0 + x_1 y_{-1} + y_0^2 + 2y_{-1}y_1 \\ & - \lambda y_1 - \mu(x_0 y_1 + x_1 y_0 + x_2 y_{-1} + 2y_{-1}y_2 + 2y_0 y_1) \\ & + (x_0 y_2 + x_1 y_1 + x_2 y_0 + x_3 y_{-1}). \end{aligned} \tag{2.91}$$

which is also trivially satisfied as all terms either cancel with another or contain a factor of x_0, y_{-1}, or y_0. Thus, we turn to $\mathcal{O}(\varepsilon^4)$ to determine x_2. Equating the coefficients to zero gives

$$\begin{aligned} 0 = {} & 2(x_0 x_1 + x_0 y_1 + x_1 y_0 + x_2 y_{-1} + y_{-1}y_2 + y_0 y_1) - \lambda y_2 \\ & - \mu\left(x_0 y_2 + x_1 y_1 + x_2 y_0 + x_3 y_{-1} + y_1^2 + 2y_{-1}y_3 + 2y_0 y_2\right) \\ & + \lambda\sigma(x_0 y_3 + x_1 y_2 + x_2 y_1 + x_3 y_0 + x_4 y_{-1}) \\ = {} & y_1(-\mu(x_1 + y_1) + \lambda\sigma x_2). \end{aligned} \tag{2.92}$$

The solution we're interested in for x_2 comes from $y_1 = 0$, which can be expressed in terms of x_2 as

$$0 = \psi_{-1}(x_2 - \phi_2), \tag{2.93}$$

and thus

$$x_2 = \phi_2 = \frac{\delta_c + \mu - \sigma}{\lambda\sigma^2}. \tag{2.94}$$

At this point, we have a second order expansion of the approximate equilibrium x^* :

$$x^* \approx \frac{1}{\sigma}\varepsilon + \frac{\delta_c + \mu - \sigma}{\lambda\sigma^2}\varepsilon^2 + \mathcal{O}(\varepsilon^3). \tag{2.95}$$

Now with the relation $w^* = \frac{\sigma}{\varepsilon}x^*$, we conclude that

$$w^* \approx 1 + \frac{\delta_c + \mu - \sigma}{\lambda\sigma}\varepsilon + \mathcal{O}(\varepsilon^2). \tag{2.96}$$

CHAPTER 3

Adaptive Network Modeling of Social Distancing Interventions

3.1. Introduction

The global COVID-19 pandemic has upended modern life an placed and enormous epidemiological, economic, and social burden on the world's resources. The gravity of events has brought the need for epidemiological modeling into sharp focus. As the pandemic spread around the world in the absence of a vaccine, non-pharmaceutical interventions including social distancing, quarantine, and lockdown measures proliferated, and bringing these interventions into modeling efforts has remained paramount.

In recent years, network-based models of epidemic spread have become an increasingly popular paradigm (Kiss et al., 2017; Pastor-Satorras et al., 2015), and network science generally has been recognized for its potential to contribute solutions to the current crisis (Eubank et al., 2020). Most network models represent individuals as nodes in a network, and their contacts as edges connecting the nodes. Moreover, many models assume that the network is static—that the edges between nodes don't change over time—and thus the epidemic spreads from node to node across these edges. Among static network models, pairwise models (Eames and Keeling, 2002; Keeling, 1999) are both frequently used and well-studied. Pairwise models track not only the number of nodes in a given state, but pairs, triples, and higher order motifs as well (Fig. 3.1). An advantage of pairwise models is that in their full form, they exactly model (in expectation) the continuous time Markov chain formulation of epidemic spread on a network (Taylor et al., 2012).

Pairwise models have been successfully applied to a number of disease natural histories and different network types. Two important network features that play a role in the theory of pairwise models are degree heterogeneity and clustering. The degree of a node in a network is the number of edges to which it is connected, and the degree distribution is the probability distribution of selecting a random node with a given degree. The degree distribution plays a fundamental role

in many network models, and is particularly powerful when described as a probability generating function. The clustering coefficient is the ratio of triangles to connected triples in the network. While clustering is an important component of network structure, it has not widely been incorporated to pairwise models. We acknowledge two major benefits of models that incorporate degree heterogeneity and clustering. First, including degree heterogeneity and/or clustering as modeling consideration affects epidemic dynamics in a nontrivial way (House and Keeling, 2011; Keeling, 1999) and second, both have been shown to be features of realistic contact networks (Read et al., 2008).

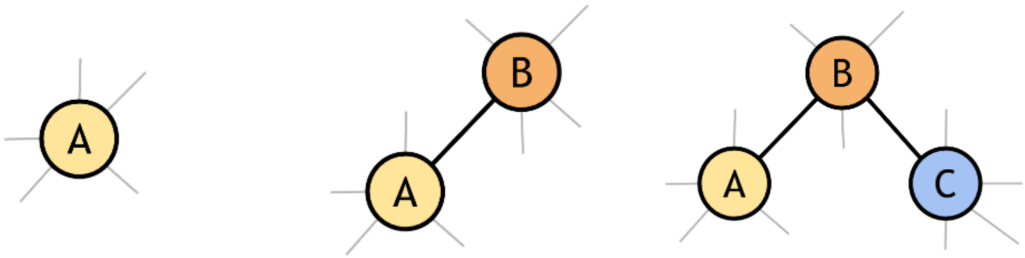

(a) (b) (c)

FIGURE 3.1. Diagrams of network structures whose evolution is modeled by the pairwise model: (a) node in state A, (b) pair in state $A-B$, (c) triple in state $A-B-C$.

Although static networks model some forms of complexity well, an important aspect of real-world contact networks is that some connections change in response to disease dynamics or public health measures. By relaxing the static network assumption, dynamic or 'adaptive" network models (Gross and Blasius, 2008) can capture both the dynamics of the network and the epidemic dynamics on the network. A number of models have been recently proposed that describe a variety of network dynamic processes. Gross et al. (2006) introduced a model of edge rewiring, where susceptible individuals break connections with infectious individuals and reconnect to susceptible individuals at random. A related model of adaptive dynamics is 'relational exchange" (Scarpino et al., 2016), where an node in contact with an infectious node are rewired to a susceptible node. Another model for network dynamics is random link addition/deletion (Kiss et al., 2012) where individuals break and form new contacts at constant rates. Their approach is notable for its intuitiveness as a simple dynamic model, and also its use of probability generating functions as a

tool to describe network dynamics. A related model is link addition/deletion on a fixed network (Shkarayev et al., 2014; Tunc et al., 2013), where individuals can temporarily deactivate contacts with infectious individuals, and reactivate them when their contact is not infectious. While much of the focus of the adaptive network literature has been involved in analyzing the resulting dynamical systems, particularly for SIS-type diseases, some works have focused specifically on the role of network dynamics in controlling or mitigating epidemic spread (Selley et al., 2015; Youssef and Scoglio, 2013).

Network models in general offer a compromise between two other common modeling techniques: compartment models and agent-based simulations. They are able to capture more complex contact structure than simple compartment models, while offering analytical tractability that many agent-based simulations lack. Despite this, models of non-pharmaceutical interventions have tended to favor simulation or compartment models (Ahmed et al., 2018; Davey et al., 2008). In the early stages of the COVID-19 pandemic, complex individual-based simulations offered major insights about the effectiveness of non-pharmaceutical interventions (Ferguson et al., 2020). However, the high computational cost can make investigating the impacts of intervention policies with a large number of parameters a challenging endeavor. Network models, especially those with a relatively small number of equations, can offer broad insights at reduced cost. While some models of social distancing have incorporated contact network structure as a major consideration (Glass et al., 2006; Valdez et al., 2012), differential equation network models of such interventions are uncommon. Adaptive network models in particular can offer a new perspective on questions surrounding social distancing and other non-pharmaceutical interventions made pressing by the COVID-19 pandemic.

In this chapter, we develop simple, novel mechanisms to incorporate social distancing into a network model of epidemic spread, using COVID-19 as the central case study to investigate the impact of a range of interventions. First, we develop a pairwise SEIR model with random link activation/deletion dynamics—that is edges are added and deleted at constant rates independent of the epidemic dynamics on the network. Furthermore, the model incorporates degree heterogeneity and clustering, which offers increased realism over simpler network or compartment models. To apply the model, we use bipartite mixing networks to generate large heterogeneous, clustered contact networks coupled with disease dynamics given by epidemiological parameters estimated

for COVID-19. Next, we develop two mechanisms of social distancing using piecewise constant link activation and deletion rates. The first is a single intervention event, where the average number of contacts decreases, is held constant, and then recovers: the second allows for multiple interventions which restart depending on the prevalence of the disease. While we investigate the implications of these policies for COVID-19 on a specific type of heterogeneous, clustered network, both the adaptive network model and the social distancing schemes are more generally applicable to a variety of networks and epidemiological parameters. Finally, we consider the public health implications of the latter model, finding that certain intervention parameters are more important than others in achieving an effective reduction in overall infections.

3.2. Model

To begin construction of the full model, we consider SEIR dynamics on a static network. Pairwise equations for an SEIR epidemic can be found in Keeling et al. (1997) and Rand (1999). Model variables include the expected number of susceptible, exposed, infectious, and recovered nodes ($[S], [E], [I]$ and $[R]$ respectively) as well as the expected number of pairs in each state. For example, $[SS]$ is the expected number of connected pairs of susceptible nodes, while $[SI]$ is the expected number of connected pairs of susceptible and infectious nodes. The expected number of connected triples is also considered ($[SSI], [ESI], [ISI]$), though differential equations for these

variables are not written. The full SEIR pairwise model is

$$[\dot{S}] = -\beta[SI], \tag{3.1}$$

$$[\dot{E}] = \beta[SI] - \eta[E], \tag{3.2}$$

$$[\dot{I}] = \eta[E] - \gamma[I], \tag{3.3}$$

$$[\dot{SS}] = -2\beta[SSI], \tag{3.4}$$

$$[\dot{SE}] = \beta[SSI] - \beta[ESI] - \eta[SE], \tag{3.5}$$

$$[\dot{SI}] = \eta[SE] - \beta[SI] - \beta[ISI] - \gamma[SI], \tag{3.6}$$

$$[\dot{EE}] = 2\beta[ESI] - 2\eta[EE], \tag{3.7}$$

$$[\dot{EI}] = \beta[ISI] + \beta[SI] + \eta[EE] - (\gamma + \eta)[EI], \tag{3.8}$$

$$[\dot{II}] = 2\eta[EI] - 2\gamma[II], \tag{3.9}$$

where β is the transmission rate, γ is the recovery rate, and η is the rate at which exposed individuals become infectious. The nodes and edges also obey conservation equations

$$N = [S] + [E] + [I] + [R] \tag{3.10}$$

and

$$\begin{aligned} \langle k \rangle N = {} & [SS] + [EE] + [II] + [RR] \\ & + 2\left([SE] + [SI] + [SR] + [EI] + [ER] + [IR]\right) \end{aligned} \tag{3.11}$$

where N is the number of nodes and $\langle k \rangle$ is the average degree of the network. We note that with the conservation equations, we do not need terms of the type $[AR]$ to determine the evolution of $[S]$, $[E]$, $[I]$, and $[R]$.

The full model requires dynamical equations for triples of the form $[ASI]$ and higher order motifs as well, leading to a system that is prohibitively large for analysis. To make the model tractable, we approximate the expected number of triples $[ASI]$ in terms of pairs and individual nodes, thus closing the system (3.1)-(3.9). An approximation of this kind is referred to as a triple closure. For

triples of the type $A - S - I$. House and Keeling (2011) give a triple closure approximation as

$$[ASI] \approx [AS][SI]\frac{\sum_k (k^2 - k)[S_k]}{\left(\sum_k k[S_k]\right)^2}\left(1 - \phi + \phi\frac{N\langle k\rangle [AI]}{\left(\sum_k k[A_k]\right)\left(\sum_k k[I_k]\right)}\right) \tag{3.12}$$

where $[A_k]$ is the expected number of nodes in state A with degree k and ϕ is the clustering coefficient. Using the network degree distribution probability generating function and introducing new dynamical variables, they develop an SIR model for heterogeneous, clustered networks. In Appendix Section 3.4.1, we derive an analogous heterogeneous, clustered SEIR model complete with link activation and deletion. However, the model complexity induced by (3.12) is not necessary to accurately capture the combined epidemic and network dynamics, and thus a simpler triple closure will suffice.

A simple yet useful assumption is that degree and state are independent, and thus $[A_k] = p_k[A]$ where p_k is the proportion of nodes with degree k. With this assumption, the resulting triple closure becomes:

$$[ASI] \approx \frac{\langle k^2 - k\rangle}{\langle k\rangle^2}\frac{[AS][SI]}{[S]}\left(1 - \phi + \phi\frac{N}{\langle k\rangle}\frac{[AI]}{[A][I]}\right), \tag{3.13}$$

where $\langle k\rangle = \sum_{k=0}^{N-1} kp_k$ and $\langle k^2 - k\rangle = \sum_{k=0}^{N-1}(k^2 - k)p_k$. We note that if a homogeneous degree distribution is assumed, the closure reduces to clustered closure from Keeling (1999).

With the static model closed, we now incorporate the effects of network dynamics. Kiss et al. (2012) introduced a simple model of network dynamics, termed random link activation/deletion (RLAD). In this model, independent of epidemic dynamics nonexistent edges are added to the network (or activated) at a constant rate α and existing edges are removed from the network (or deleted) at a constant rate ω. Ignoring epidemic spread and looking at the effects of activation/deletion only, the equation for edges of type $[AA]$ is

$$\dot{[AA]} = \alpha\left([A](|A| - 1) - [AA]\right) - \omega[AA] \tag{3.14}$$

and for type $[AB]$ we have

$$\dot{[AB]} = \alpha\left([A][B] - [AB]\right) - \omega[AB]. \tag{3.15}$$

Next, we have to consider the effect of activation/deletion on the now time-dependent network quantities: degree distribution moment terms $\langle k \rangle(t)$, $\langle k^2 - k \rangle(t)$ and the clustering coefficient $\phi(t)$. Following the example of Kiss et al. (2012), dynamical equations for the first two can be easily derived by finding the partial differential equation for the degree distribution generating function

$$g(x,t) = \sum_{k=0}^{N-1} p_k(t) x^k. \tag{3.16}$$

The Kolmogorov equations describe the evolution of $p_k(t)$, the proportion of degree k nodes at time t :

$$\dot{p_k} = \alpha\,(N-k)\,p_{k-1} - (\alpha(N-1-k) + \omega k)\,p_k + \omega(k+1)p_{k+1}. \tag{3.17}$$

With some straightforward algebra, we derive a partial differential equation for the degree distribution generating function:

$$\frac{\partial g}{\partial t} = (x-1)\left(\alpha(N-1)g - (\alpha x + \omega)\frac{\partial g}{\partial x}\right). \tag{3.18}$$

The network quantities $\langle k \rangle$ and $\langle k^2 - k \rangle$ can be computed from the generating function as $\langle k \rangle = g_x(1,t)$ and $\langle k^2 - k \rangle = g_{xx}(1,t)$. Then, from (3.18) we derive the dynamical equations

$$\langle \dot{k} \rangle = \alpha(N-1) - (\alpha + \omega)\langle k \rangle, \tag{3.19}$$

$$\langle \dot{k^2 - k} \rangle = 2\alpha(N-2)\langle k \rangle - 2(\alpha + \omega)\langle k^2 - k \rangle. \tag{3.20}$$

The clustering coefficient is defined as the ratio of triangles to connected triples in the network. To compute $\dot{\phi}$, we start with the Kolmogorov equations for $q_k(t)$, the probability that there are k triangles in the network at time t:

$$\dot{q_k} = \alpha(L - 3(k-1))q_{k-1} - (\alpha(L-3k) + 3\omega k)q_k + 3\omega(k+1)q_{k+1} \tag{3.21}$$

where $L = N\langle k^2 - k\rangle/2$ is the number of connected triples. From this we derive the differential equation for the expected number of triangles $\langle T\rangle$ as

$$\langle \dot{T}\rangle = \alpha L - 3(\alpha+\omega)\langle T\rangle, \tag{3.22}$$

and compute the equation for the clustering coefficient $\phi(t)$:

$$\dot{\phi} = 3\alpha - \left(\alpha+\omega+2\alpha(N-2)\frac{\langle k\rangle}{\langle k^2-k\rangle}\right)\phi. \tag{3.23}$$

Finally, we have a full set of equations for a pairwise SEIR for a heterogeneous, clustered network with random link activation and deletion:

$$[\dot{S}] = -\beta[SI], \tag{3.24}$$

$$[\dot{E}] = \beta[SI] - \eta[E], \tag{3.25}$$

$$[\dot{I}] = \eta[E] - \gamma[I], \tag{3.26}$$

$$[\dot{SS}] = -2\beta[SSI] + \alpha[S](|S|-1) - (\alpha+\omega)[SS], \tag{3.27}$$

$$[\dot{SE}] = \beta[SSI] - \beta[ESI] - \eta[SE] + \alpha[S][E] - (\alpha+\omega)[SE], \tag{3.28}$$

$$[\dot{SI}] = \eta[SE] - \beta[SI] - \beta[ISI] - \gamma[SI] + \alpha[S][I] - (\alpha+\omega)[SI], \tag{3.29}$$

$$[\dot{EE}] = 2\beta[ESI] - 2\eta[EE] + \alpha[E](|E|-1) - (\alpha+\omega)[EE], \tag{3.30}$$

$$\begin{aligned}[\dot{EI}] = {} & \beta[ISI] + \beta[SI] + \eta[EE] - (\gamma+\eta)[EI] \\ & + \alpha[E][S] - (\alpha+\omega)[EI],\end{aligned} \tag{3.31}$$

$$[\dot{II}] = 2\eta[EI] - 2\gamma[II] + \alpha[I](|I|-1) - (\alpha+\omega)[II], \tag{3.32}$$

$$\langle \dot{k}\rangle = \alpha(N-1) - (\alpha+\omega)\langle k\rangle, \tag{3.33}$$

$$\langle \dot{k^2-k}\rangle = 2\alpha(N-2)\langle k\rangle - 2(\alpha+\omega)\langle k^2-k\rangle, \tag{3.34}$$

$$\dot{\phi} = 3\alpha - \left(\alpha+\omega+2\alpha(N-2)\frac{\langle k\rangle}{\langle k^2-k\rangle}\right)\phi, \tag{3.35}$$

where

$$[SSI] = \frac{\langle k^2 - k \rangle}{\langle k \rangle^2} \frac{[SS][SI]}{[S]} \left(1 - \phi + \phi \frac{N}{\langle k \rangle} \frac{[SI]}{[S][I]}\right), \tag{3.36}$$

$$[ESI] = \frac{\langle k^2 - k \rangle}{\langle k \rangle^2} \frac{[SE][SI]}{[S]} \left(1 - \phi + \phi \frac{N}{\langle k \rangle} \frac{[EI]}{[E][I]}\right), \tag{3.37}$$

$$[ISI] = \frac{\langle k^2 - k \rangle}{\langle k \rangle^2} \frac{[SI]^2}{[S]} \left(1 - \phi + \phi \frac{N}{\langle k \rangle} \frac{[II]}{[I]^2}\right). \tag{3.38}$$

To demonstrate the validity of this model, we test it against numerical simulations (Fig. 3.2) on a

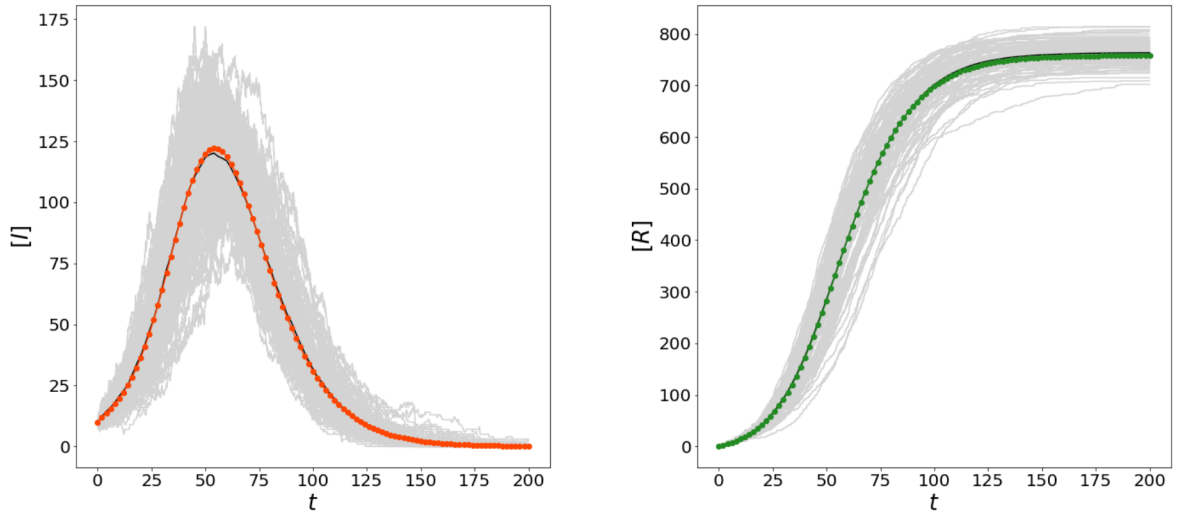

(a) (b)

FIGURE 3.2. Comparison of the model to simulation. 100 trials were run on a unipartite contact network generated from a bipartite network with Poisson degree distributions and $N = 500, M = 125, \lambda = 4$. Initial conditions are $[E]_0 = [I]_0 = 10, [S]_0 = 480, [R]_0 = 0$. Epidemiological and network parameters are $R_0 = 2.4, \eta = 1/5, \gamma = 1/10, \alpha \approx 2.3 \times 10^{-5}, \omega = 3.4 \times 10^{-5}$. Individual simulations are shown in light gray with the mean in black. Model results are (a) $[I](t)$, red circles, (b) $[R](t)$, green circles.

heterogeneous, clustered network—the construction of which is described in Section 3.2.1. Clearly, the model (3.24)-(3.35) is in excellent agreement with the simulations.

(a)

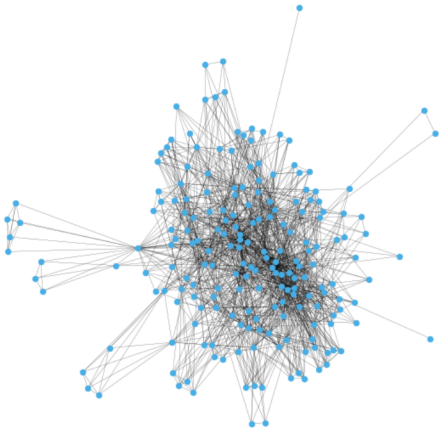

(b)

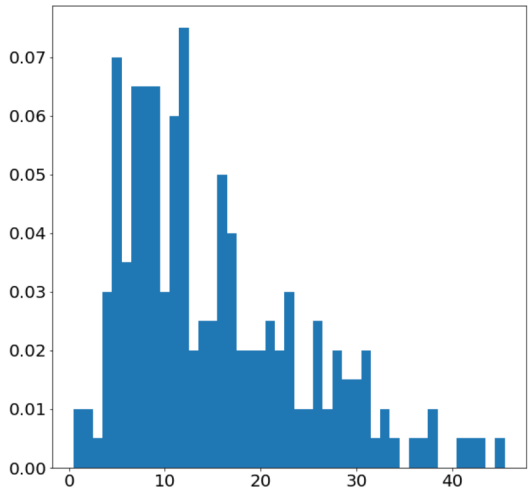

(c)

FIGURE 3.3. Example contact network (b) and its degree distribution (c) generated from a bipartite mixing network (a). Degree distributions for the individuals and mixing locations are Poisson (as described in Section 3.2.1) with $N = 200$, $M = 50$, and $\lambda = 2$. For (c), the horizontal axis is node degree and the vertical axis is the proportion of nodes.

3.2.1. Network and Epidemiological Parameters. The goal of this chapter is to investigate social distancing policies through random link activation/deletion dynamics, which are controlled by the activation and deletion rates α and ω. Moreover, in building intervention schemes in Section 3.3 new parameters are introduced. In order to consistently compare the efficacy of intervention schemes, network and epidemiological parameters are held the same across schemes.

As such, we restrict our attention to a particular heterogeneous, clustered network and epidemiological parameters that are plausible for COVID-19. For completeness, other network types and epidemiological parameters are considered in Appendix Section 3.4.2.

A consistent challenge of network models is constructing realistic contact networks. In particular, degree heterogeneity and significant clustering are observed in real world social networks (Read et al., 2008). To construct such a contact network, we consider a bipartite mixing network (Eubank et al., 2004) with N individuals and M mixing locations (Fig. 3.3a). Two individuals are in contact if they both connect to the same mixing location, so we form a contact network as the unipartite projection of the bipartite mixing network (Fig. 3.3b). To introduce degree heterogeneity, we construct a bipartite mixing network where both individuals and mixing locations have Poisson degree distributions (Newman et al., 2001). The average individual degree λ and average mixing location degree μ are related by

$$N\lambda = M\mu, \tag{3.39}$$

so only $N, M,$ and λ are needed to characterize this network. Using generating function techniques (Newman et al., 2001), we compute

$$\langle k \rangle = \frac{N}{M}\lambda^2, \tag{3.40}$$

$$\langle k^2 - k \rangle = \left(\frac{N}{M}\right)^2 \lambda^3(\lambda + 1), \tag{3.41}$$

$$\phi = \frac{1}{\lambda + 1}, \tag{3.42}$$

for the unipartite contact network, which exhibits both degree heterogeneity (Fig. 3.3c) and clustering. Unless otherwise specified, the networks in this chapter are generated using $N = 10,000$, $M = 2,500$, and $\lambda = 4$. We acknowledge that though we use a bipartite mixing network to generate a heterogeneous, clustered unipartite contact network, our network dynamics are limited to the contact network. Mobility networks (Chang et al., 2021) have been used to great effect for COVID-19, and suggest a fruitful path forward for bipartite network dynamics.

Numerous recent studies have estimated important epidemiological quantities for the spread of Sars-CoV-2, including the length of the incubation period, the length of the infectious period, and the basic reproduction number R_0. We choose the plausible estimates in line with recent studies[1]: average incubation period of 5 days (Linton et al., 2020; Zhang et al., 2020), average infectious period of 10 days (You et al., 2020), and $R_0 = 2.4$ (Anastassopoulou et al., 2020; Li et al., 2020). To incorporate these into the model, we note that $1/\eta$ and $1/\gamma$ are the average lengths of the incubation and infectious periods respectively, and thus $\eta = 0.2, \gamma = 0.1$. We do not derive R_0 for the model (3.24)-(3.35), but instead consider the basic reproduction number for a heterogeneous, clustered population from Miller (2009), which is given as the series

$$R_0 = \frac{\langle k^2 - k \rangle}{\langle k \rangle} \frac{\beta}{\beta + \gamma} - \phi \frac{\langle k^2 - k \rangle}{\langle k \rangle} \left(\frac{\beta}{\beta + \gamma} \right)^2 + \dots \tag{3.43}$$

Ignoring higher order terms, we can compute β from (3.43) when $R_0 = 2.4$ With these parameters, we plausibly model the spread of COVID-19 through a moderately sized heterogeneous, clustered population in the following sections, while introducing various social distancing interventions to mitigate or control the epidemic.

3.3. Analysis of Interventions

Social distancing and lockdown measures have been used to curb the spread of infectious diseases throughout history, and are some of the most ubiquitous non-pharmaceutical interventions in the current COVID-19 pandemic. Many compartment-based models that incorporate social distancing do so in a phenomenological manner through the transmission rate, but adaptive network models present an opportunity to describe a social distancing mechanism in a fundamental way. A simple model of such interventions can be naturally characterized by the link activation/deletion process. During periods of social distancing and lockdown, individual contacts break; during periods of relaxation of the measures, individual contacts form. In this section, we develop two social distancing schemes (Fig. 3.4). Both social distancing schemes begin when the prevalence $[I](t)$ reaches some specified threshold level. For the simple intervention scheme, contacts break as the intervention is implemented, then contacts stay fixed as the intervention is in place, and finally contacts form

[1]It is worth noting that at the time this chapter was written, these represented the most recent estimates. Subsequent studies and the emergence of variants of SARS-Cov-2 have altered some estimates of the epidemiological parameters.

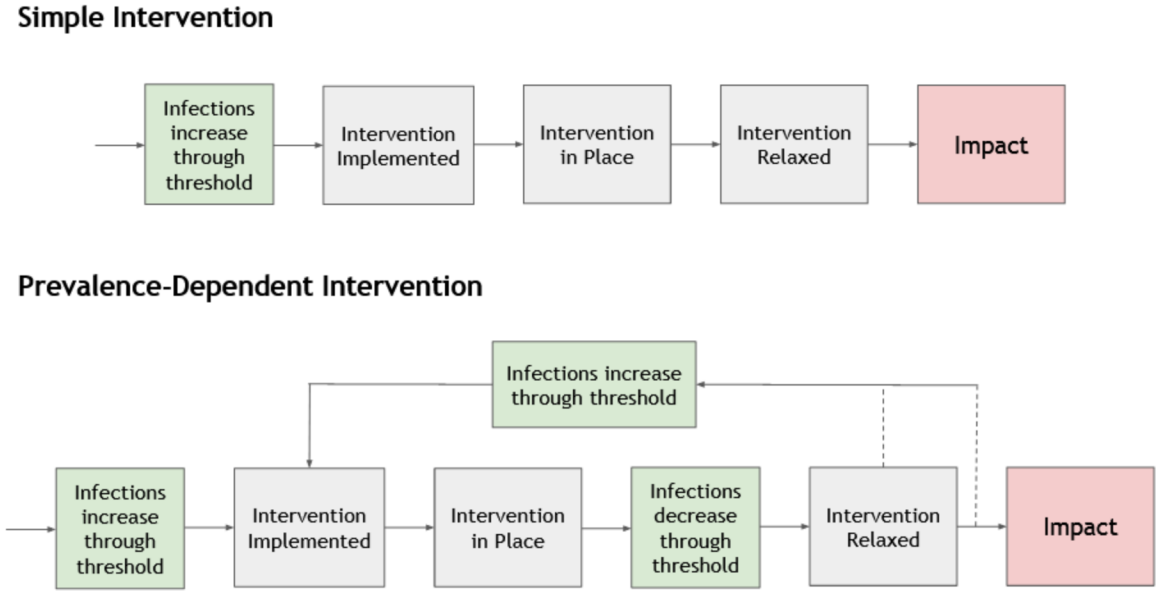

FIGURE 3.4. Schematic of the Simple and Prevalence-Dependent Interventions. Both interventions are triggered by a threshold condition, and proceed through the described intervention until the epidemic ends and the impacts of the interventions can be evaluated.

until they reach their pre-intervention levels. The prevalence-dependent scheme unfolds similarly, but with two notable differences. First, after the intervention, contacts do not start forming again until the prevalence has dropped below the threshold. Second, any time the prevalence reaches the threshold again, the intervention restarts. This allows for multiple implementations of a social distancing intervention throughout the course of the epidemic.

Critically, we do not treat these schemes as a mere modeling exercise, but are interested in the impact of each intervention scheme at the end of the epidemic. We develop two simple metrics to evaluate the effectiveness of the simple and prevalence-dependent interventions. First, we consider each intervention's ability to reduce the cumulative number of infections, known as the final size of the epidemic. Second, we also consider how many infections occur above the threshold value for prevalence. These two measures reflect two different yet crucial public health goals, and do not necessarily agree on which interventions are the most effective. Both must be considered to get a complete picture of an intervention's impact. In this section, we derive these two metrics

mathematically, and describe the simple and prevalence-dependent interventions while assessing their overall effects.

3.3.1. Evaluation Metrics. The first measure of intervention effectiveness we introduce is the *Relative Change in the Final Size* (RCFS). The final size of an epidemic is the cumulative number of infections that occur over the course of the epidemic. In terms of the model, the final size can be found as the limiting value of the recovered individuals $[R]$:

$$\lim_{t\to\infty}[R](t) = R_\infty.$$

We compare the final size of the epidemic with no intervention R_∞ to the final size where an intervention has been implemented R_∞^{int}. We then define the RCFS as

$$\text{RCFS} = \frac{R_\infty^{\text{int}} - R_\infty}{R_\infty}. \tag{3.44}$$

An effective intervention will lead to a decrease in final size, so an RCFS near 0 is unsuccessful, while an RCFS near -1 is extraordinarily successful. However, it is important to note that for brief, intense intervention schemes, it is possible that the final size actually increases. In this case, the network parameters change quickly, before significant disease spread, so the epidemic unfolds on a fundamentally different static network.

While the relative change in the final size provides an overall measure of the effectiveness of interventions, reducing cumulative infections alone is not the only public health goal that an intervention scheme might seek to accomplish. In some schemes, a large number of infections occur above the threshold despite a large reduction in the final size of the epidemic. This can be particularly pernicious if the threshold represents some fixed resource such as healthcare capacity, where a large number of infections above the threshold could lead to higher mortality and other negative outcomes. To account for this, we compute the *Cumulative Infections Above Threshold* (CIAT). Let $t_1, t_2, \ldots$ be the sequence of times when $[I] = qN$. Assuming $[\dot{I}] \neq 0$ at any time in the sequence[2], the continuity of $[I](t)$ implies that the prevalence is above the threshold on the intervals

[2]This assumption is made simply so that the times when I increases or decreases through the threshold alternate, and the CIAT can be defined as a sum of integrals.

$[t_{2i-1}, t_{2i}]$ for $i = 1, 2, 3, \ldots$ Thus, the CIAT may be defined as

$$\text{CIAT} = \sum_i \int_{t_{2i-1}}^{t_{2i}} [I](t) - qN dt. \tag{3.45}$$

We note that the units of CIAT are person-time—for a metric with units of population, we compute the *Average Infections Above Threshold* (AIAT):

$$\text{AIAT} = \frac{\text{CIAT}}{\sum_i t_{2i} - t_{2i-1}} \tag{3.46}$$

Using the relation $[\dot{R}] = \gamma[I]$, equation (3.46) becomes

$$\text{AIAT} = \frac{\sum_i [R](t_{2i}) - [R](t_{2i-1})}{\gamma \sum_i t_{2i} - t_{2i-1}} - qN, \tag{3.47}$$

which is convenient for computations.

3.3.2. Simple Intervention. For a simple model of social distancing, we consider a scheme that unfolds in three successive phases, each with variable length. The effects of the intervention scheme on the contact network are characterized through the average number of contacts $\langle k \rangle(t)$. The intensity of the intervention can be thought of as how severely the average number of contacts are reduced, so we introduce a severity parameter $p \in [0, 1)$. The top panel of Figure 3.5 shows how the $\langle k \rangle$ changes over time as the result of the intervention. In the first phase, as social distancing measures are put into place, the average number of contacts decreases from its pre-intervention level $\langle k \rangle_0$ to $p\langle k \rangle_0$. In the second phase, with the measures fully in place, the average number of contacts remains constant at $p\langle k \rangle$. In the third phase, social distancing measures are relaxed and the average number of contacts increases to its pre-intervention level $\langle k \rangle_0$.

To achieve this effect in the evolution of the average number of contacts, we consider link activation rate $\alpha(t)$ and deletion rate $\omega(t)$ functions that are piecewise constant. These rate functions can be seen in the bottom two panels of Figure 3.5. Since contacts are only broken in the first phase, $\omega(t) = \omega^*$ in the first phase and 0 otherwise. Since contacts are only formed in the third phase, $\alpha(t) = \alpha^*$ in the third phase and 0 otherwise. As the dynamical equation for $\langle k \rangle$ (3.33) is a first-order linear ODE, the resulting curve for $\langle k \rangle(t)$ will be piecewise exponential, and the values of α^* and ω^* are easily computed for a given p. Other than p, four other parameters characterize the

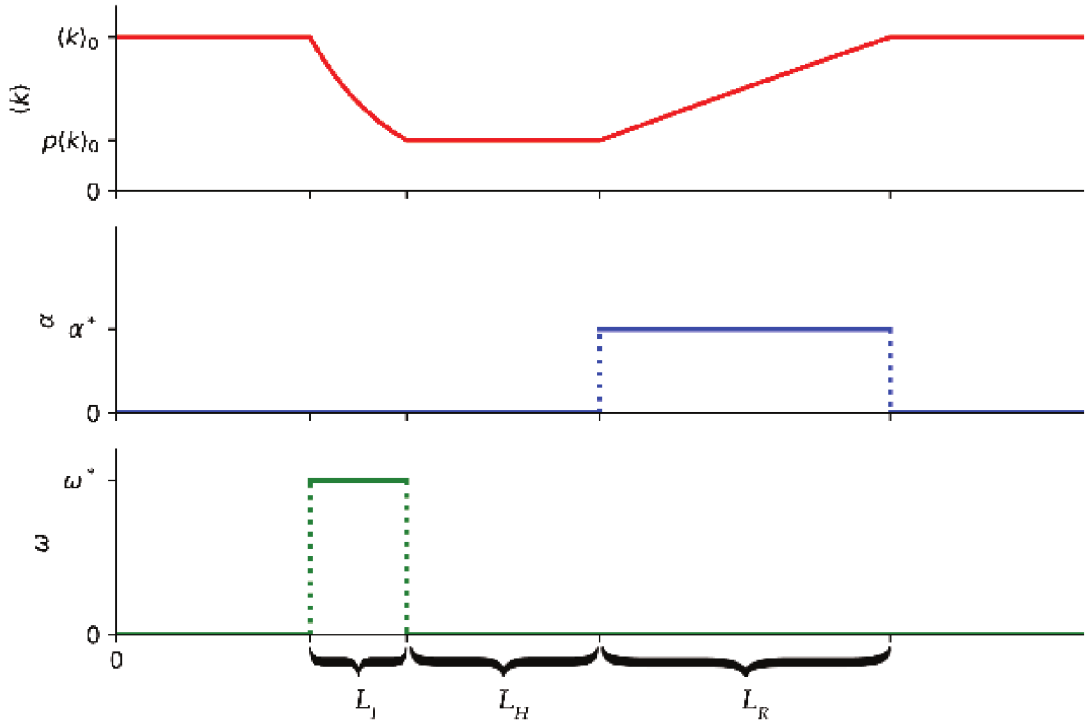

FIGURE 3.5. Simple Intervention. Once the intervention begins, edges are deleted at rate ω^* for L_I days until the average number of contacts $\langle k \rangle$ drops to $p\langle k \rangle_0$. For the next L_H days, no changes are made to the nework. Then, edges are added at rate α^* for L_R days, until the average number of contacts $\langle k \rangle$ increases to back to $\langle k \rangle_0$

simple intervention: the lengths of the three phases L_I, L_H, and L_R, and the threshold proportion of the population $q \in [0, 1)$ to initiate the intervention. The full simple intervention scheme can be described as follows:

- No intervention: the epidemic spreads unabated until $[I]$ increases through qN ($\alpha = \omega = 0$).
- Intervention Phase (length L_I): intervention occurs, edges are removed at a constant rate ($\alpha = 0, \omega = \omega^*$).
- Holding Phase (length L_H): intervention holds, edges are neither removed nor added ($\alpha = \omega = 0$).

- Relaxation Phase (length L_R): interventions are relaxed, edges are added at a constant rate ($\alpha = \alpha^*, \omega = 0$).

As this scheme requires five 'intervention" parameters, p, q, L_I, L_H, and L_R, exploring the full impact of the interventions is difficult. To better see the effects, we consider an example scheme where we fix two parameter values in each and allow the other three to vary. To focus on the impact of the severity parameter p and the lengths of the intervention and relaxation phases L_I and L_R, we set $L_H = 15$ and $q = 0.01$ for the remainder of this section. Thus, the intervention begins when infections reach one percent of the population, and the holding phase is fixed at 15 days for all interventions. The other three parameters are allowed to vary. This allows for both abrupt and gradual implementations of interventions and relaxation of measures, and different levels of intervention intensity. Figure 3.6 shows the prevalence of some example intervention schemes, showing rich qualitative behavior. To assess the effectiveness of the simple intervention we plot the

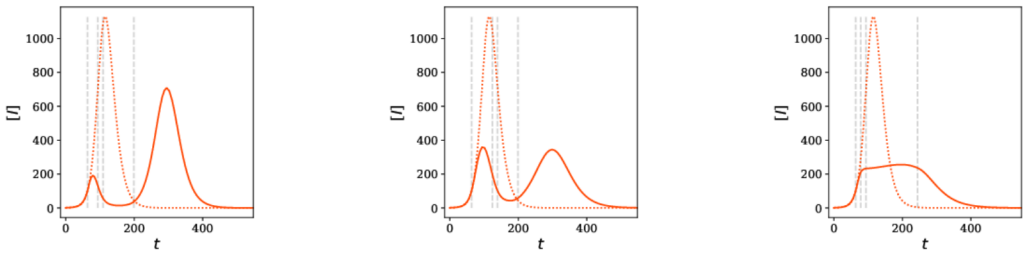

(a) (b) (c)

FIGURE 3.6. Example infection curves $[I](t)$ for the simple intervention with $q = 0.01$. The other intervention parameters are (a) $p = 0.125$, $L_I = 30$, $L_R = 90$, (b) $p = 0.25$, $L_I = 60$, $L_R = 60$, and (c) $p = 0.5$, $L_I = 15$, $L_R = 150$. Solid orange curves are $[I](t)$ under the intervention, while dashed orange curves are $[I](t)$ without any intervention. Gray dashed lines denote the starts of the intervention, holding, and relaxation periods.

RCFS and the AIAT for a large number of parameter combinations. We allow the lengths of both the intervention and relaxation periods L_I and L_R to vary from 2 to 180 days, and consider three different intensities $p = 0.125, 0.25, 0.5$. The results are shown in Figure 3.7.

A significant common feature of the plots in Figure 3.7a is a qualitative boundary (solid white curve) that divides (L_I, L_R) space into two distinct classes of the resulting infection curve (for $p = 0.125$, this occurs outside the boundaries of the plot). To the right of the boundary, infection

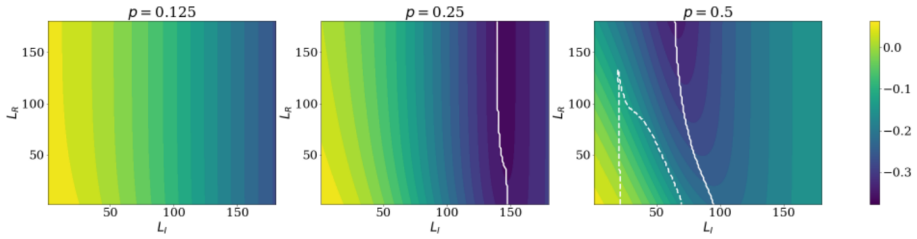

(a)

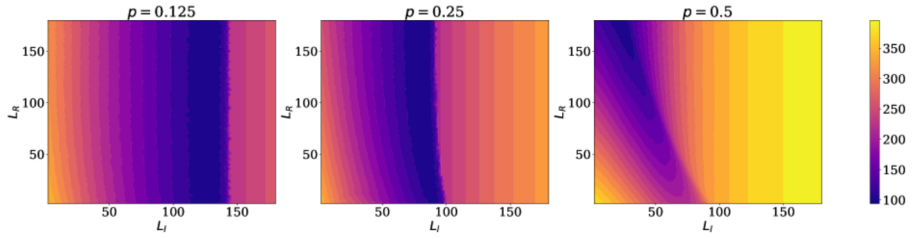

(b)

FIGURE 3.7. Plots of the RCFS (a) and AIAT (b) for the $L_H = 15$ and $q = 0.01$. For intensities $p = 0.125, 0.25$, and 0.5, the intervention period and relaxation period lengths L_I and L_R vary from 2 to 180 days. In (a), the solid white curve denotes the qualitative boundary, to the right of which uniform spikes occur. The dashed white line in the third panel denotes the boundary of the region where two spikes occur.

curves are characterized by a single 'uniform spike," defined by an prevalence curve $[I](t)$ with two inflection points and a single local maximum (Fig. 3.8a). To the left of the boundary, infection curves take the form of either a single 'non-uniform spike" (Fig. 3.8b), with more than two inflection points but only one local maximum, or multiple spikes (Fig. 3.8c), with more than two inflection points and multiple local maxima. For $p = 0.125$ and $p = 0.25$, only multiple spikes occur to the left of the boundary. For small L_I, the first spike is small and the second spike is large, and occasionally the final size of the epidemic surpasses the static case due to network alterations. As L_I approaches the qualitative boundary, the second spike becomes shorter and occurs later until negligible. This phenomenon can also be seen in Figure 3.7b: as L_I increases, the AIAT decreases until the second spike drops below the threshold qN, at which point the AIAT increases as the first spike grows taller. For $p = 0.5$ on the other hand, both nonuniform spikes and multiple spikes are possible to the left of the boundary. Multiple spikes occur in the region of (L_I, L_R) space enclosed by the dashed white curve, while a single nonuniform spike occurs elsewhere left of the qualitative boundary.

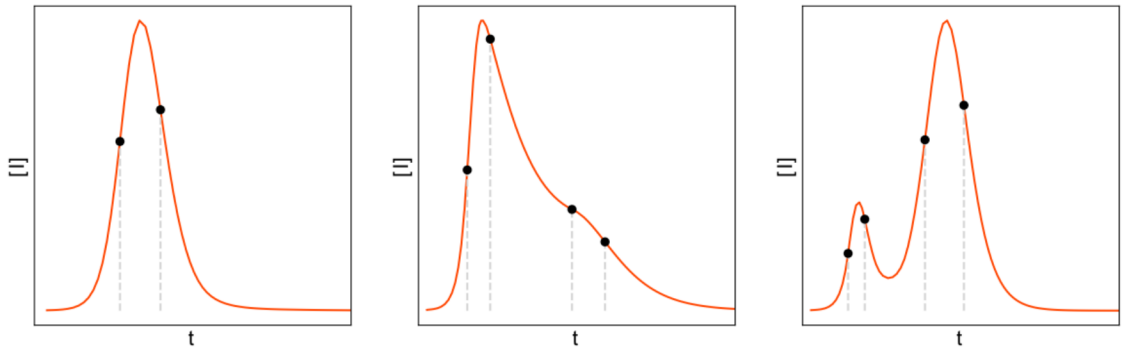

(a) (b) (c)

FIGURE 3.8. Types of infection curves with the simple intervention: (a) uniform spike, (b) non-uniform spike, (c) multiple spikes. Black dots denote inflection points.

A few other observations warrant comment. First, the length of the intervention L_I appears to be more important in determining epidemic's final size compared to L_R. This is intuitive, as the most significant changes to network structure occur during the intervention phase. Second, as p increases, the qualitative boundary shifts generally left. This means that for less severe interventions, single uniform spikes will occur for smaller L_I values. This observation carries weight for repeated interventions, explored in Section 3.3.3, as single uniform spikes are heavily penalized by the AIAT. Third, nonuniform spikes occur for $p = 0.5$, but not for $p = 0.125$ or $p = 0.25$. We hypothesize that there may exist some threshold p^* where nonuniform spikes don't occur below p^*, but do above p^*.

3.3.3. Prevalence-Dependent Intervention. While the simple intervention scheme provides a simple yet general model of social distancing, its implementation lacks a degree of realism. Interventions are put into place only once, and the epidemic continues, often with infections spiking after measures begin to relax. In reality, we would expect public health measures to be responsive to rising prevalence. Moreover, continued interventions might be triggered by some indicator, such as case numbers, deaths, hospital capacity, etc... In this section, we adapt the intervention scheme from Section 3.3.2 so that it may be reimplemented when a prevalence-based condition is satisfied, forming the prevalence-dependent intervention. We begin with two more realistic assumptions about how a public health response might unfold. First, interventions are reimplemented any time the prevalence increases through some threshold. Second, the relaxation phase of an intervention

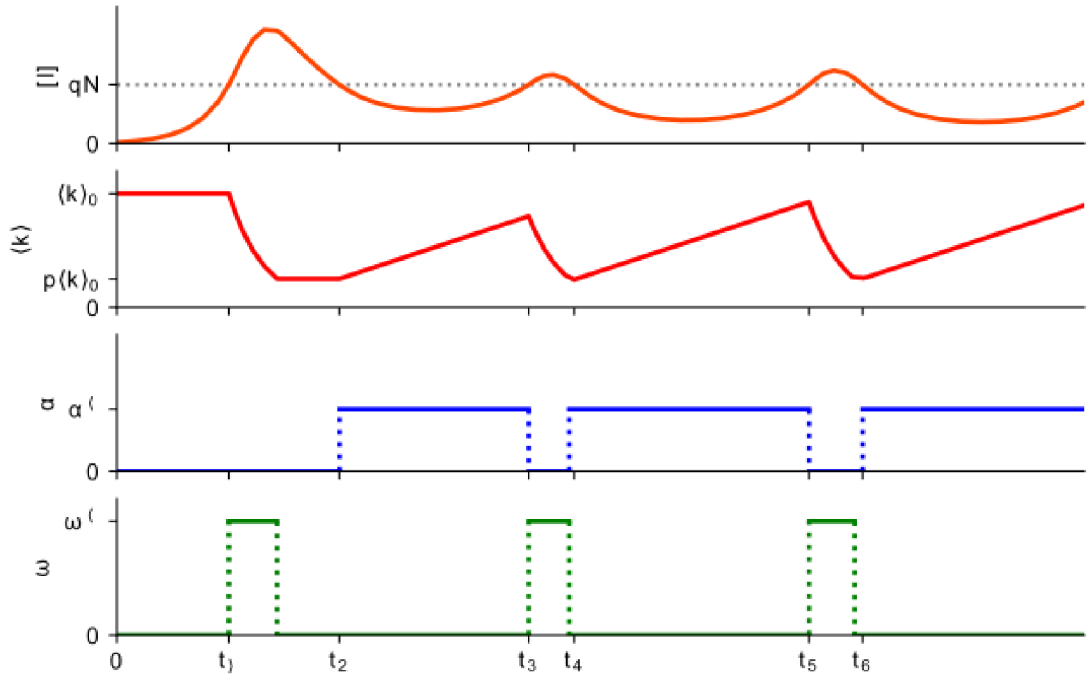

FIGURE 3.9. Prevalence-Dependent Intervention. The intervention begins when $[I] = qN$, and edges are deleted at a constant rate ω^* until $\langle k \rangle$ decreases to $p\langle k \rangle_0$, at which point there is no change to the network until $[I]$ drops below the threshold qN. Then, edges are added at a constant rate α^* until $\langle k \rangle$ returns to $\langle k \rangle_0$ or $[I]$ increases through the threshold qN, at which point the intervention begins again.

doesn't begin until the prevalence has dropped below the threshold. We incorporate these assumptions into a new prevalence-dependent intervention scheme. The scheme is determined by four parameters: q, p, L_I, and L_R. As before, interventions begin when $[I]$ reaches qN, p is the severity of the intervention, and L_I and L_R are now the maximum lengths of the intervention and relaxation periods, which determine ω^* and α^* as in Section 3.3.2. We can define the new scheme as follows:

- As $[I]$ increases through qN, a new intervention is implemented.
- Intervention Phase: Once an intervention is implemented, edges are deleted at rate $\omega = \omega^*$ until $\langle k \rangle = p\langle k \rangle_0$.

- Holding Phase: At the end of the intervention period, a holding period begins ($\alpha = \omega = 0$) until the prevalence has dropped below the threshold qN. If the prevalence drops below the threshold during the intervention period, the holding period has length 0.
- Relaxation Phase: Edges are added at rate $\alpha = \alpha^*$ until $\langle k \rangle = \langle k \rangle_0$, or a new intervention is implemented.

It worth noting that compared to the simple intervention in Section 3.3.2, the intervention, holding, and relaxation phases can all be of variable length. For instance, if the average number of contacts $\langle k \rangle$ has not rebounded to $\langle k \rangle_0$ by the time a new implementation begins, the resulting relaxation period is shorter than L_R. Moreover, in the subsequent intervention phase, edges delete until $\langle k \rangle = p\langle k \rangle_0$ and the phase is shorter than L_I. In sum, while ω^* and α^* are fixed, the average number of contacts is never less than $p\langle k \rangle_0$ and the effective lengths of different intervention and relaxation phases may vary. An example implementation of the prevalence-dependent scheme is shown in Figure 3.9, which shows both holding periods of nonzero length as well as intervention and relaxation periods that are shorter than L_I and L_R respectively.

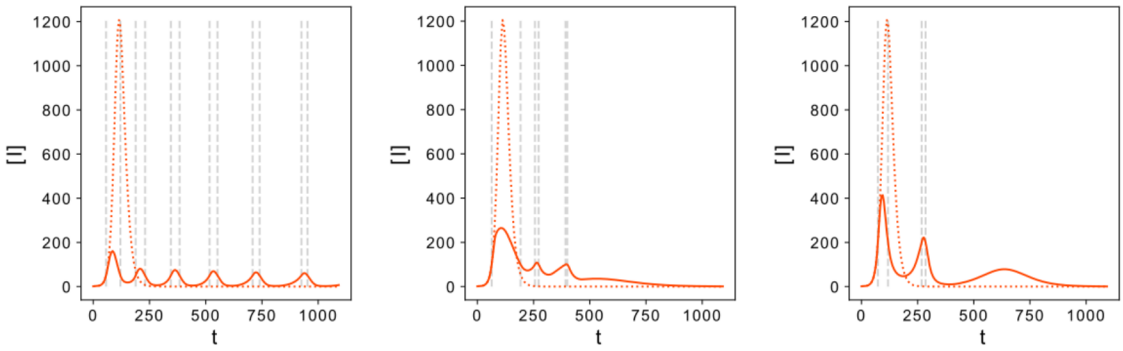

(a) (b) (c)

FIGURE 3.10. Example infection curves $[I](t)$ for the prevalence-dependent intervention. Parameters shown are (a) $q = 0.005, p = 0.125, L_I = 60, L_R = 60$, (b) $q = 0.01, p = 0.5, L_I = 15, L_R = 60$, (c) $q = 0.02, p = 0.25, L_I = 30, L_R = 120$. Solid orange curves are $[I](t)$ under the intervention, while dashed orange curves are $[I](t)$ without any intervention. Dashed gray lines denote times when $[I] = qN$.

A notable feature of the prevalence-dependent intervention is its ability to generate infection curves with multiple spikes as the epidemic progresses. Examples of this behavior are shown in Figure 3.10. To fully explore the intervention, we again consider the RCFS for a variety of parameter

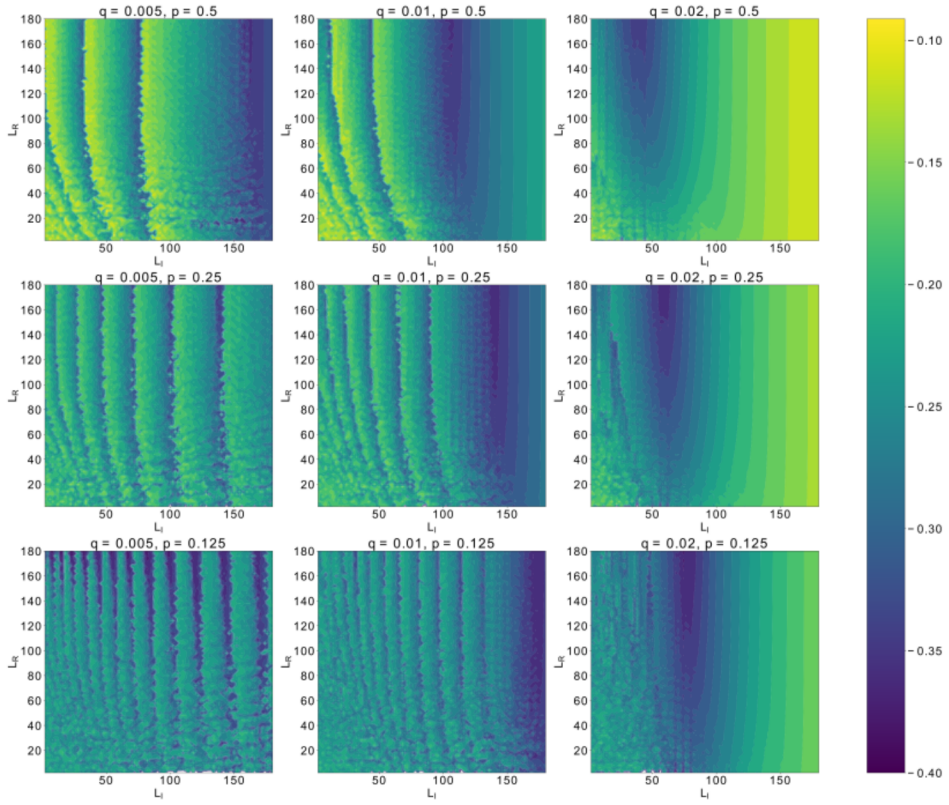

FIGURE 3.11. Relative change in final size (RCFS) for the prevalence-dependent intervention. Each plot represents a choice of p and q, with L_I and L_R on the axes, ranging from 2 for 180.

combinations. Figure 3.11 shows the RCFS for different thresholds ($q = 0.005, 0.01, 0.02$) and intensities ($p = 0.125, 0.25, 0.5$) as L_I and L_R both vary from 2 to 180 days. Though not shown, as with the simple intervention each case has a qualitative boundary, to the right of which infection curves are single, uniform spikes. The most significant departure from the simple intervention though is to the left of the qualitative boundary. In the simple case, infection curves from this region took the form of either two spikes or a single nonuniform spike. With the prevalence-dependent intervention, the infection curve behavior is richer.

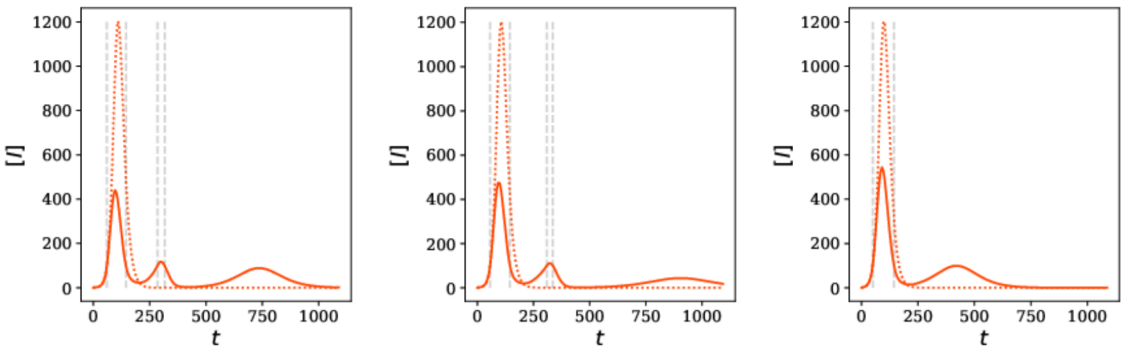

(a) (b) (c)

FIGURE 3.12. Progression of the infection curve $[I](t)$ as L_I increases, showing the shrinking of the final spike and the penultimate spike dropping below the threshold qN. Parameters are $q = 0.01, p = 0.25, L_R = 90$ and $L_I = 70$ (a), 78 (b), 92 (c). Solid orange curves are $[I](t)$ under the intervention, while dashed orange curves are $[I](t)$ without any intervention. Dashed gray lines denote times when $[I] = qN$.

The region is characterized by 'waves" in the RCFS, particularly for lower values of p. The boundaries of these waves can be described by the number of spikes that occur over the course of the epidemic. Holding L_R fixed and increasing L_I through one of these contours helps explain the behavior of the infection curve in this region (Fig. 3.12). At the crest, the final spike peaks just below the threshold qN (Fig. 3.12a). As L_I increases, the final spike occurs later and peaks lower (Fig. 3.12b) and the RCFS decreases until the spike vanishes. Then, the penultimate spike becomes the new final spike, peaking just below the threshold (Fig. 3.12c) and the RCFS jumps up as a new wave crests. This underscores a potential limitation of a threshold-based intervention: if a spike does not reach the threshold and no intervention occurs, the spike occurs over a longer period of time and more infections accumulate than if the spike had triggered an intervention. A practical implication of this observation is that no spike in infections should go unaddressed by interventions if the goal is only to reduce the number of cumulative infections. We also consider the AIAT for the same parameter combinations (Fig. 3.13), though the conclusions by this metric are less complex. For any combination of p and q, increasing L_I leads to a larger AIAT. This suggests that when considering interventions with the same RCFS, more abrupt interventions (smaller L_I) are preferable. However, an interesting observation is that the AIAT increases rapidly as the epidemic changes from three to two spikes.

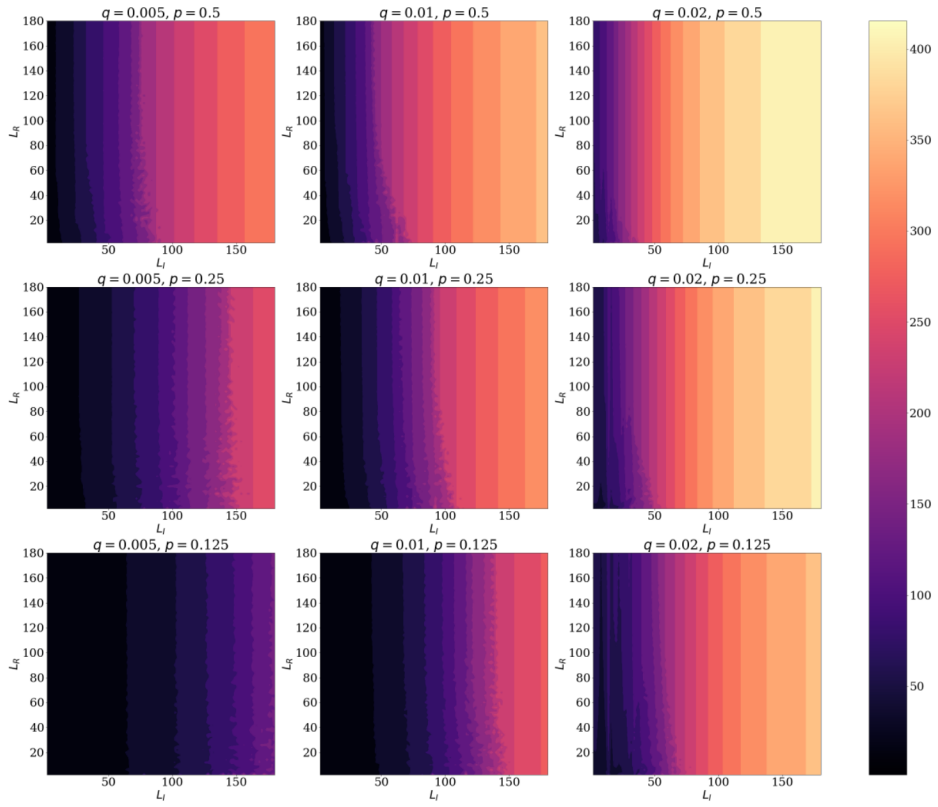

FIGURE 3.13. Average infections above threshold (AIAT) for the prevalence-dependent intervention. Each plot represents a choice of p and q, with L_I and L_R on the axes, ranging from 2 for 180.

While Figs. 3.11 and 3.13 show the overall behavior of the prevalence-dependent intervention, by considering fixed values of L_I and L_R and allowing p and q to vary, we get a more pointed perspective on the effectiveness of this type of intervention. Figure 3.14 shows increasingly gradual interventions from left to right with plots of the RCFS and AIAT as p and q vary on the axes. Notably, regardless of L_I, low values of p and q are able to produce interventions that both greatly decrease the final size of the epidemic, and the average infections above threshold. An important factor in this decrease in the final size is the time at which the measurements of the RCFS and AIAT are taken. In Figure 3.14, the epidemic is allowed to run for three years before both are measured.

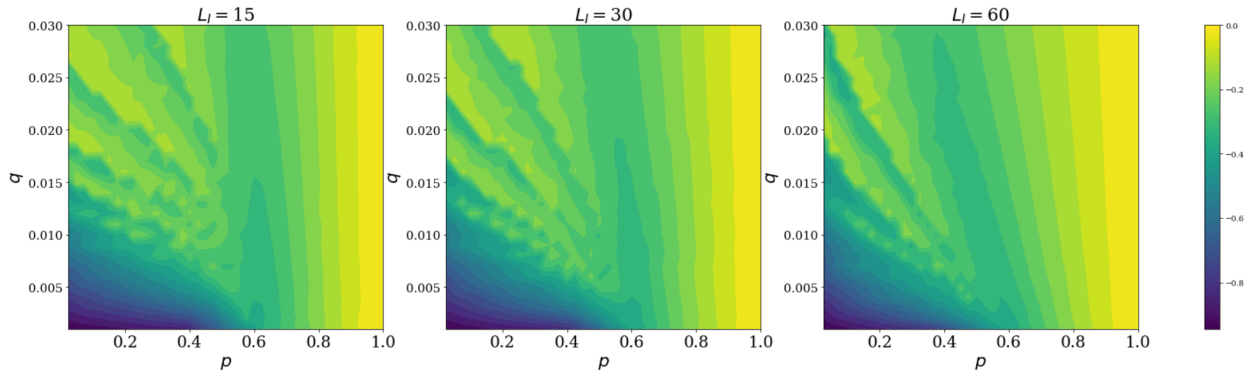

(a)

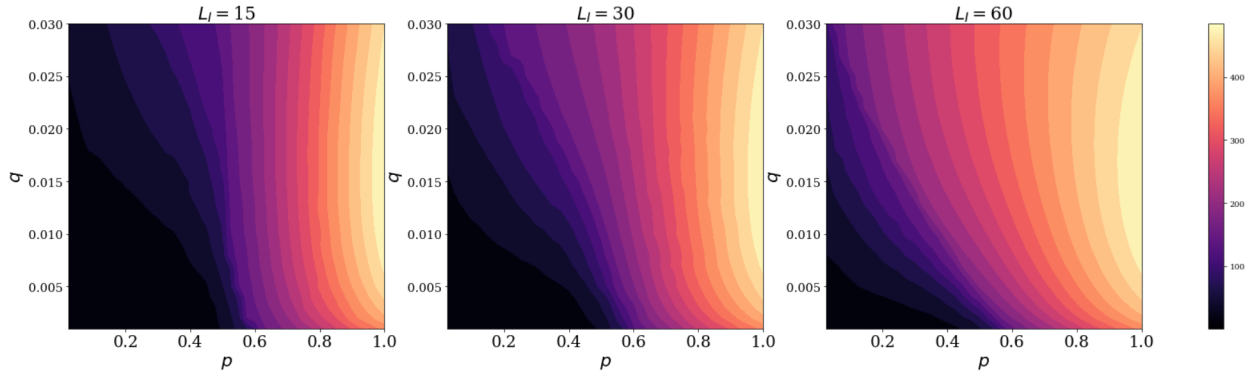

(b)

FIGURE 3.14. Plots of the RCFS (a) and AIAT (b) for the prevalence-dependent intervention with $L_I = 15, 30, 60$ and $L_R = 90$ as p varies from 0 to 1 and q varies from 0 to 0.03. Both RCFS and AIAT are measured after the epidemic has run for 3 years. Notably, both measures indicate highly-effective interventions for small values of p and q.

Measuring earlier results in a larger portion of p, q space that greatly decreases the RCFS, while measuring later results in a smaller portion. This may have important control impacts. For instance, if a vaccine is expected to be designed, produced, and distributed, the estimated time frame for that to occur can influence which levels of p and q can produce highly effective interventions. Regardless, the region of highly effective interventions appears mostly the same for the different values of L_I. This suggests that for sufficiently low thresholds (q) and sufficiently severe decreases in contacts (p), the length over which the decrease in contacts occurs (L_I) does not play an important role in the effectiveness of interventions. However, as q or p increases, L_I has a more pronounced impact. In particular, for low values of p and large values of q, a longer, more gradual intervention can

lead to more average infections above threshold. Moreover, a stark change in both effectiveness metrics occurs for large values of p, (around $p = 0.5$ for $L_I = 15$ and $L_I = 30$). This suggests that if an intervention doesn't reduce average contacts sufficiently, a highly effective intervention isn't possible, regardless of the other parameter values.

3.4. Discussion

In this chapter, we have developed a new SEIR model on a network with random link activation/deletion dynamics. Using piecewise constant activation and deletion rate functions, we propose two simple mechanisms for social distancing interventions. The simple intervention models a single intervention event, where contacts are decreased over a period of time, stay constant, and then return to pre-intervention levels. The prevalence-dependent intervention expands the simple case to more complex scenarios, where interventions can be reintroduced in the face of rising prevalence. Using the unipartite projection of a bipartite network, and epidemiological parameters representative of COVID-19, we examine the effectiveness of a wide range of potential social distancing policies on relatively large heterogeneous, clustered networks.

Both intervention schemes are shown to capture a wide variety of behaviors in the prevalence "curve," which has received considerable attention in both academic studies and public health messaging. The simple intervention manifests curves with one or two spikes, while the curves for prevalence-dependent intervention can (unsurprisingly) have many more. Moreover, the behavior of the prevalence curve is consistent across a number of parameters and can be described qualitatively, which has an impact on which metrics reward or punsish the intervention. This is despite the simplicity of social distancing mechanism introduced by the piecewise constant activation and deletion rates $\alpha(t)$ and $\omega(t)$, which take on values α^* or ω^* respectively, or zero. We have not considered the cases where the values of α^* and ω^* may change over time, or where $\alpha(t)$ and $\omega(t)$ are not piecewise constant. As such, our model has natural extensions that may capture an even richer variety of qualitative behaviors.

Furthermore, the mechanisms proposed in this chapter offer insights into what makes for a successful intervention. We have used two metrics as simplified public health goals to evaluate the effectiveness of interventions: the relative change in final size (RCFS) and the average infections

above threshold (AIAT). For the more realistic prevalence-dependent intervention scheme, we find that the most effective interventions come when the threshold number of infections is low and the intervention severely decreases average contacts. When these conditions are met, the relative change in the final size is greatly decreased and the length over which the intervention is implemented has little impact on the effectiveness. However, even small increases in the threshold value can greatly impact the effectiveness of interventions over a fixed period of time. As well, if interventions do not sufficiently reduce contacts (around fifty percent), they are rendered significantly less effective by both measures.

While this is a first foray into the use of adaptive networks to model social distancing for an SEIR disease, we acknowledge some limitations of our model. First, there is a trade-off between complexity of the disease natural history model and the number of equations of the pairwise model: age-structured models or other more complex compartmental models are popular for COVID-19, but added compartments require tracking an increasing number of edge types. However, even simple extensions (such as the inclusion of an asymptomatic infectious state) present interesting opportunities. Second, while the random link activation/deletion process is simple to implement, it has some unrealistic features. In particular, in the $t \to \infty$ limit, one can show from the degree distribution generating function that the resulting network approaches an Erdős-Renyi random graph, with vanishing clustering and an approximately Poisson degree distribution. One manifestation of this property is a rapidly declining clustering coefficient over time. While the piecewise constant activation and deletion rates mitigate this to an extent, the network resulting from these social distancing policies is fundamentally different than the initial network state. To overcome this limitation, future investigations might involve new processes for network dynamics, such as activation/deletion on a fixed network or network dynamics on an underlying bipartite mixing network.

Appendix

3.4.1. Adaptive SEIR model with Complex Closure. In this appendix, we develop an adaptive network SEIR pairwise model for heterogeneous, clustered networks. The model is analogous to the SIR model for heterogeneous, clustered networks in House and Keeling (2011) with random link activation/ deletion dynamics included.

The generic triple closure (12) from the main text, proposed by House and Keeling (2011), can be further developed by introducing a new variable $\theta(t)$, the proportion of edges that have not transmitted the infection. With the observation that $[S_k] = Np_k\theta^k$, the triple closure becomes

$$[ASI] \approx [AS][SI]\frac{g''(\theta)}{N(g'(\theta))^2}\left((1-\phi) + \phi g'(1)N\frac{[AI]}{(\sum_k k[A_k])\,(\sum_k k[I_k])}\right) \tag{3.48}$$

Moreover, we can express $\sum_k k[S_k] = N\theta g'(\theta)$, and we introduce auxiliary variables $Y = \sum_k k[E_k]$, $Z = \sum_k k[I_k]$, and θ. Observing that $\sum_k k[A_k] = [AS]+[AE]+[AI]+[AR]$, it follows that the dynamical equations for Y and Z (without network dynamics) are

$$\dot{Y} = \beta\frac{\theta g''(\theta)}{g'(\theta)}[SI] - \eta Y \tag{3.49}$$

$$\dot{Z} = \eta Y - \gamma Z \tag{3.50}$$

Now we incorporate the effects of link activation and deletion. Notably, the probability generating function for the degree distribution is now time- dependent, taking the form

$$g(x,t) = \sum_{k=0}^{N-1} p_k(t)x^k. \tag{3.51}$$

As a consequence, the ordinary derivatives of g in (3.48)-(3.50) become partial derivatives with respect to x. From (14) and (15) in the main text, we can derive network- dynamical versions of (3.49) and (3.50):

$$\dot{Y} = \beta\frac{\theta g_{xx}(\theta,t)}{g_x(\theta,t)}[SI] - (\eta+\alpha+\omega)Y + \alpha(N-1)[E] \tag{3.52}$$

$$\dot{Z} = \eta Y - (\gamma+\alpha+\omega)Z + \alpha(N-1)[I] \tag{3.53}$$

Next, the non-epidemiological network quantities in this model are entirely determined by the degree distribution probability generating function $g(x,t)$ and the clustering coefficient $\phi(t)$. We can express (23) from the main text in terms of the generating function $g(x,t)$ as

$$\dot{\phi} = 3\alpha - \left(\alpha + \omega + 2\alpha(N-2)\frac{g_x(1,t)}{g_{xx}(1,t)}\right)\phi. \tag{3.54}$$

Equations (3.48),(3.52), and (3.54) require $g(x,t)$ and its derivatives explicitly, which can be found by solving (18) from the main text using the method of characteristics:

$$\begin{aligned} g(x,t) = g_0 &\left(\frac{\omega + \alpha x + \omega(x-1)e^{-(\alpha+\omega)t}}{\omega + \alpha x - \alpha(x-1)e^{-(\alpha+\omega)t}}\right) \\ &\cdot \left(\frac{\omega + \alpha x - \alpha(x-1)e^{-(\alpha+\omega)t}}{\alpha+\omega}\right)^{N-1} \end{aligned} \tag{3.55}$$

where $g_0(x) = g(x,0)$. Finally, we derive the evolution equation for $\theta(t)$ by differentiating $[\dot{S}] = Ng(\theta(t),t)$ and solving for $\dot{\theta}$:

$$\dot{\theta} = -\frac{\beta[SI]}{Ng_x(\theta,t)} - (1-\theta)\left(\alpha\theta + \omega - \alpha(N-1)\frac{g(\theta,t)}{g_x(\theta,t)}\right). \tag{3.56}$$

Thus, we arrive at the pairwise SEIR for a heterogeneous, clustered network with random link activation and deletion:

$$|S] = Ng(\theta, t) \tag{3.57}$$

$$|\dot{E}] = \beta|SI] - \eta|E], \tag{3.58}$$

$$|\dot{I}] = \eta|E] - \gamma|I], \tag{3.59}$$

$$|\dot{SS}] = -2\beta|SSI] + \alpha|S](|S] - 1) - (\alpha + \omega)|SS], \tag{3.60}$$

$$|\dot{SE}] = \beta|SSI] - \beta|ESI] - \eta|SE] + \alpha|S]|E] - (\alpha + \omega)|SE], \tag{3.61}$$

$$|\dot{SI}] = \eta|SE] - \beta|SI] - \beta|ISI] - \gamma|SI] + \alpha|S]|I] - (\alpha + \omega)|SI], \tag{3.62}$$

$$|\dot{EE}] = 2\beta|ESI] - 2\eta|EE] + \alpha|E](|E] - 1) - (\alpha + \omega)|EE], \tag{3.63}$$

$$|\dot{EI}] = \beta|ISI] + \beta|SI] + \eta|EE] - (\gamma + \eta)|EI] + \alpha|E]|S] - (\alpha + \omega)|EI], \tag{3.64}$$

$$|\dot{II}] = 2\eta|EI] - 2\gamma|II] + \alpha|I](|I] - 1) - (\alpha + \omega)|II], \tag{3.65}$$

$$\dot{Y} = \beta\frac{\theta g_{xx}(\theta, t)}{g_x(\theta, t)}|SI] - (\eta + \alpha + \omega)Y + \alpha(N-1)|E], \tag{3.66}$$

$$\dot{Z} = \eta Y - (\gamma + \alpha + \omega)Z + \alpha(N-1)|I], \tag{3.67}$$

$$\dot{\theta} = -\frac{\beta|SI]}{Ng_x(\theta, t)} - (1-\theta)\left(\alpha\theta + \omega - \alpha(N-1)\frac{g(\theta, t)}{g_x(\theta, t)}\right), \tag{3.68}$$

$$\dot{\phi} = 3\alpha - \left(\alpha + \omega + 2\alpha(N-2)\frac{g_x(1, t)}{g_{xx}(1, t)}\right), \phi \tag{3.69}$$

where

$$|SSI] = |SS]|SI]\frac{g_{xx}(\theta, t)}{N(g_x(\theta))^2}\left((1-\phi) + \phi g'(1)\frac{|SI]}{\theta g_x(\theta, t)Z}\right), \tag{3.70}$$

$$|ESI] = |SE]|SI]\frac{g_{xx}(\theta, t)}{N(g_x(\theta, t))^2}\left((1-\phi) + \phi g'(1)N\frac{|EI]}{YZ}\right), \tag{3.71}$$

$$|ISI] = |SI]^2\frac{g_{xx}(\theta, t)}{N(g_x(\theta, t))^2}\left((1-\phi) + \phi g'(1)\frac{|II]}{\theta g_x(\theta, t)Y}\right). \tag{3.72}$$

3.4.2. Interventions with Additional Network and Epidemiological Parameters. In this section, we consider the prevalence-dependent intervention on two alternative heterogeneous, clustered networks with our COVID-19 parameters $R_0 = 2.4, \eta = 0.2$ and $\gamma = 0.1$. We also consider

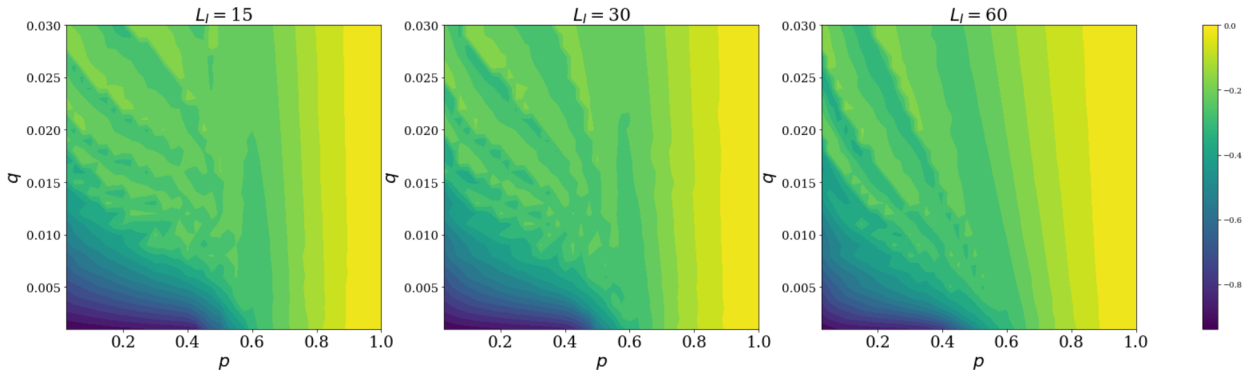

(a)

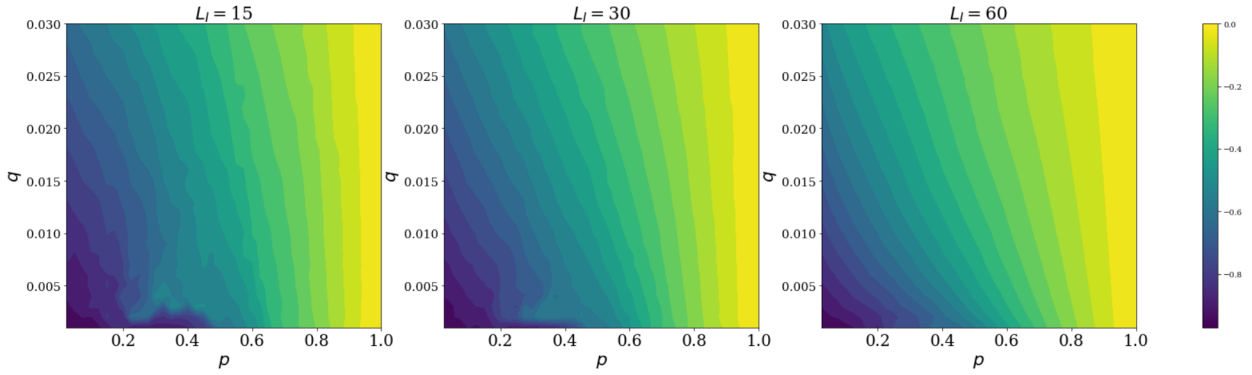

(b)

FIGURE 3.15. Plots of the RCFS for the prevalence-dependent intervention on the (a) small world network and (b) power law network with clustering for $R_0 = 2.4, \eta = 0.2, \gamma = 0.1$ and a fixed $L_R = 90$.

the case where R_0 has increased to 5 on the same networks, as well as the original unipartite projection contact network from the main text. The two networks considered are a Watts-Strogatz 'small world" network (Watts and Strogatz, 1998) and a power law network with clustering (Holme and Kim, 2002). Both networks consist of $N = 10,000$ nodes, as with the contact network in the main text. For the small world network, $\langle k \rangle \approx 30, \langle k^2 - k \rangle \approx 900, \phi \approx 0.25$; for the the power law network with clustering, the relevant initial network parameters are $\langle k \rangle \approx 30, \langle k^2 - k \rangle \approx 2000, \phi \approx 0.1$. For all cases, the system is run for 3 years.

For each network, we report two sets of figures, analogous to Figure 3.14. We consider the the relative change in final size (RCFS) and the average infections above threshold (AIAT) while fixing $L_R = 90$ and $L_I = 15, 30, 60$ and allow p and q to vary on the axes, with p ranging from 0 to 1 and q ranging from 0 to 0.03.

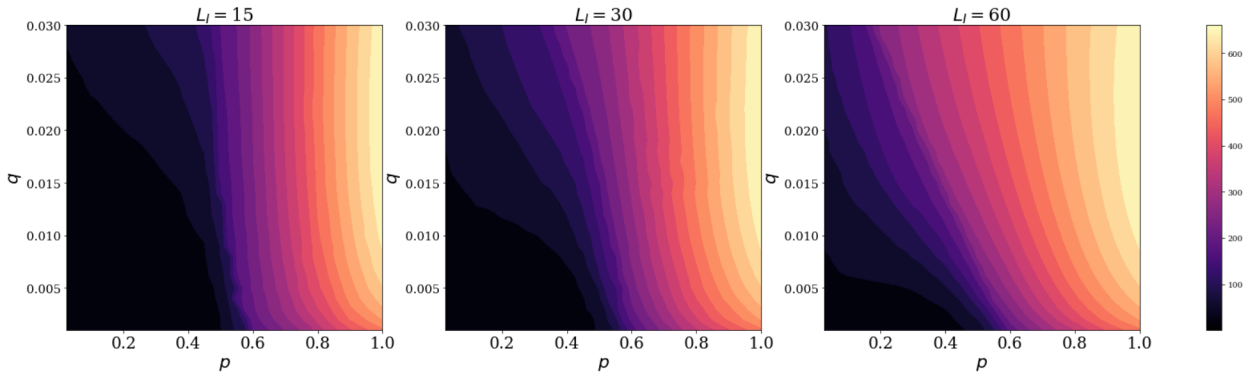

(a)

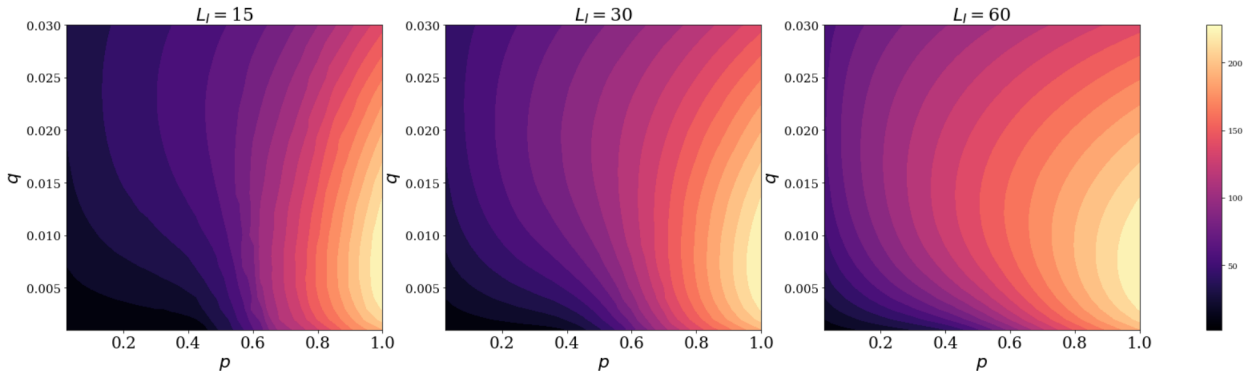

(b)

FIGURE 3.16. Plots of the AIAT for the prevalence-dependent intervention on the (a) small world network and (b) power law network with clustering for $R_0 = 2.4, \eta = 0.2, \gamma = 0.1$ and a fixed $L_R = 90$.

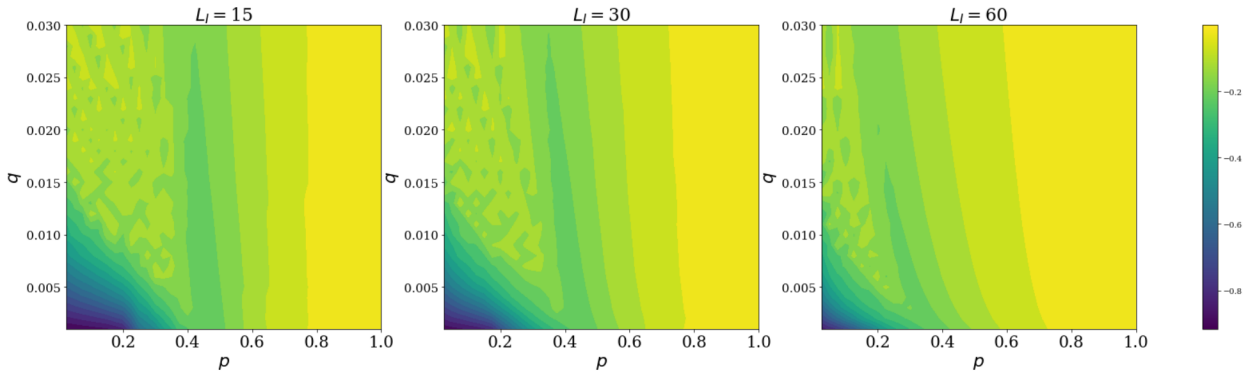

(a)

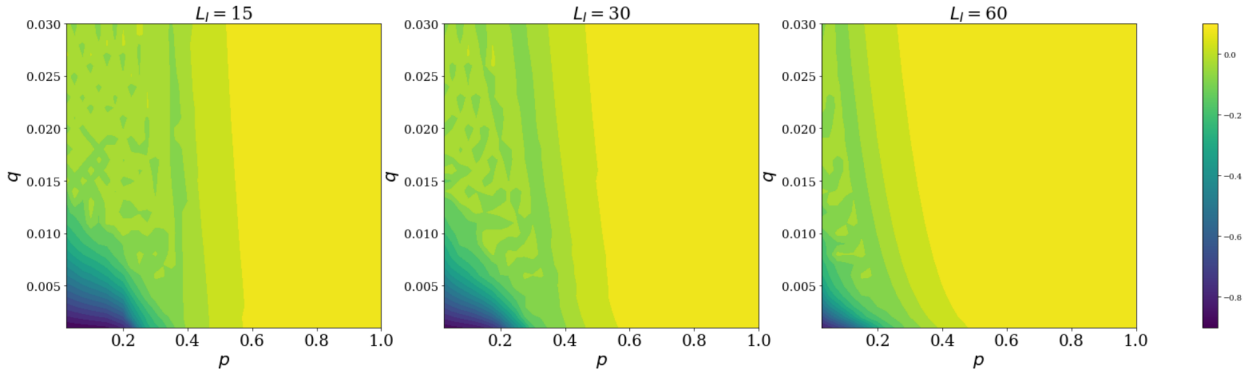

(b)

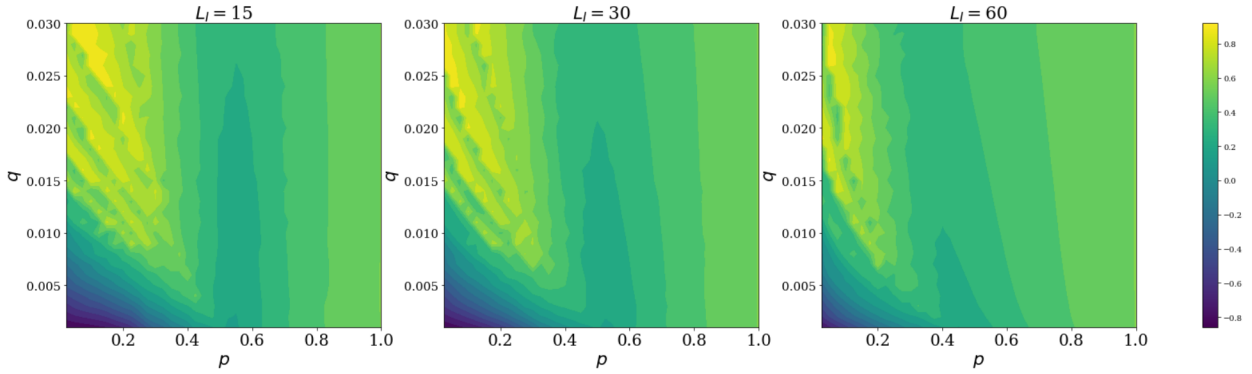

(c)

FIGURE 3.17. Plots of the RCFS for the prevalence-dependent intervention on the (a) unipartite projection network, (b) small world network and (c) power law network with clustering for $R_0 = 5, \eta = 0.2, \gamma = 0.1$ and a fixed $L_R = 90$.

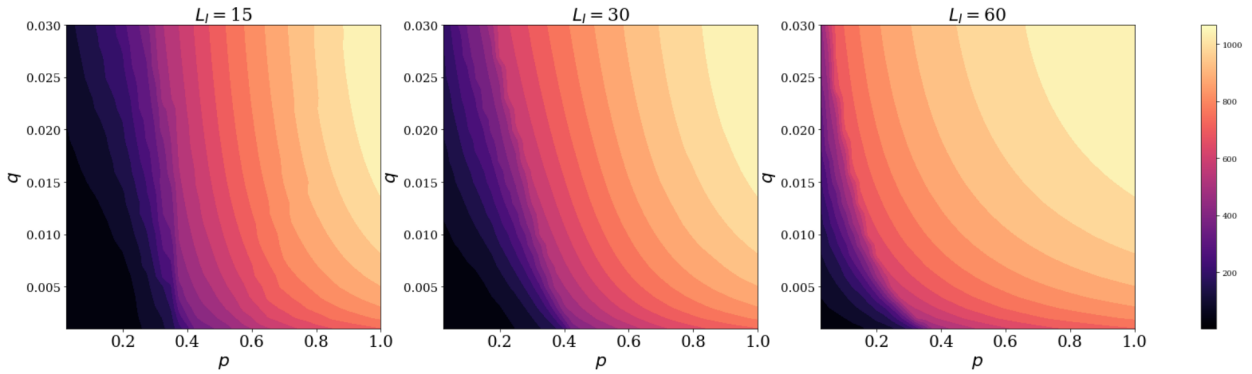

(a)

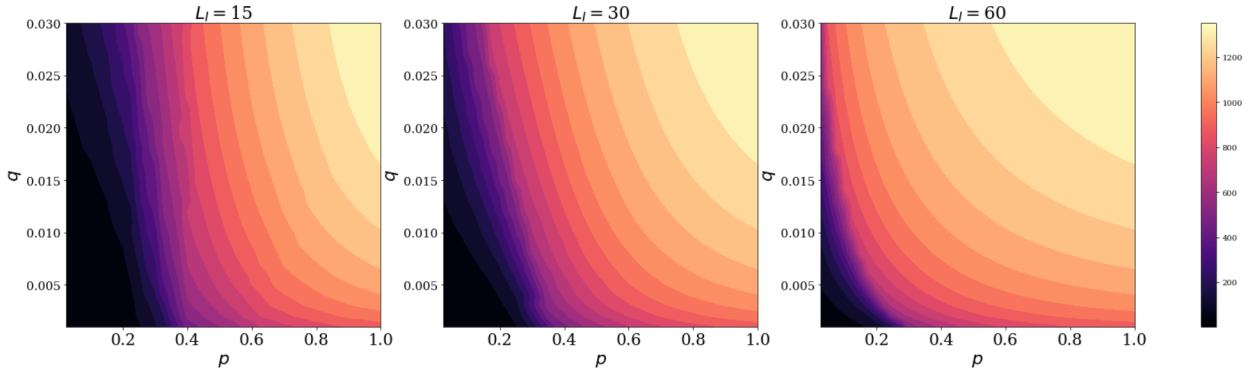

(b)

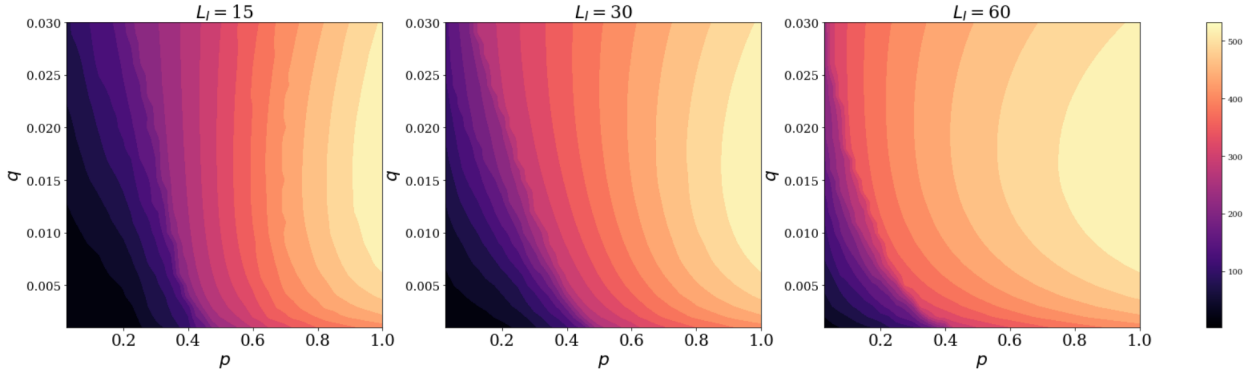

(c)

FIGURE 3.18. Plots of the AIAT for the prevalence-dependent intervention on the (a) unipartite projection network, (b) small world network and (c) power law network with clustering for $R_0 = 5, \eta = 0.2, \gamma = 0.1$ and a fixed $L_R = 90$.

CHAPTER 4

A Simple Dynamic Process on Bipartite Networks

4.1. Introduction

Network models have made a significant impact on the epidemiological modeling landscape in the past two decades (Kiss et al., 2017; Pastor-Satorras et al., 2015). The network (a collection of nodes and edges) considered is often a contact network, where individuals are represented by nodes and potential disease-transmitting contacts are represented by edges. Pairwise models (Eames and Keeling, 2002; Keeling, 1999) form a prominent family of models of epidemics on networks. The models consider the number of individuals (nodes) in each state, but also the number of pairs, triples, and higher-order motifs, leading to large systems of ordinary differential equations. A common approach used to reduce the number of equations is to employ a triple closure—that is, an approximation of the number of triples in a given state in terms of individuals, pairs, and non-epidemic network quantities. The most fundamental pairwise models assume that the number of nodes and the edges connecting them do not change over time, or that the network is 'static". Intuitively, however, during an epidemic changing contacts can be just as dynamic as disease spreading. In recent years, an effort has been made to integrate the effects of disease dynamics and network dynamics into cohesive models.

Dynamic or 'adaptive" network models (Gross and Blasius, 2008) consider disease dynamics on the network, as well as the time-evolution of the network itself and crucially the interaction between the two processes. A variety of network dynamic processes have been proposed. One of the first adaptive network processes was an edge-rewiring model (Gross et al., 2006), where susceptible-infectious edges were randomly rewired to create a new susceptible- susceptible edge at a constant rate. This rewiring process was extended to occur with infectious-infectious edges as well in Scarpino et al. (2016), a process known as 'relational exchange." Another intuitive dynamic process is random link activation/deletion (Kiss et al., 2012), abbreviated RLAD, where

edges in the network are randomly activated (added) or deleted (removed) at separate constant rates. The RLAD process has been extended to the case of a fixed network (Shkarayev et al., 2014; Tunc et al., 2013), where susceptible-infectious edges can temporarily deactivate and reactivate when they are susceptible-susceptible. The fundamental network dynamic process in each of these models takes place at the level of an individual edge in the contact network. Thus, the dynamic process models individual behavior change in response to the condition of their contacts. In this chapter, we present an alternative perspective on individual behavior change which relies on a bipartite network structure underlying the contact network.

The use of a bipartite network to produce a contact network on which an epidemic spreads has been used in both agent-based simulations (Eubank et al., 2004) and theoretical models (Newman, 2003). Here, the two bipartite sets represent individuals and either locations or groups where individuals interact and contact each other. The bipartite network, which we refer to as the bipartite mixing network, is then projected onto the set of nodes representing individuals resulting in a unipartite network which we refer to as the contact network. Essential properties of the contact network can be recovered from the bipartite network using probability generating functions (Newman et al., 2001). The inherently dynamic nature of bipartite mixing networks has received recent attention due to the availability of mobile phone mobility data (Chang et al., 2021), and warrants further attention from a modeling perspective. While the contact network can evolve through time due to changes in individual behavior, it can also change due to large-scale public health interventions such as school or business closures, lockdowns, and social distancing policies, or simply seasonal changes in mobility patterns. These changes are reflected at the bipartite level, with the motivating concept being that rather than individuals ad or delete their connection to mixing locations, rather than adding or deleting contacts with other individuals. To accommodate this change, we extend the RLAD process to occur on the bipartite mixing network rather than the unipartite contact network—a process we term bipartite random link activation deletion (BRLAD). When coupled with disease dynamics, this results in a model where the epidemic dynamics occur on the contact network, and the contact network dynamics are the result of a dynamic process in the bipartite mixing network.

Aside from more general questions of modeling epidemic spread, adaptive networks can be naturally applied to questions of seasonally-forced diseases. The periodic time series of childhood infectious diseases such as measles and mumps (London and Yorke, 1973) as well as respiratory diseases such as influenza (Dushoff et al., 2004) have all been investigated using seasonally-forced epidemic models. Changes to weather and social behavior (London and Yorke, 1973) or other factors (Dushoff et al., 2004) have been proposed as drivers of the observed periodicity. From a modeling perspective, the adoption of a time-varying transmission rate has been the predominant mechanism of seasonal forcing. Such transmission rates often take on a sinusoidal (Dietz, 1976) or piecewise-constant form (Earn, 2000). Adaptive network models offer the potential to treat the seasonality of transmission and mobility separately, as social behavior processes are explicitly described alongside disease transmission. To this end, we consider simple sinusoidal seasonal rate functions for activation on top of the more traditional seasonal transmission rate, and investigate the effects as the varying magnitudes of seasonality interact.

In this chapter, we introduce and analyze the BRLAD process coupled with SIS disease dynamics on the contact network. We then apply the model to a seasonally-forced epidemic, examining the interaction of multiple mechanisms for periodicity. In Section 2, we describe the BRLAD process and derive evolution equations for important network quantities using a probability generating function approach. These equations are coupled with a pairwise SIS model to create the full SIS with BRLAD model, which is validated by simulations. In Section 3, we analyze the model, looking at its bifurcation structure as well as the effects of differing timescales in the disease and network dynamics. In Section 4, we consider seasonal activation, deletion, and transmission rates and their effect on periodic epidemic dynamics. Finally, in Section 5 we discuss some implications of the model and potential future directions of modeling bipartite-level network dynamics.

4.2. Model Construction

We begin construction of the SIS with BRLAD model by considering a bipartite mixing network where the two sets of nodes represent individuals and mixing locations. Disease dynamics play out on the unipartite projection of the bipartite network onto the set of individuals, which we call the contact network. Our network dynamic process, however, plays out on the bipartite network:

edges in the bipartite network are activated at rate α and deleted at rate ω. To understand the effect of the network dynamics on disease dynamics, we have to understand the resulting process on the contact network. Using probability generating functions, we can determine the how important network parameters evolve over time. After the evolution equations for the network parameters are derived, we follow the approach of Gross et al. (2006) and Kiss et al. (2012) to construct the coupled model: we find equations for edges in the presence of static node labels, and finally combine the network and disease dynamics into a single model.

4.2.1. Network Dynamics. Let $\mathcal{A}$ and $\mathcal{B}$ be the left and right sets of nodes in the time-evolving bipartite mixing network, where $\mathcal{A} = N$ and $\mathcal{B} = M$. Let the degree distribution probability generating functions (PGFs) for $\mathcal{A}$ and $\mathcal{B}$ respectively be given by:

$$A(x, t) = \sum_{k=0}^{M} a_k(t) x^k, \tag{4.1}$$

$$B(x, t) = \sum_{k=0}^{N} b_k(t) x^k. \tag{4.2}$$

There are many important properties of PGFs. One of particular interest to the current question is that the first moment can be recovered by differentiating and setting $x = 1$. In the succeeding text, we will use the subscript notation (rather than Leibniz notation) for partial derivatives to make the equations more readily readable. Let $\langle k_A \rangle$ and $\langle k_B \rangle$ denote the average degree of the sets $\mathcal{A}$ and $\mathcal{B}$ respectively. Then, $\langle k_A \rangle(t) = A_x(1, t)$ and $\langle k_B \rangle(t) = B_x(1, t)$. Higher moments can be obtained through a similar process using higher derivatives. Bipartite networks have the useful property that both sets of nodes are connected to each other by the same number of edges. This can be expressed in terms of average degree as

$$N\langle k_A \rangle(t) = M\langle k_B \rangle(t). \tag{4.3}$$

Ultimately, we are interested in the moments of the degree distribution for the contact network, as that is what will affect disease dynamics. From Newman et al. (2001), we get the PGF for the

degree distribution of the unipartite contact network (modified for time-dependence):

$$G(x,t) = A\left(\frac{B_x(x,t)}{B_x(1,t)}, t\right) \tag{4.4}$$

Two key network quantities can be recovered from this PGF: the average degree of the contact network $\langle k \rangle$ and the average number of connected triples per node $\langle k^2 - k \rangle$. In terms of the PGF, we have

$$\langle k \rangle(t) = G_x(1,t), \tag{4.5}$$

$$\langle k^2 - k \rangle(t) = G_{xx}(1,t). \tag{4.6}$$

To facilitate the derivation of evolution equations for $\langle k \rangle$ and $\langle k^2 - k \rangle$, it will be useful to characterize G_x and G_{xx} in terms of A, B and their derivatives.

$$G_x(1,t) = \frac{M}{N} B_{xx}(1,t), \tag{4.7}$$

$$G_{xx}(1,t) = A_{xx}(1,t)\left(\frac{G_x(1,t)}{A_x(1,t)}\right)^2 + \frac{M}{N} B_{xxx}(1,t). \tag{4.8}$$

Another crucial network quantity to consider for the contact network is the clustering coefficient ϕ, which is defined as the ratio of triangles to connected triples in a network. In the case of a unipartite projection from a bipartite network, Newman et al. (2001) give an expression for the clustering coefficient, which can be modified for time dependence as

$$\phi(t) = \frac{M}{N} \frac{B_{xxx}(1,t)}{G_{xx}(1,t)}. \tag{4.9}$$

One insight from the forms of (4.7),(4.8), and (4.9) is that the dynamical equations for $\langle k \rangle$, $\langle k^2 - k \rangle$, and ϕ can be derived from dynamical equations for A, B and their derivatives (with respect to x). For simplicity, we will often not write the dependence on t, as all terms depend on t. As well, we also drop the dependence on x when $x = 1$; for instance, $B_x(1,t) = B_x$.

From Kiss et al. (2012), we know that under the RLAD process, the PGF of the degree distribution of a network obeys a simple partial differential equation for activation rate α and deletion rate ω. In our characterization of BRLAD (Fig. 4.1), the bipartite network is altered using RLAD,

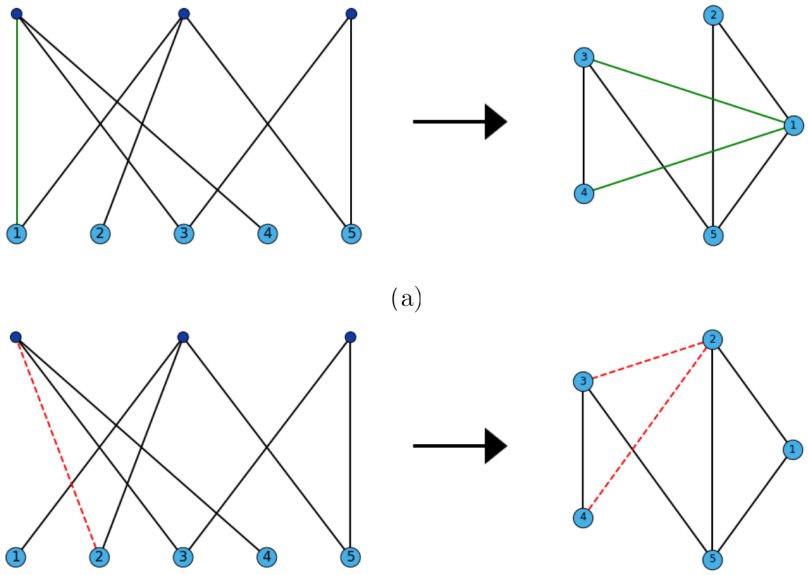

FIGURE 4.1. Schematic of the bipartite random link activation/deletion (BRLAD) process. Link activation (a) is shown in green, while link deletion (b) is shown in red.

so the equations for the PGFs A and B are readily found.

$$A_t(x,t) = (1-x)\left((\alpha x+\omega)A_x(x,t) - \alpha M A(x,t)\right), \tag{4.10}$$

$$B_t(x,t) = (1-x)\left((\alpha x+\omega)B_x(x,t) - \alpha N B(x,t)\right). \tag{4.11}$$

From these we can derive equations for the higher derivatives of A and B. It can be shown through induction that these equations are

$$\begin{aligned}\frac{\partial^k A_t(x,t)}{\partial x^k} &= k\alpha(M-(k-1))\frac{\partial^{k-1}A}{\partial x^{k-1}} - k(\alpha x+\omega)\frac{\partial^k A}{\partial x^k} \\ &\quad - (1-x)\left(\alpha(M-k)\frac{\partial^k A}{\partial x^k} - (\alpha x+\omega)\frac{\partial^{k+1}A}{\partial x^{k+1}}\right),\end{aligned} \tag{4.12}$$

$$\begin{aligned}\frac{\partial^k B_t(x,t)}{\partial x^k} &= k\alpha(N-(k-1))\frac{\partial^{k-1}B}{\partial x^{k-1}} - k(\alpha x+\omega)\frac{\partial^k B}{\partial x^k} \\ &\quad - (1-x)\left(\alpha(N-k)\frac{\partial^k B}{\partial x^k} - (\alpha x+\omega)\frac{\partial^{k+1}B}{\partial x^{k+1}}\right).\end{aligned} \tag{4.13}$$

Evaluating at $x = 1$ yields

$$\frac{\partial^k A_t}{\partial x^k} = k\alpha(M - (k-1))\frac{\partial^{k-1} A}{\partial x^{k-1}} - k(\alpha+\omega)\frac{\partial^k A}{\partial x^k} \tag{4.14}$$

$$\frac{\partial^k B_t}{\partial x^k} = k\alpha(N - (k-1))\frac{\partial^{k-1} B}{\partial x^{k-1}} - k(\alpha+\omega)\frac{\partial^k B}{\partial x^k}. \tag{4.15}$$

Now, we differentiate (4.7) with respect to t and apply (4.15) and (4.3) to obtain

$$G_{xt} = 2\alpha(N-1)A_x - 2(\alpha+\omega)G_x. \tag{4.16}$$

Notably, this partial differential equation depends on A_x as well as G_x, and we will need an evolution equation for A_x for the full system describing our network dynamics. We now differentiate (4.8) with respect to t, and apply (4.14),(4.15),(4.16) and simplify to obtain

$$\begin{aligned} G_{xxt} = &\left(4\alpha(N-1)\frac{A_x}{G_x} - 2\alpha\frac{M}{A_x} - 4(\alpha+\omega)\right)\left(G_{xx} - \frac{M}{N}B_{xxx}\right) - 3(\alpha+\omega)\frac{M}{N}B_{xxx} \\ &+ 2\alpha(M-1)\frac{G_x^2}{A_x} + 3\alpha(N-2)G_x. \end{aligned} \tag{4.17}$$

We note that though B_{xxx} is present in (4.17), we will not need an additional dynamical equation, as B_{xxx} can be expressed in terms of G_{xx} and ϕ. Finally, we turn our attention to the dynamical equation for ϕ. Differentiating (4.9) yields

$$\begin{aligned} \dot{\phi} = &\left(3\alpha(N-2)\frac{G_x}{G_{xx}} - \left(4\alpha(N-1)\frac{A_x}{G_x} - 2\alpha\frac{M}{A_x} - (\alpha+\omega)\right)\phi\right)(1-\phi) \\ &- 2\alpha(M-1)\frac{G_x^2}{A_x G_{xx}}\phi. \end{aligned} \tag{4.18}$$

Substituting in the appropriate network parameters, equations (4.14), (4.16), (4.17), and (4.18), we get the dynamical equations for the network parameters:

$$\dot{\langle k_A \rangle} = \alpha M - (\alpha + \omega)\langle k_A \rangle, \tag{4.19}$$

$$\dot{\langle k \rangle} = 2\alpha(N-1)\langle k_A \rangle - 2(\alpha + \omega)\langle k \rangle, \tag{4.20}$$

$$\begin{aligned}\dot{\langle k^2 - k \rangle} = &\left(4\alpha(N-1)\frac{\langle k_A \rangle}{\langle k \rangle} - 2\alpha\frac{M}{\langle k_A \rangle} - 4(\alpha+\omega)\right)\langle k^2 - k \rangle(1-\phi) \\ &- 3(\alpha+\omega)\langle k^2 - k \rangle\phi + 2\alpha(M-1)\frac{\langle k \rangle^2}{\langle k_A \rangle} + 3\alpha(N-2)\langle k \rangle,\end{aligned} \tag{4.21}$$

$$\begin{aligned}\dot{\phi} = &\left(3\alpha(N-2)\frac{\langle k \rangle}{\langle k^2 - k \rangle} - \left(4\alpha(N-1)\frac{\langle k_A \rangle}{\langle k \rangle} - 2\alpha\frac{M}{\langle k_A \rangle} - (\alpha+\omega)\right)\phi\right)(1-\phi) \\ &- 2\alpha(M-1)\frac{\langle k \rangle^2}{\langle k_A \rangle\langle k^2 - k \rangle}\phi.\end{aligned} \tag{4.22}$$

In the case of constant rates α and ω, the network quantities can be expressed explicitly as functions of time. Perhaps the most straightforward way of doing this is to solve (4.14) and (4.15) successively and substitute into (4.7), (4.8), and (4.9). Moreover, with constant α and ω, the steady-state values of the network parameters can be easily found.

$$\langle k_A \rangle^* = \frac{\alpha M}{\alpha + \omega}, \tag{4.23}$$

$$\langle k \rangle^* = \frac{\alpha^2 M(N-1)}{(\alpha+\omega)^2}, \tag{4.24}$$

$$\langle k^2 - k \rangle^* = \frac{\alpha^3 M(N-1)(N-2)}{(\alpha+\omega)^3}\left(1 + \frac{\alpha}{\alpha+\omega}\frac{N-1}{N-2}(M-1)\right), \tag{4.25}$$

$$\phi^* = \frac{1}{1 + \frac{\alpha}{\alpha+\omega}\frac{N-1}{N-2}(M-1)}. \tag{4.26}$$

To demonstrate the validity of this model, we test it against numerical simulations (Fig. 4.2). To construct a bipartite mixing network, we use a configuration model-like algorithm (Molloy and Reed, 1995) to connect stubs from the left and right sets of nodes, both of which have Poisson degree distributions. We take $N = 100, M = 25$ and $\langle k_A \rangle(0) = 3.62$, which sufficiently determine both degree distributions. The corresponding contact network shows considerable degree heterogeneity and clustering, with $\langle k \rangle(0) = 53.5, \langle k^2 - k \rangle(0) = 3637.4$, and $\phi(0) \approx 0.22$. The activation and deletion rates considered are $\alpha = 0.005$ and $\omega = 0.1$. Clearly, the model equations (4.19)-(4.22) are in excellent agreement with the simulations, even on a relatively small network.

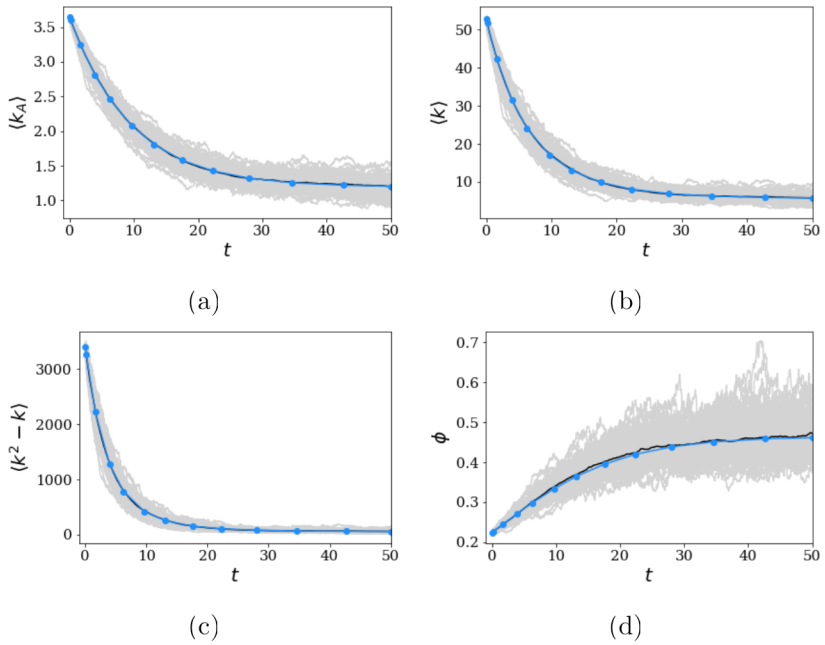

FIGURE 4.2. Comparison of the model against simulations. One hundred trials were run on a bipartite network with Poisson degree distributions and $N = 100, M = 25$, and $\langle k_A \rangle(0) = 3.62$. The initial corresponding contact network parameters were $\langle k \rangle(0) = 53.5, \langle k^2 - k \rangle(0) = 3637.4, \phi(0) \approx 0.22$. Activation and deletion rates are $\alpha = 0.005, \omega = 0.1$. Individual simulations are shown in light gray, with the mean in black. Model results (blue circles) are shown for (a) $\langle k_A \rangle(t)$, (b) $\langle k \rangle(t)$, (c) $\langle k^2 - k \rangle(t)$ and (d) $\phi(t)$.

4.2.2. Disease Dynamics. With the network dynamics described for both the bipartite mixing network and the unipartite contact network, we turn our attention to the disease dynamics that unfold on the contact network. The interaction between the network and disease dynamics on an epidemic can be challenging to describe. Our approach here differs slightly from that of Gross et al. (2006) and Kiss et al. (2012). When describing the network dynamics in the presence of node labeling, both allow for the network dynamics to differ for each edge type. This allows for a more general model, as well as allowing for more feedback between the network and disease dynamics. With BRLAD, this is more complicated: since the network dynamics fundamentally occur in the bipartite mixing network, any status-dependent rates would have to depend on the node state of the individual. The edge dynamics in the contact network would be more complicated, and thus we do not attempt to consider that case here. Instead, we simply consider the effects of the rates α and ω on the evolution of edge types in the contact network.

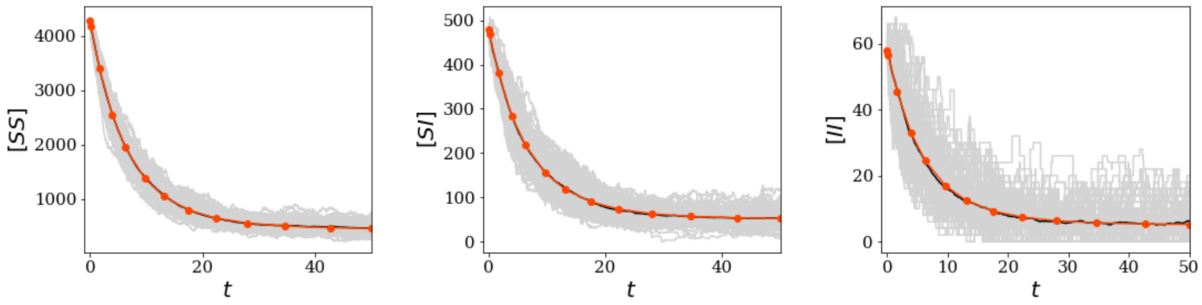

(a) (b) (c)

FIGURE 4.3. Comparison of the model results (orange circles) for (a) $[SS](t)$, (b) $[SI](t)$, and (c) $[II](t)$ without disease dynamics against simulations. Initial conditions are $[SS](0) = 4044$, $[SI](0) = 485$, and $[II](0) = 58$. One hundred trials were run on a bipartite network with Poisson degree distributions and $N = 100$, $M = 25$, and $\langle k_A \rangle(0) = 3.62$. The initial corresponding contact network parameters were $\langle k \rangle(0) = 53.5$, $\langle k^2 - k \rangle(0) = 3637.4$, $\phi(0) \approx 0.22$. Activation and deletion rates are $\alpha = 0.005, \omega = 0.1$. Individual simulations are shown in light gray, with the mean in black.

Looking forward to the epidemic model, we suppose the nodes in set $\mathcal{A}$ representing individuals have labels S or I, so the resulting edge types in the contact network are SS, SI, and II. An exact derivation of the evolution equations for the edge types would require complicated calculations with the Kolmogorov equations. Instead, we heuristically write down the mean field edge evolution equations:

$$\dot{[SS]} = 2\alpha[S](|S| - 1)\langle k_A \rangle - 2(\alpha + \omega)[SS], \tag{4.27}$$

$$\dot{[SI]} = 2\alpha[S][I]\langle k_A \rangle - 2(\alpha + \omega)[SI], \tag{4.28}$$

$$\dot{[II]} = 2\alpha[I](|I| - 1)\langle k_A \rangle - 2(\alpha + \omega)[II]. \tag{4.29}$$

Notably, (4.27)-(4.29) satisfy the desired edge conservation relation $\dot{[SS]} + 2\dot{[SI]} + \dot{[II]} = N\dot{\langle k \rangle}$. For validation, we compare the model to numerical simulations (Fig. 4.3) on the same adaptive network described in Section 4.2.1, and clearly the agreement is excellent.

Next, we turn our attention to the disease dynamics. Our starting point is the full pairwise model for an SIS disease on a static network (Eames and Keeling, 2002):

$$|\dot{S}] = -\beta|SI] + \gamma|I] \tag{4.30}$$

$$|\dot{I}] = \beta|SI] - \gamma|I] \tag{4.31}$$

$$|\dot{SS}] = -2\beta|SSI] + 2\gamma|SI] \tag{4.32}$$

$$|\dot{SI}] = \beta(|SSI] - |ISI] - |SI]) + \gamma(|II] - |SI]) \tag{4.33}$$

$$|\dot{II}] = 2\beta(|ISI] + |SI]) - 2\gamma|II] \tag{4.34}$$

As is typical of pairwise models, the full pairwise SIS model requires tracking the expected number of susceptible and infectious nodes ($|S], |I]$) and the expected number of susceptible-susceptible, susceptible-infectious, and infectious-infectious pairs ($|SS], |SI], |II]$). The equations for the pairs depend on triples $|SSI]$ and $|ISI]$, and the evolution equations for triples in turn depend on higher-order motifs. As such, the full model is prohibitively large, and we take the common approach of closing the system at the triple level using an approximation. In this case, we use the heterogeneous, clustered approximation introduced in Chapter 3:

$$|ASI] = \frac{\langle k^2 - k\rangle}{\langle k\rangle^2}\frac{|AS]|SI]}{|S]}\left(1 - \phi + \phi\frac{N}{\langle k\rangle}\frac{|AI]}{|A]|I]}\right). \tag{4.35}$$

The incorporation of the clustering coefficient in the triple approximation here is influenced by the nature of the unipartite projection—many choices of degree distribution for the bipartite mixing network lead to nontrivial clustering in the contact network. Moreover, the BRLAD dynamics of the three network parameters in this approximation ($\langle k\rangle, \langle k^2 - k\rangle, \phi$) can be tracked by including (4.19)-(4.22) in the full coupled model. Thus, by combining (4.30)-(4.34) with (4.19)-(4.22) and

augmenting (4.32)-(4.34) with (4.27)-(4.29), we arrive at the SIS model with BRLAD dynamics[1]:

$$|\dot{S}] = -\beta|SI] + \gamma|I] \tag{4.36}$$

$$|\dot{I}] = \beta|SI] - \gamma|I] \tag{4.37}$$

$$|\dot{SS}] = -2\beta|SSI] + 2\gamma|SI] + 2\alpha|S](|S] - 1)\langle k_A\rangle - 2(\alpha+\omega)|SS] \tag{4.38}$$

$$|\dot{SI}] = \beta(|SSI] - |ISI] - |SI]) + \gamma(|II] - |SI]) + 2\alpha|S]|I]\langle k_A\rangle - 2(\alpha+\omega)|SI] \tag{4.39}$$

$$|\dot{II}] = 2\beta(|ISI] + |SI]) - 2\gamma|II] + 2\alpha|I](|I] - 1)\langle k_A\rangle - 2(\alpha+\omega)|II] \tag{4.40}$$

$$\langle\dot{k_A}\rangle = \alpha M - (\alpha+\omega)\langle k_A\rangle, \tag{4.41}$$

$$\langle\dot{k}\rangle = 2\alpha(N-1)\langle k_A\rangle - 2(\alpha+\omega)\langle k\rangle, \tag{4.42}$$

$$\begin{aligned}\langle\dot{k^2 - k}\rangle = &\left(4\alpha(N-1)\frac{\langle k_A\rangle}{\langle k\rangle} - 2\alpha\frac{M}{\langle k_A\rangle} - 4(\alpha+\omega)\right)\langle k^2 - k\rangle(1-\phi)\\ &- 3(\alpha+\omega)\langle k^2-k\rangle\phi + 2\alpha(M-1)\frac{\langle k\rangle^2}{\langle k_A\rangle} + 3\alpha(N-2)\langle k\rangle,\end{aligned} \tag{4.43}$$

$$\begin{aligned}\dot{\phi} = &\left(3\alpha(N-2)\frac{\langle k\rangle}{\langle k^2-k\rangle} - \left(4\alpha(N-1)\frac{\langle k_A\rangle}{\langle k\rangle} - 2\alpha\frac{M}{\langle k_A\rangle} - (\alpha+\omega)\right)\phi\right)(1-\phi)\\ &- 2\alpha(M-1)\frac{\langle k\rangle^2}{\langle k_A\rangle\langle k^2-k\rangle}\phi,\end{aligned} \tag{4.44}$$

where the triple approximation for $|SSI]$ and $|ISI]$ is given by (4.35). This model performs quite well when compared to simulations, even for a relatively small network. Figure 4.4 shows a comparison of the model results for $[I](t)$ against simulations on the adaptive network described in Section 4.2.1 with the epidemiological parameters $\beta = 0.05$ and $\gamma = 0.1$. In the following section, we will analyze the SIS with BRLAD model, exploring the effects of BRLAD on the qualitative behavior of the prevalence curve and the nontrivial endemic equilibrium, when it exists. In Section 4.4, we turn our attention to investigating how periodic activation/deletion rates affect epidemic dynamics, and how they interact with periodic (seasonal) transmission rates.

[1]The SIS with BRLAD model (4.36)-(4.44) can be easily altered to give the SIR dynamics. By eliminating the $+\gamma|I]$ term from (4.36), the $+2\gamma|SI]$ term from (4.38), and the $+\gamma|II]$ from (4.39), the SIR with BRLAD dynamics can be recovered (along with the conservation relation $|S] + |I] + |R] = N$).

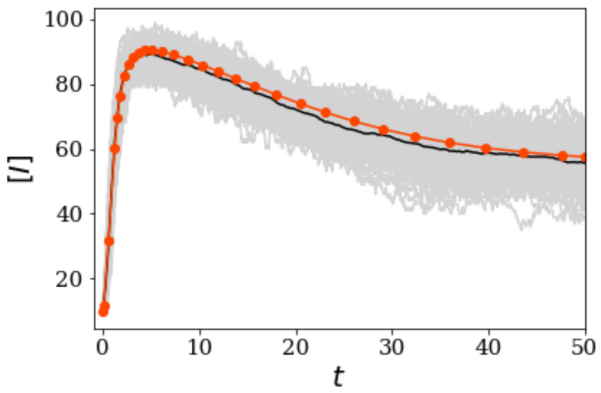

FIGURE 4.4. Comparison of the model results (orange circles) for $[I](t)$ against simulations. Initial conditions are $[S](0) = 90, [I](0) = 10, [SS](0) = 4044, [SI](0) = 485$, and $[II](0) = 58$. Epidemiological parameters are $\beta = 0.05$ and $\gamma = 0.1$. One hundred trials were run on a bipartite network with Poisson degree distributions and $N = 100, M = 25$, and $\langle k_A \rangle(0) = 3.62$. The initial corresponding contact network parameters are $\langle k \rangle(0) = 53.5, \langle k^2 - k \rangle(0) = 3637.4, \phi(0) \approx 0.22$. Activation and deletion rates are $\alpha = 0.005, \omega = 0.1$. Individual simulations are shown in light gray, with the mean in black.

4.3. Analysis of the SIS with BRLAD model

In this section, we analyze the SIS with BRLAD model (4.36)-(4.44) from a dynamical systems perspective. Network models of SIS-type diseases on static networks are well understood (Kiss et al., 2017), and many adaptive network SIS models have been thoroughly analyzed as well (Gross et al., 2006; Kiss et al., 2012). With the adaptive network models, particular attention has been paid to link-status-dependent network dynamic rates. The feedback in these models can produce behavior such as bistability and limit cycles. However, the SIS with BRLAD model as introduced in Section 4.2.2 exhibits bifurcation behavior much more akin to a static SIS model. Despite this, the coupling of SIS dynamics and BRLAD dynamics introduces rich qualitative behavior with the prevalence curve, which depends on the relative timescales of the disease dynamics and the network dynamics.

Our numerical investigation of the system at steady state suggests the following classic SIS model behavior: the existence of a disease-free steady state ($[S] = N, [I] = 0, [SS] = N\langle k \rangle, [SI] = 0, [II] = 0$) which loses stability as β increases through a bifurcation point (known as the epidemic threshold), at which point a stable equilibrium emerges (known as the endemic equilibrium). Figure

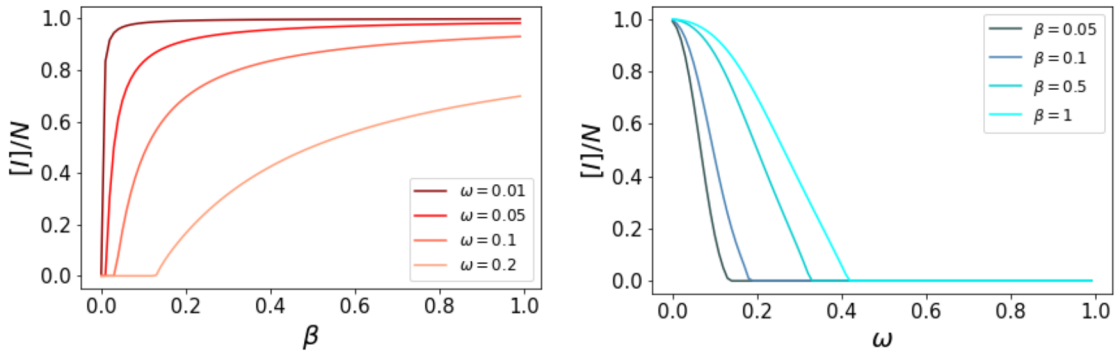

(a) (b)

FIGURE 4.5. Bifurcation diagrams for the parameters (a) β and (b) ω with $\alpha = 0.01$ and $\gamma = 1$ fixed. Stable branches of equilibria are solid, unstable branches not shown. $N = 100$ and $M = 25$ for the underlying bipartite mixing network.

4.5a shows the stable branches of equilibria as β varies and for several values of ω, while α and γ are fixed. As expected, β and ω have opposing effects on the progression of the disease. As the deletion rate ω increases, a higher transmission rate β is required for the disease to persist, and the epidemic threshold increases. On the other hand, as ω decreases the epidemic threshold vanishes, though we note that for fixed α decreasing ω will lead to an increasingly connected network facilitating disease spread. Figure 4.5b shows the stable equilibria as ω varies and for various values of β. Notably, for the parameter combinations shown, even small changes to ω can lead to drastically different endemic equilibria and even disease extinction—an observation that may have important public health implications. However, it is important to note that while some parameter combinations may lead to similar behavior at steady state, the varying timescales of the network and disease dynamic processes may lead to outbreaks with qualitatively different prevalence.

Following Kiss et al. (2012), we consider three possible regimes of relative timescales: slow network dynamics relative to disease dynamics, comparable timescales, and fast network dynamics relative to disease dynamics. We will refer to these as the slow, comparable, and fast regimes respectively. We also consider effects of starting network parameters by looking at the model under two different bipartite mixing networks. In the first case, both individuals and mixing locations have Poisson degree distributions (Fig. 4.6, solid), and in the second case, both individuals and mixing locations have geometric degree distributions (Fig. 4.6, dashed). The distributions are

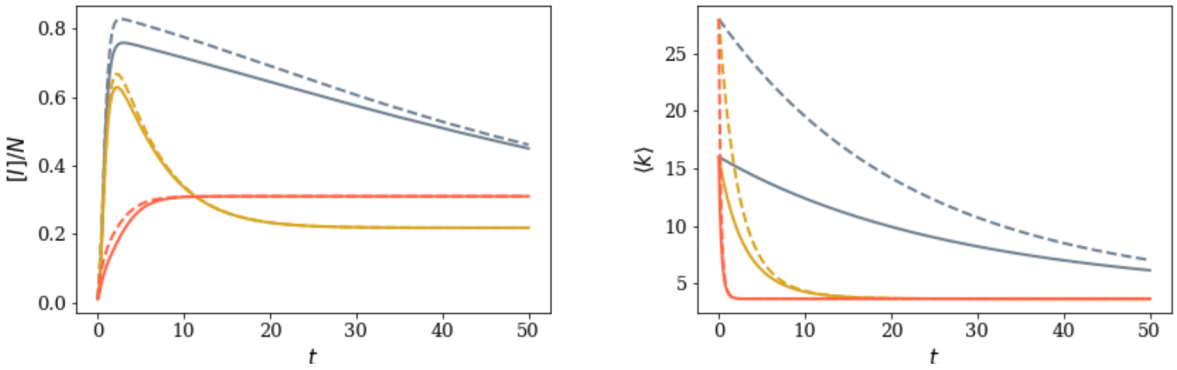

(a) (b)

FIGURE 4.6. Plots of (a) the prevalence $[I]/N$ and (b) the average contact network degree $\langle k \rangle$ under the slow, comparable, and fast network dynamic regimes. The epidemiological parameters in both cases are $\beta = 0.4, \gamma = 1$. The slow regime (blue) parameters are $\alpha = 0.001, \omega = 0.025$. The comparable regime (gold) parameters are $\alpha = 0.01, \omega = 0.25$. The fast regime (red) parameters are $\alpha = 0.1, \omega = 2.5$. Results for two starting bipartite mixing networks are shown: $\mathcal{A}$ and $\mathcal{B}$ both with Poisson degree distributions (solid) and $\mathcal{A}$ and $\mathcal{B}$ with geometric distributions (dashed). For both, $N = 100, M = 25$, and $\langle k_A \rangle(0) = 2$. The initial network parameters for the Poisson-Poisson network are $\langle k \rangle(0) = 16, \langle k^2 - k \rangle(0) = 384$, and $\phi(0) = 1/3$ and for the geometric-geometric network they are $\langle k \rangle(0) = 28, \langle k^2 - k \rangle(0) = 1372, \phi(0) = 0.6$.

chosen so that $\langle k_A \rangle$ is the same for both cases, which results in higher initial values for $\langle k \rangle, \langle k^2 - k \rangle$, and ϕ for the geometric case. In the slow regime, network parameters converge to equilibrium much more slowly than the prevalence reaches its static endemic equilibrium. The effect of this is a slow correction, which for some values of α and ω can eventually drive an otherwise stable epidemic to extinction in the long run. In the comparable regime, the initial epidemic spread is more prominently affected, which can result in a qualitatively different prevalence curve. In the fast regime, the equilibrium values of the network parameters are reached quickly—effectively before the epidemic has a chance to spread. In effect, the epidemic essentially spreads on a static network. These regimes capture essentially the same behavior as that of the RLAD dynamics in Kiss et al. (2012). As such, a relevant question is whether or not 'similar" BRLAD and RLAD processes result in similar epidemics. To investigate, we consider two epidemics on the same contact network generated from a bipartite mixing network. We note that the triple closure (4.35) is used for a more direct comparison of both models, and the network evolution equations required for

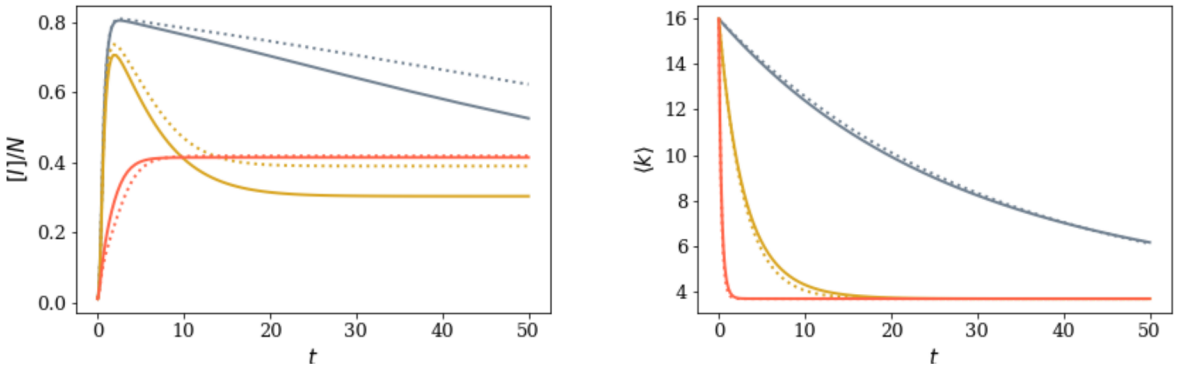

(a) (b)

FIGURE 4.7. Plots of (a) the prevalence $[I]/N$ and (b) the average contact network degree $\langle k \rangle$ for similar BRLAD (solid) and RLAD (dotted) processes under the slow (blue), comparable (gold), and fast (red) network dynamic regimes. The epidemiological parameters are $\beta = 0.4, \gamma = 1$. The BRLAD network dynamic parameters are slow: $\alpha = 0.001, \omega = 0.025$; comparable: $\alpha = 0.01, \omega = 0.25$; fast: $\alpha = 0.1, \omega = 2.5$. The RLAD network dynamic parameters are slow: $\alpha = 0.0012, \omega = 0.03125$; comparable: $\alpha = 0.013, \omega = 0.339$; fast: $\alpha = 0.13, \omega = 3.39$. The initial network parameters for the bipartite mixing network are $N = 100, M = 25$, and $\langle k_A \rangle(0) = 2$, and the initial network parameters for both contact networks are $\langle k \rangle(0) = 16, \langle k^2 - k \rangle(0) = 384$ and $\phi(0) = 1/3$.

the RLAD model are found in Chapter 3. The two network dynamic processes we consider are 'similar" insofar as they result in almost identical dynamics for the average degree $\langle k \rangle$ (Fig. 4.7b). As expected, with the fast regime, both processes result in similar epidemics as they unfold on effectively static networks with similar network parameters. However, for the comparable and slow regimes, the endemic equilibrium reached is quite different (Fig. 4.7a). For the parameters chosen, the RLAD epidemic reaches a greater endemic equilibrium in both regimes. This may not always be the case—as such a more complete look at such 'similar" processes may be appropriate.

4.4. Seasonal Forcing in Activation/Deletion and Transmission

As an application of the SIS with BRLAD model, we investigate the effects of seasonal forcing of an SIS disease. Explanations of observed periodicity in prevalence time series has historically been attributed to weather and climatic factors, changing social behaviors, or other phenomena including stochasticity. On the deterministic side, periodicity has been incorporated through a time-varying transmission rate $\beta(t)$, which takes on a sinusoidal, piecewise-constant, or other form.

With the inclusion of separate network and disease dynamics, adaptive network models provide a mechanism for modeling the seasonality in disease characteristics and seasonality in social behavior separately. The BRLAD process is particularly well-suited to this question as it can more directly model changing mobility patterns in the bipartite mixing network. To this end, we take the SIS model with BRLAD and introduce simple sinusoidal forms of the activation and deletion rates $\alpha(t)$ and $\omega(t)$ to model seasonal social behavior and examine their effect on the time-evolving network parameters, as well as the disease dynamics. Moreover, we also introduce a simple sinusoidal transmission rate $\beta(t)$ (Dietz, 1976), exploring the interaction between differing mechanisms of seasonal forcing and its effect on an SIS epidemic.

To define simple time-varying activation and deletion rate functions, we consider a periodic perturbation to the constant rates α_0 and ω_0 :

$$\alpha(t) = \alpha_0(1 - \varepsilon_\alpha \cos(Tt)), \tag{4.45}$$

$$\omega(t) = \omega_0(1 + \varepsilon_\omega \cos(Tt)). \tag{4.46}$$

Here, ε_α and ε_ω describe the magnitude of the seasonal perturbation of those rates with $0 \leq \varepsilon_\alpha, \varepsilon_\omega \leq 1$, and T is the frequency of oscillation, being $T = 2\pi/365$ for a period of one year (seasonal dynamics). These forms are motivated by simple assumptions about seasonal mobility patterns that occur at the scale of the whole population—that the activation and deletion of links peak out of phase by half a period. Heuristically, this can be thought of as activation peaking in summer, and deletion peaking in winter.

In terms of the network dynamics, the effect of these rates on the evolution of $\langle k_A \rangle$ and $\langle k \rangle$ is important: how does the seasonality affect the average number of mixing locations visited, as well as the average number of contacts per individual. As these may be observable quantities, the choice of parameters $\alpha_0, \omega_0, \varepsilon_\alpha$, and ε_ω may be constrained by plausibility for a given scenario. With (4.45) and (4.46) the evolution equations for $\langle k_A \rangle$ and $\langle k \rangle$ can be written

$$\dot{\langle k_A \rangle} = \alpha_0(1 - \varepsilon_\alpha \cos(Tt))M - (\alpha_0 + \omega_0 - (\alpha_0\varepsilon_\alpha - \omega_0\varepsilon_\omega)\cos(Tt))\langle k_A \rangle, \tag{4.47}$$

$$\dot{\langle k \rangle} = 2\alpha_0(1 - \varepsilon_\alpha \cos(Tt))(N-1)\langle k_A \rangle - 2(\alpha_0 + \omega_0 - (\alpha_0\varepsilon_\alpha - \omega_0\varepsilon_\omega)\cos(Tt))\langle k \rangle. \tag{4.48}$$

While both are still first-order linear ordinary differential equations, they no longer have constant coefficients. Moreover, an exact solution cannot be found for either equation. However, we assume that ε_α and ε_ω to be small, insofar as we assume that there are likely small perturbations to large-scale mobility behaviors seasonally rather than large swings. Thus, we approach solving (4.47) and (4.48) as a regular perturbation problem. We expand $\langle k_A \rangle$ and $\langle k \rangle$ in the two parameters:

$$\langle k_A \rangle(t) = \langle k_A \rangle_0(t) + \varepsilon_\alpha \langle k_A \rangle_{1,\alpha}(t) + \varepsilon_\omega \langle k_A \rangle_{1,\omega}(t) + \dots, \tag{4.49}$$

$$\langle k \rangle(t) = \langle k \rangle_0(t) + \varepsilon_\alpha \langle k \rangle_{1,\alpha}(t) + \varepsilon_\omega \langle k \rangle_{1,\omega}(t) + \dots. \tag{4.50}$$

First we substitute (4.49) into (4.47). Solving to first order in ε_α and ε_ω yields

$$\begin{aligned} \langle k_A \rangle(t) = {} & \frac{\alpha_0 M}{\alpha_0 + \omega_0} + C e^{-(\alpha_0+\omega_0)t} \\ & + \left(\frac{\alpha_0 \omega_0 M(\varepsilon_\alpha + \varepsilon_\omega)}{(\alpha_0+\omega_0)^2 + T^2} + \frac{\alpha_0 \varepsilon_\alpha - \omega_0 \varepsilon_\omega}{T} C \sin(Tt) \right) e^{-(\alpha_0+\omega_0)t} \\ & - \frac{\alpha_0 \omega_0 M(\varepsilon_\alpha + \varepsilon_\omega)}{(\alpha_0+\omega_0)^2 + T^2} \left(\cos(Tt) + \frac{T}{\alpha_0+\omega_0} \sin(Tt) \right) \Bigg) + \dots \end{aligned} \tag{4.51}$$

where

$$C = \left(\langle k_A \rangle(0) - \frac{\alpha_0 M}{\alpha_0 + \omega_0} \right).$$

Next, we substitute (4.50) into (4.48). Solving to first order in ε_α and ε_ω yields

$$\begin{aligned} \langle k \rangle(t) = {} & \frac{\alpha_0^2 M(N-1)}{(\alpha_0+\omega_0)^2} + \frac{2\alpha_0(N-1)}{\alpha_0+\omega_0} C e^{-(\alpha_0+\omega_0)t} + D e^{-2(\alpha_0+\omega_0)t} \\ & + \left(\frac{2\alpha_0\omega_0(N-1)C}{T^2 + (\alpha_0+\omega_0)^2} (\varepsilon_\alpha + \varepsilon_\omega) + \frac{2(\alpha\varepsilon_\alpha - \omega\varepsilon_\omega)}{T} D \sin(Tt) \right) e^{-2(\alpha_0+\omega_0)t} \\ & + \Bigg(\left(\frac{\alpha_0\omega_0 M}{\alpha_0+\omega_0)} - C\omega_0 \left(\cos(Tt) - \frac{T}{\alpha_0+\omega_0} \sin(Tt) \right) \right) (\varepsilon_\alpha + \varepsilon_\omega) \\ & \quad - \frac{C(T^2 + (\alpha_0+\omega_0)^2)(\alpha_0\varepsilon_\alpha - \omega_0\varepsilon_\omega)}{T(\alpha_0+\omega_0)} \sin(Tt) \Bigg) e^{-(\alpha_0+\omega_0)t} \\ & - \frac{2\alpha_0^2\omega_0 M(N-1)(\varepsilon_\alpha+\varepsilon_\omega)}{(\alpha_0+\omega_0)(T^2+(\alpha_0+\omega_0)^2)} \left(\cos(Tt) + \frac{T}{\alpha_0+\omega_0} \sin(Tt) \right) + \dots \end{aligned} \tag{4.52}$$

where

$$D = \langle k \rangle(0) - \frac{2\alpha_0(N-1)}{\alpha_0+\omega_0} C - \frac{(\alpha_0)^2 M(N-1)}{(\alpha_0+\omega_0)^2}.$$

The asymptotic approximations perform quite well (Fig. 4.8), but even to first order in ε_α and ε_ω

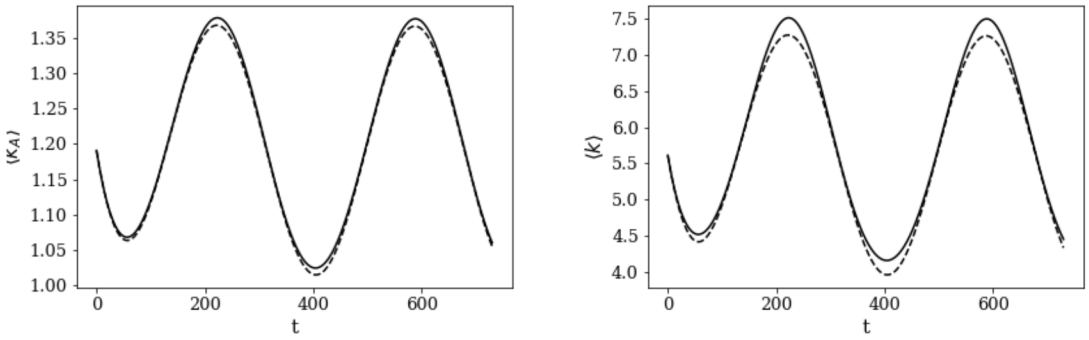

(a) (b)

FIGURE 4.8. Exact (solid) and approximate (dashed) solutions to the dynamical equations for (a) $k_A\rangle(t)$ and (b) $\langle k\rangle$ with periodic activation and deletion rates. Initial conditions are $\langle k_A\rangle(0) = 1.2$ and $\langle k\rangle(0) = 5.6$, while activation/deletion rate parameters are $\alpha_0 = 0.001, \omega_0 = 0.02, \varepsilon_\alpha = \varepsilon_\omega = 0.1$.

the expressions for $\langle k_A\rangle$ and $\langle k\rangle$ are quite complicated, owing to the combination of exponential and periodic change over time. However, we are more interested in the long-term effects of seasonal activation and deletion. For this, we consider a large t approximation, where the network is relatively stable and the network quantities are fluctuating about the equilibrium of the unperturbed case. Then, the exponential terms vanish and we have the approximations

$$\langle k_A\rangle(t) \approx \frac{\alpha_0 M}{\alpha_0+\omega_0} - (\varepsilon_\alpha+\varepsilon_\omega)\frac{\alpha_0\omega_0 M}{T^2+(\alpha_0+\omega_0)^2}\left(\cos(Tt)+\frac{T}{\alpha_0+\omega_0}\sin(Tt)\right), \tag{4.53}$$

$$\langle k\rangle(t) \approx \frac{\alpha_0^2 M(N-1)}{(\alpha_0+\omega_0)^2} - \frac{2\alpha_0^2\omega_0 M(N-1)(\varepsilon_\alpha+\varepsilon_\omega)}{(\alpha_0+\omega_0)(T^2+(\alpha_0+\omega_0)^2)}\left(\cos(Tt)+\frac{T}{\alpha_0+\omega_0}\sin(Tt)\right). \tag{4.54}$$

The amplitude of these oscillations is easily found:

$$\text{Amplitude of } \langle k_A\rangle \approx (\varepsilon_\alpha+\varepsilon_\omega)\frac{\alpha_0\omega_0 M}{(\alpha_0+\omega_0)\sqrt{(T^2+(\alpha_0+\omega_0)^2)}}; \tag{4.55}$$

$$\text{Amplitude of } \langle k\rangle \approx (\varepsilon_\alpha+\varepsilon_\omega)\frac{2\alpha_0^2\omega_0 M(N-1)}{(\alpha_0+\omega_0)^2\sqrt{T^2+(\alpha_0+\omega_0)^2}}. \tag{4.56}$$

From (4.55) and (4.56), it is clear that the amplitude of $\langle k_A\rangle$ and $\langle k\rangle$ will depend on the relationship between T and α_0 and ω_0. If the period is one year (i.e. $T = 2\pi/365$) and the dynamics are slow, the amplitude of oscillations will be relatively small. In this case, an epidemic spreading under the slow regime will not deviate much from the nonseasonal dynamics. On the other

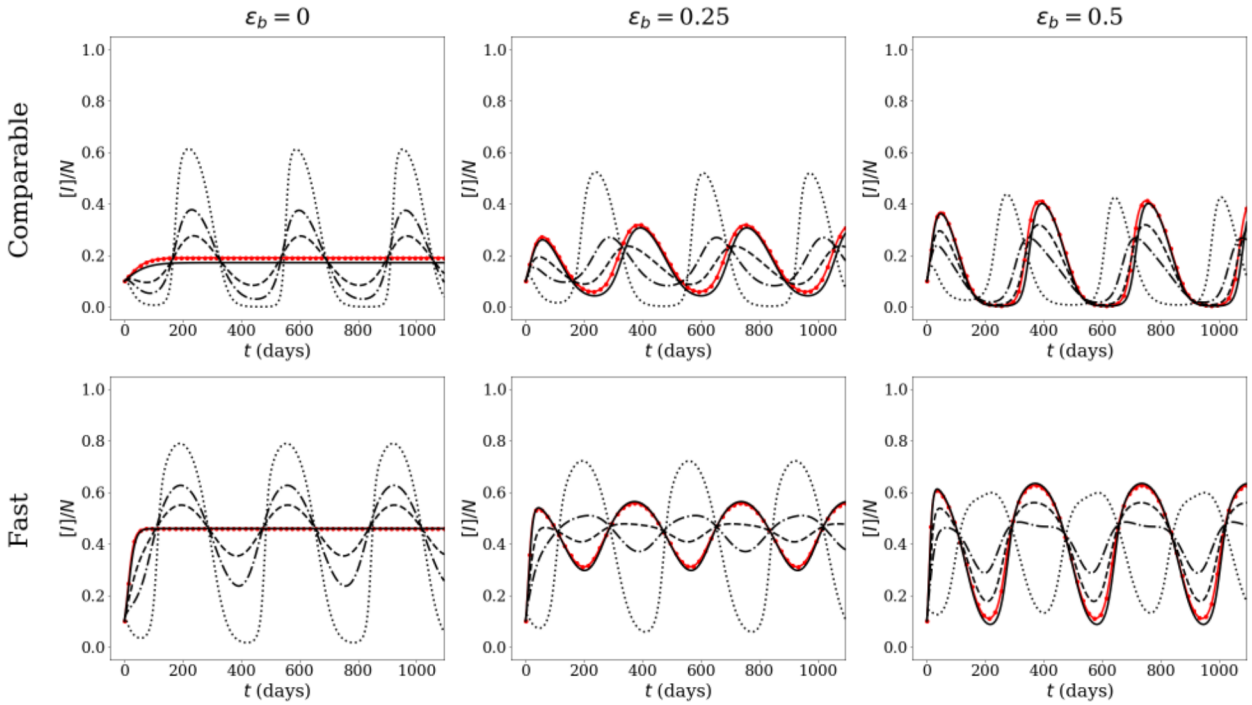

FIGURE 4.9. Plots of prevalence for an SIS with BRLAD epidemic (black) with seasonal transmission and seasonal activation/deletion. The top row shows a comparable regime with $\alpha_0 = 0.001, \omega_0 = 0.032$ and the bottom shows a fast regime with $\alpha_0 = 0.01, \omega_0 = 0.25$. Seasonality parameters for network dynamics are $\varepsilon_\alpha = \varepsilon_\omega = \varepsilon$, varying ε as 0 (solid), 0.05 (dashed), 0.01 (dash-dotted), and 0.25 (dotted); the static network case is shown in red. Epidemiological parameters are $\gamma = 0.1$ with $\beta_0 = 0.0005$, with transmission seasonality parameters $\varepsilon_\beta = 0$ (left), $\varepsilon_\beta = 0.25$ (center), and $\varepsilon_\beta = 0.5$ (right). Underlying bipartite network parameters are $N = 1000, M = 250$ and initial values of $\langle k_A \rangle, \langle k \rangle, \langle k^2 - k \rangle$, and ϕ are all taken from the BRLAD equilibria with the respective α_0 and ω_0. All model runs are initialized with $I_0 = 100$, and time is shifted so the epidemic begins at $t_0 = 365/2$.

hand, if the dynamics are fast enough that $\alpha_0 + \omega_0 >> T$ (as often happens in the comparable and fast regimes), the oscillations are relatively large and will have a significant impact on the epidemic spread. This is shown in the left panels of Figure 4.9, where increasingly large periodic perturbations to the activation and deletion rates result in oscillating epidemics with increasingly large peaks.

While seasonal dynamics in activation and deletion are sufficient to induce an oscillatory epidemic on their own, we can further unpack the role of seasonal forcing by considering a time-dependent transmission rate $\beta(t)$. Following Dietz (1976), we introduce a simple sinusoidal transmission function

$$\beta(t) = \beta_0(1 + \varepsilon_\beta \cos(Tt)), \tag{4.57}$$

where ε_β is the magnitude of the periodic perturbation to the constant transmission rate β_0. This formulation of the transmission rate peaks at the same time as the deletion rate, which corresponds to a disease such as a respiratory infection that is more transmissible in the winter, when individual mobility decreases.

The center and right panels of Figure 4.9 show the effects of low ($\varepsilon_\beta = 0.25$) and high ($\varepsilon_\beta = 0.5$) levels of seasonality in transmission. In both the comparable and fast regimes, seasonality in transmission has a tempering effect on the scale of the epidemic when activation and deletion are also seasonal, decreasing peak prevalence. Perhaps more interesting is to take the perspective of an epidemic with seasonal transmission and then increasing the magnitude of the perturbations to activation and deletion. In both regimes and for both $\varepsilon_\beta = 0.25$ and $\varepsilon_\beta = 0.5$, as ε_α and ε_ω increase, the epidemic dynamics undergo two notable changes. First, the peak prevalence decreases initially and then increases beyond that of the unperturbed case. Second, the oscillations undergo a phase shift, reaching nearly half a period for $\varepsilon_\alpha = \varepsilon_\omega = 0.25$. These observations underscore the importance understanding the dynamics and variation of individual mobility, rather than simply looking at seasonal forcing through transmission alone.

4.5. Discussion

In this chapter, we have developed a novel process of contact network dynamics known as bipartite random link activation/deletion (BRLAD), where edges are randomly added and removed from a bipartite mixing network at specified rates, leading to a time-evolving unipartite contact network. The derivation of evolution equations for critical network parameters was done using probability generating function techniques, and full model encompassing both BRLAD network dynamics and SIS disease dynamics was presented. We followed with an investigation of the SIS

with BRLAD model, including its equilibria and bifurcations, as well as the effect of varying timescales between network and disease dynamics. Finally, we applied the SIS with BRLAD model to a seasonally-forced epidemic, where we defined periodic activation and deletion rates α and ω, as well as a periodic transmission rate β. We found that by treating transmission and social behavior as separate periodic processes, more complex behavior can be captured than in the case of periodic transmission alone.

As BRLAD is one of the simplest adaptive processes that can occur at the bipartite level, it inherently has its limitations. The assumption of constant (or even periodic) activation and deletion rates may not realistically model real-world social behavior, which may depend on an individual's status, or may involve another process entirely, such as rewiring. Another drawback is that for constant rates, the network properties tend to equilibrium values as $t \to \infty$, leading to a fundamentally different network that the initial conditions (in most cases), regardless of what those initial conditions are.

However, there are numerous future directions to describe more complex bipartite-level dynamics. Bipartite-level dynamics based on existing processes may be particularly fruitful, such as allowing differing activation and deletion rates depending on node status or RLAD on a fixed bipartite network. New lines of inquiry may be warranted as well. One such potential modification is to define differing activation and deletion rates for groups of mixing locations, which would allow modelers and public health scientists to consider the effects of closure or limited capacity of mixing locations such as schools, restaurants, religious organizations, etc... A more thorough look at seasonality is another potential extension of the BRLAD process. First, other periodic forms of transmission, activation, and deletion rates may be considered, such as piecewise constant. Second, though we have considered an SIS disease here, many childhood infectious diseases are modeled using an SIR or SEIR model with vital dynamics (see Dietz (1976)). The combination of vital dynamics and adaptive processes has intriguing potential. Perhaps the most exciting application of BRLAD and similar processes is to incorporate the now-abundant cell phone mobility data that helps characterize the real-world bipartite mixing network. When combined with prevalence data, this mobility data could be used to fit realistic dynamic network models without resorting to computationally expensive simulations. There may be great benefits to public health officials of being

able to test the effects of non-pharmaceutical interventions such as lockdowns, business closures, and social distancing in a flexible yet relatively parsimonious modeling framework.

Bibliography

Faruque Ahmed, Nicole Zviedrite, and Amra Uzicanin. Effectiveness of workplace social distancing measures in reducing influenza transmission: A systematic review. *BMC Public Health*, 18(1): 518, December 2018.

Cleo Anastassopoulou, Lucia Russo, Athanasios Tsakris, and Constantinos Siettos. Data-based analysis, modelling and forecasting of the COVID-19 outbreak. *PLOS ONE*, 15(3):e0230405, March 2020.

Rosanna C. Barnard, Luc Berthouze, Peter L. Simon, and Istvan Z. Kiss. Epidemic threshold in pairwise models for clustered networks: Closures and fast correlations. *Journal of Mathematical Biology*, 79(3):823–860, August 2019.

Marian Boguña and Romualdo Pastor-Satorras. Epidemic spreading in correlated complex networks. *Physical Review E*, 66(4):047104, October 2002.

Carlos Castillo-Chavez, Baojun Song, 1. Mathematics, Computational and Modeling Sciences Center, Arizona State University, PO Box 871904, Tempe, AZ 85287, and 2. Department of Mathematical Sciences, Montclair State University, Upper Montclair, NJ 07043. Dynamical Models of Tuberculosis and Their Applications. *Mathematical Biosciences and Engineering*, 1(2):361–404, 2004.

Serina Chang, Emma Pierson, Pang Wei Koh, Jaline Gerardin, Beth Redbird, David Grusky, and Jure Leskovec. Mobility network models of COVID-19 explain inequities and inform reopening. *Nature*, 589(7840):82–87, January 2021.

Shirshendu Chatterjee and Rick Durrett. Contact processes on random graphs with power law degree distributions have critical value 0. *The Annals of Probability*, 37(6), November 2009.

Nicholas A. Christakis and James H. Fowler. Social Network Sensors for Early Detection of Contagious Outbreaks. *PLoS ONE*, 5(9):e12948, September 2010.

Carl Corcoran and Alan Hastings. A Low-Dimensional Network Model for an SIS Epidemic: Analysis of the Super Compact Pairwise Model. *Bulletin of Mathematical Biology*, 83(7):77, July 2021.

Victoria J. Davey, Robert J. Glass, H. Jason Min, Walter E. Beyeler, and Laura M. Glass. Effective, Robust Design of Community Mitigation for Pandemic Influenza: A Systematic Examination of Proposed US Guidance. *PLoS CNE*, 3(7):e2606, July 2008.

O. Diekmann and J. A. P. Heesterbeek. *Mathematical Epidemiology of Infectious Diseases: Model Building, Analysis, and Interpretation*. Wiley Series in Mathematical and Computational Biology. John Wiley, Chichester : New York, 2000. ISBN 978-0-471-98682-9.

K. Dietz. The Incidence of Infectious Diseases under the Influence of Seasonal Fluctuations. In S. Levin, Jürgen Berger, Wolfgang J. Bühler, Rudolf Repges, and Petre Tautu, editors, *Mathematical Models in Medicine*, volume 11, pages 1–15. Springer Berlin Heidelberg, Berlin, Heidelberg, 1976. ISBN 978-3-540-07802-9 978-3-642-93048-5. doi: 10.1007/978-3-642-93048-5_1.

J. Dushoff, J. B. Plotkin, S. A. Levin, and D. J. D. Earn. Dynamical resonance can account for seasonality of influenza epidemics. *Proceedings of the National Academy of Sciences*, 101(48): 16915–16916, November 2004.

K. T. D. Eames and M. J. Keeling. Modeling dynamic and network heterogeneities in the spread of sexually transmitted diseases. *Proceedings of the National Academy of Sciences*, 99(20):13330–13335, October 2002.

D. J. Earn. A Simple Model for Complex Dynamical Transitions in Epidemics. *Science*, 287(5453): 667–670, January 2000.

P. Erdös and A. Renyi. On Random Graphs I. *Publicationes Mathematicae*, 6:290–297, 1959.

S. Eubank, I. Eckstrand, B. Lewis, S. Venkatramanan, M. Marathe, and C. L. Barrett. Commentary on Ferguson, et al., 'Impact of Non-pharmaceutical Interventions (NPIs) to Reduce COVID-19 Mortality and Healthcare Demand". *Bulletin of Mathematical Biology*, 82(4):52, April 2020.

Stephen Eubank, Hasan Guclu, V. S. Anil Kumar, Madhav V. Marathe, Aravind Srinivasan, Zoltan Toroczkai, and Nan Wang. Modelling disease outbreaks in realistic urban social networks. *Nature*, 429(6988):180–184, May 2004.

N Ferguson, D Laydon, G Nedjati Gilani, N Imai, K Ainslie, M Baguelin, S Bhatia, A Boonyasiri, ZULMA Cucunuba Perez, G Cuomo-Dannenburg, A Dighe, I Dorigatti, H Fu, K Gaythorpe, W Green, A Hamlet, W Hinsley, L Okell, S Van Elsland, H Thompson, R Verity, E Volz, H Wang, Y Wang, P Walker, P Winskill, C Whittaker, C Donnelly, S Riley, and A Ghani. Report 9: Impact of non-pharmaceutical interventions (NPIs) to reduce COVID19 mortality and healthcare demand. Technical report, Imperial College London, March 2020.

Neil M. Ferguson, Derek A. T. Cummings, Christophe Fraser, James C. Cajka, Philip C. Cooley, and Donald S. Burke. Strategies for mitigating an influenza pandemic. *Nature*, 442(7101):448–452, July 2006.

E. N. Gilbert. Random Graphs. *The Annals of Mathematical Statistics*, 30(4):1141–1144, December 1959.

Robert Glass, Laura Glass, Walter Beyeler, and H. Min. Targeted Social Distancing Designs for Pandemic Influenza. *Emerging Infectious Diseases*, 12(11):1671–1681, 2006.

Thilo Gross and Bernd Blasius. Adaptive coevolutionary networks: A review. *Journal of The Royal Society Interface*, 5(20):259–271, March 2008.

Thilo Gross, Carlos J. Dommar D'Lima, and Bernd Blasius. Epidemic Dynamics on an Adaptive Network. *Physical Review Letters*, 96(20):208701, May 2006.

Petter Holme and Beom Jun Kim. Growing scale-free networks with tunable clustering. *Physical Review E*, 65(2):026107, January 2002.

Thomas House and Matt J. Keeling. Insights from unifying modern approximations to infections on networks. *Journal of The Royal Society Interface*, 8(54):67–73, January 2011.

Thomas House, Geoffrey Davies, Leon Danon, and Matt J. Keeling. A Motif-Based Approach to Network Epidemics. *Bulletin of Mathematical Biology*, 71(7):1693–1706, October 2009.

Brian Karrer and M. E. J. Newman. Message passing approach for general epidemic models. *Physical Review E*, 82(1):016101, July 2010.

M. J. Keeling. The effects of local spatial structure on epidemiological invasions. *Proceedings of the Royal Society of London. Series B: Biological Sciences*, 266(1421):859–867, April 1999.

M. J. Keeling, D. A. Rand, and A. J. Morris. Correlation models for childhood epidemics. *Proceedings of the Royal Society of London. Series B: Biological Sciences*, 264(1385):1149–1156, August

1997.

Matt J. Keeling, Thomas House, Alison J. Cooper, and Lorenzo Pellis. Systematic Approximations to Susceptible-Infectious-Susceptible Dynamics on Networks. *PLOS Computational Biology*, 12 (12):e1005296, December 2016.

W. O. Kermack and A. G. McKendrick. A contribution to the mathematical theory of epidemics. *Proceedings of the Royal Society of London. Series A, Containing Papers of a Mathematical and Physical Character*, 115(772):700–721, August 1927.

Istvan Z. Kiss, Luc Berthouze, Timothy J. Taylor, and Peter L. Simon. Modelling approaches for simple dynamic networks and applications to disease transmission models. *Proceedings of the Royal Society A: Mathematical, Physical and Engineering Sciences*, 468(2141):1332–1355, May 2012.

Istvan Z. Kiss, Joel C. Miller, and Peter L. Simon. *Mathematics of Epidemics on Networks: From Exact to Approximate Models*, volume 46 of *Interdisciplinary Applied Mathematics*. Springer International Publishing, Cham, 2017. ISBN 978-3-319-50804-7 978-3-319-50806-1.

Qun Li, Xuhua Guan, Peng Wu, Xiaoye Wang, Lei Zhou, Yeqing Tong, Ruiqi Ren, Kathy S.M. Leung, Eric H.Y. Lau, Jessica Y. Wong, Xuesen Xing, Nijuan Xiang, Yang Wu, Chao Li, Qi Chen, Dan Li, Tian Liu, Jing Zhao, Man Liu, Wenxiao Tu, Chuding Chen, Lianmei Jin, Rui Yang, Qi Wang, Suhua Zhou, Rui Wang, Hui Liu, Yinbo Luo, Yuan Liu, Ge Shao, Huan Li, Zhongfa Tao, Yang Yang, Zhiqiang Deng, Boxi Liu, Zhitao Ma, Yanping Zhang, Guoqing Shi, Tommy T.Y. Lam, Joseph T. Wu, George F. Gao, Benjamin J. Cowling, Bo Yang, Gabriel M. Leung, and Zijian Feng. Early Transmission Dynamics in Wuhan, China, of Novel Coronavirus–Infected Pneumonia. *New England Journal of Medicine*, 382(13):1199–1207, March 2020.

Natalie Linton, Tetsuro Kobayashi, Yichi Yang, Katsuma Hayashi, Andrei Akhmetzhanov, Sung-mok Jung, Baoyin Yuan, Ryo Kinoshita, and Hiroshi Nishiura. Incubation Period and Other Epidemiological Characteristics of 2019 Novel Coronavirus Infections with Right Truncation: A Statistical Analysis of Publicly Available Case Data. *Journal of Clinical Medicine*, 9(2):538, February 2020.

Wayne P. London and James A. Yorke. Recurrent outbreaks of measles, chickenpox, and mumps. *American Journal of Epidemiology*, 98(6):453–468, December 1973.

Joel C. Miller. Spread of infectious disease through clustered populations. *Journal of The Royal Society Interface*, 6(41):1121–1134, December 2009.

Joel C. Miller, Anja C. Slim, and Erik M. Volz. Edge-based compartmental modelling for infectious disease spread. *Journal of The Royal Society Interface*, 9(70):890–906, May 2012.

Michael Molloy and Bruce Reed. A critical point for random graphs with a given degree sequence. *Random Structures & Algorithms*, 6(2-3):161–180, 1995.

M. E. J. Newman. Properties of highly clustered networks. *Physical Review E*, 68(2):026121, August 2003.

M. E. J. Newman. *Networks: An Introduction*. Oxford University Press, Oxford ; New York, 2010. ISBN 978-0-19-920665-0.

M. E. J. Newman, S. H. Strogatz, and D. J. Watts. Random graphs with arbitrary degree distributions and their applications. *Physical Review E*, 64(2):026118, July 2001.

Romualdo Pastor-Satorras and Alessandro Vespignani. Epidemic dynamics and endemic states in complex networks. *Physical Review E*, 63(6):066117, May 2001.

Romualdo Pastor-Satorras and Alessandro Vespignani. Epidemic dynamics in finite size scale-free networks. *Physical Review E*, 65(3):035108, March 2002.

Romualdo Pastor-Satorras, Claudio Castellano, Piet Van Mieghem, and Alessandro Vespignani. Epidemic processes in complex networks. *Reviews of Modern Physics*, 87(3):925–979, August 2015.

D. A. Rand. Correlation Equations and Pair Approximations for Spatial Ecologies. In Jacqueline McGlade, editor, *Advanced Ecological Theory*, pages 100–142. Blackwell Publishing Ltd., Oxford, UK, April 1999. ISBN 978-1-4443-1150-1 978-0-86542-734-1.

Prapanporn Rattana, Konstantin B. Blyuss, Ken T. D. Eames, and Istvan Z. Kiss. A Class of Pairwise Models for Epidemic Dynamics on Weighted Networks. *Bulletin of Mathematical Biology*, 75(3):466–490, March 2013.

Jonathan M Read, Ken T.D Eames, and W. John Edmunds. Dynamic social networks and the implications for the spread of infectious disease. *Journal of The Royal Society Interface*, 5(26): 1001–1007, September 2008.

R. Ross. Some a priori pathometric equations. *British Medical Journal*, 1(2830):546–547, March 1915.

M. Salathe, M. Kazandjieva, J. W. Lee, P. Levis, M. W. Feldman, and J. H. Jones. A high-resolution human contact network for infectious disease transmission. *Proceedings of the National Academy of Sciences*, 107(51):22020–22025, December 2010.

Marcel Salathe and James H. Jones. Dynamics and Control of Diseases in Networks with Community Structure. *PLoS Computational Biology*, 6(4):e1000736, April 2010.

Samuel V. Scarpino, Antoine Allard, and Laurent Hebert-Dufresne. The effect of a prudent adaptive behaviour on disease transmission. *Nature Physics*, 12(11):1042–1046, November 2016.

Fanni Selley, Adam Besenyei, Istvan Z. Kiss, and Peter L. Simon. Dynamic Control of Modern, Network-Based Epidemic Models. *SIAM Journal on Applied Dynamical Systems*, 14(1):168–187, January 2015.

Kieran J. Sharkey, Carmen Fernandez, Kenton L. Morgan, Edmund Peeler, Mark Thrush, James F. Turnbull, and Roger G. Bowers. Pair-level approximations to the spatio-temporal dynamics of epidemics on asymmetric contact networks. *Journal of Mathematical Biology*, 53(1):61–85, July 2006.

Maxim S Shkarayev, Ilker Tunc, and Leah B Shaw. Epidemics with temporary link deactivation in scale-free networks. *Journal of Physics A: Mathematical and Theoretical*, 47(45):455006, November 2014.

Peter L. Simon and Istvan Z. Kiss. Super compact pairwise model for SIS epidemic on heterogeneous networks. *Journal of Complex Networks*, 4(2):187–200, June 2016.

Peter L. Simon, Michael Taylor, and Istvan Z. Kiss. Exact epidemic models on graphs using graph-automorphism driven lumping. *Journal of Mathematical Biology*, 62(4):479–508, April 2011.

Michael Taylor, Peter L. Simon, Darren M. Green, Thomas House, and Istvan Z. Kiss. From Markovian to pairwise epidemic models and the performance of moment closure approximations. *Journal of Mathematical Biology*, 64(6):1021–1042, May 2012.

Ilker Tunc, Maxim S. Shkarayev, and Leah B. Shaw. Epidemics in Adaptive Social Networks with Temporary Link Deactivation. *Journal of Statistical Physics*, 151(1-2):355–366, April 2013.

L. D. Valdez, P. A. Macri, and L. A. Braunstein. Intermittent social distancing strategy for epidemic control. *Physical Review E*, 85(3):036108, March 2012.

P. van den Driessche and James Watmough. Reproduction numbers and sub-threshold endemic equilibria for compartmental models of disease transmission. *Mathematical Biosciences*, 180(1-2): 29–48, November 2002.

Piet Van Mieghem. The N-intertwined SIS epidemic network model. *Computing*, 93(2-4):147–169, December 2011.

Duncan J. Watts and Steven H. Strogatz. Collective dynamics of 'small-world' networks. *Nature*, 393(6684):440–442, June 1998.

Herbert S. Wilf. *Generatingfunctionology*. A K Peters, Wellesley, Mass, 3rd ed edition, 2006. ISBN 978-1-56881-279-3.

Chong You, Yuhao Deng, Wenjie Hu, Jiarui Sun, Qiushi Lin, Feng Zhou, Cheng Heng Pang, Yuan Zhang, Zhengchao Chen, and Xiao-Hua Zhou. Estimation of the time-varying reproduction number of COVID-19 outbreak in China. *International Journal of Hygiene and Environmental Health*, 228:113555, July 2020.

Mina Youssef and Caterina Scoglio. Mitigation of epidemics in contact networks through optimal contact adaptation. *Mathematical Biosciences and Engineering*, 10(4):1227–1251, 2013.

Juanjuan Zhang, Maria Litvinova, Wei Wang, Yan Wang, Xiaowei Deng, Xinghui Chen, Mei Li, Wen Zheng, Lan Yi, Xinhua Chen, Qianhui Wu, Yuxia Liang, Xiling Wang, Juan Yang, Kaiyuan Sun, Ira M Longini, M Elizabeth Halloran, Peng Wu, Benjamin J Cowling, Stefano Merler, Cecile Viboud, Alessandro Vespignani, Marco Ajelli, and Hongjie Yu. Evolving epidemiology and transmission dynamics of coronavirus disease 2019 outside Hubei province, China: A descriptive and modelling study. *The Lancet Infectious Diseases*, 20(7):793–802, July 2020.